Regulation of temozolomide-induced death of glioblastoma cells: dose responses and role of HIPK2

Dissertation

zur Erlangung des Grades

Doktors der Naturwissenschaften

Am Fachbereich Biologie

Der Johannes Gutenberg-Universität Mainz

vorgelegt von:

Yang He

geb. am 01.06.1989 in Shaanxi, China

Mainz 2019

Table of contents

1 Summary

Astrocytoma WHO grade IV, also called glioblastoma multiforme or glioblastoma, is the most frequent and aggressive kind of high-grade malignant glioma. Due to the dismal prognosis faced by patients suffering from this disease, there is a need for identifying new targets that might improve its therapy. O^6-methylguanine (O^6-MeG) is the most toxic DNA adduct caused by temozolomide (TMZ). The damage induces DNA double-strand breaks (DSBs), which trigger apoptosis in cells. Since TMZ is utilized for the treatment of glioblastoma multiforme and the dual function of p53 regulates both cell death and cell survival mechanisms, the question arises as to the possible threshold to start apoptosis that is evoked by TMZ. To determine whether there is a threshold for the TMZ-induced DNA damage response and exploring the factors regulating the switch in p53 dependent death or survival in glioblastoma cells, the glioblastoma lines LN229, LN308 and LN229MGMT were exposed to different doses of TMZ. p53 protein expression, phosphorylation levels of p53ser15 and p53ser46 were determined by Western blotting. Apoptosis, senescence and autophagy levels were checked after different doses of TMZ. The results showed that pro-survival (p53ser15) and pro-death (p53ser46) factors are induced by *O*^{6}-MeG in a dose and time-dependent manner. We observed that *O*^{6}-MeG triggers apoptosis at later time points. A survival shoulder was observed in p53 deficient LN308 cells, but not in p53 proficient LN229 cells after TMZ treatment. LN308 also shows more resistance in senescence and autophagy than LN229 after TMZ treatment, while the two cell lines have the same level of DSBs induced by TMZ. These data suggest that the p53 status may influence the threshold of TMZ-induced damage responses in glioblastoma cells, and the phosphorylation level of p53ser46 can be used as an index of *O*^{6}-MeG triggered apoptosis.

The DNA damage-activated kinase HIPK2 serves as a potent cell death activator through engaging tumor suppressor p53. Whether HIPK2 is involved in therapy-induced glioblastoma cell death is unknown. In this work, the evidence is provided that HIPK2 and its negative regulatory E3 ubiquitin ligase SIAH1 are critical factors controlling TMZ- induced glioblastoma cell death. We show that HIPK2 downregulation (HIPK2kd) significantly reduced the level of TMZ-induced apoptosis. This was not the case in cells expressing the DNA repair enzyme MGMT, which removes TMZ-induced O^6-alkylations, suggesting that the primary DNA lesion responsible for triggering HIPK2-mediated death is *O*^{6}-methylguanine. Following TMZ treatment p53 was phosphorylated at Ser46, and HIPK2kd had an impact exclusively on p53Ser46 while left Ser15 phosphorylation unaffected. TMZ-induced apoptosis in p53 wild-type glioblastoma cells is driven by activation of the death receptor FAS (alias CD95/APO1), which becomes upregulated following TMZ. Accordingly, the expression level of FAS was clearly attenuated upon HIPK2 downregulation, supporting the conclusion that HIPK2 regulates TMZ-induced apoptosis via p53Ser46 driven FAS expression. Using

chromatin-immunoprecipitation studies we found that binding of p53 to the FAS promoter is positively regulated by HIPK2. Remarkably, other proapoptotic proteins like PUMA, NOXA, BAX and PTEN were not affected in HIPK2kd. Finally, we show that downregulation of the E3 ubiquitin ligase SIAH1, but not SIAH2, significantly ameliorates TMZ-induced apoptosis, suggesting that the ATM/ATR target SIAH1 plays a key role in TMZ-induced apoptotic death. Since our database analysis revealed that SIAH1 is frequently overexpressed in gliomas, the results bear important implications for TMZ-based malignant brain cancer therapy and suggest the HIPK2-SIAH1 module as a potential target in glioma therapy.

Zusammenfassung

Glioblastoma multiforme ist die häufigste und aggressivste Form eines hochgradigen malignen Glioms. Aufgrund der bedrückenden Prognose von Patienten, die an dieser Krankheit leiden, müssen neue Zielstrukturen („Targets“) identifiziert werden, die die Therapie verbessern könnten. *O*^{6}-Methylguanin (*O*^{6}-MeG) ist das toxischste DNA-Addukt, das durch Temozolomid (TMZ) verursacht wird. *O*^{6}-MeG induziert DNA-Doppelstrangbrüche (DSBs), die Apoptose auslösen. Da TMZ zur Behandlung von Glioblastomen verwendet wird und die Doppelfunktion von p53 sowohl den Zelltod als auch das Überleben der Zellen reguliert, stellt sich die Frage nach der möglichen Schwelle für den Beginn der Apoptose, die von TMZ ausgelöst wird. Um zu bestimmen, ob es einen Schwellenwert für die TMZ-induzierte DNA-Schadensreaktion gibt, und um die Faktoren zu untersuchen, die den Wechsel des p53-abhängigen Todes oder Überlebens in Glioblastomzellen regulieren, wurden die Glioblastom-Linien LN229, LN308 und LN229MGMT verschiedenen TMZ-Dosen ausgesetzt. p53-Proteinexpression, Phosphorylierungsniveaus von p53ser15 und p53ser46 wurden durch Western-Blotting bestimmt. Apoptose, Seneszenz und Autophagie wurden nach verschiedenen TMZ-Dosen überprüft. Die Ergebnisse zeigten, dass die Faktoren Pro-Survival (p53ser15) und Pro-Death (p53ser46) durch *O*^{6}-MeG dosis- und zeitabhängig induziert werden. Wir haben beobachtet, dass *O*^{6}-MeG zu späteren Zeitpunkten Apoptose auslöst. Eine Überlebensschulter wurde in p53-defizienten LN308-Zellen beobachtet, nicht aber in p53-wildtypischen LN229-Zellen nach niedrigen TMZ-Dosen. LN308 zeigte auch eine stärkere Resistenz hinsichtlich Seneszenz und Autophagie als LN229 nach TMZ-Behandlung, während die beiden Zelllinien nach TMZ-Behandlung das gleiche Maß an Doppelstrangbrüchen aufweisen. Diese Daten legen nahe, dass der p53-Status die Schwelle für die TMZ-induzierte Schadensreaktion in Glioblastomzellen beeinflussen kann, und der Phosphorylierungsgrad von p53ser46 kann folglich als Index der durch O^6-MeG ausgelösten Apoptose verwendet werden.

Die durch DNA-Schädigung aktivierte Kinase HIPK2 dient durch Aktivierung des Tumorsuppressors p53 als potenter Zelltodaktivator. Ob HIPK2 eine Rolle bei dem durch TMZ-Therapie induzierten Gliomzelltod spielt, ist nicht bekannt. In dieser Arbeit wird nachgewiesen, dass HIPK2 und seine negativ regulierende E3-Ubiquitin-Ligase SIAH1 kritische Faktoren sind, die den durch TMZ induzierten Glioblastomzelltod steuern. Wir zeigen, dass die Herabregulierung von HIPK2 (HIPK2kd) die Menge an TMZ-induzierter Apoptose signifikant reduziert. Dies war nicht der Fall bei Zellen, die das DNA-Reparaturenzym MGMT exprimieren, wodurch TMZ-induzierte *O*^{6}-Alkylierungen entfernt werden. Dies legt den Schluss nahe, dass die primäre DNA-Läsion, die für das Auslösen des HIPK2-vermittelten Todes verantwortlich ist, *O*^{6}-Methylguanin ist. Nach der TMZ-Behandlung wurde p53 am Ser46 phosphoryliert, und HIPK2kd hatte ausschließlich Einfluss auf p53Ser46, während die Ser15-Phosphorylierung nicht beeinflusst wurde. Die durch TMZ induzierte Apoptose in p53-Wildtyp-Glioblastomzellen wird durch die Aktivierung des Todesrezeptors FAS (Alias

CD95 / APO1) gesteuert, der nach TMZ hochreguliert wird. Dementsprechend wurde das Expressionsniveau von FAS nach der HIPK2-Herunterregulierung deutlich abgeschwächt, was die Schlussfolgerung stützt, dass HIPK2 die durch TMZ induzierte Apoptose über die p53Ser46-gesteuerte FAS-Expression reguliert. In Chromatin-Immunopräzipitationsstudien wurde festgestellt, dass die Bindung von p53 an den Fas-Promotor durch HIPK2 positiv reguliert wird. Bemerkenswerterweise waren andere proapoptotische Proteine wie PUMA, NOXA, BAX und PTEN in HIPK2kd nicht betroffen. Schließlich zeigen wir, dass die Herunterregulierung der E3-Ubiquitin-Ligase SIAH1, nicht aber SIAH2, die durch TMZ induzierte Apoptose signifikant verbessert, was darauf hindeutet, dass das ATM / ATR-Ziel, SIAH1, eine Schlüsselrolle beim durch TMZ induzierten apoptotischen Tod spielt. Da eine Datenbankanalyse ergab, dass SIAH1 häufig in Gliomen überexprimiert wird, haben unsere Ergebnisse wichtige Implikationen für die TMZ-basierte Krebs-Chemotherapie, indem sie das HIPK2-SIAH1-Modul als potenzielles "Target" in der Gliomtherapie vorschlagen.

2 Introduction

2.1 Brain tumors and the treatment

2.1.1 Types of brain tumors

Brain tumors, also known as brain cancers, arise from cells that grow abnormally in the brain. Brain tumors can be subgrouped into benign and malignant tumors. Benign tumors do not attack tissues nearby or disseminate to other distant areas(Dandy 1933). Usually, benign tumors are less severe than malignant tumors, but sometimes they still cause many problems in the brain because benign tumors can grow extensively and therefore may press nearby tissues, sometimes they even turn into malignant tumors, which occurs notably after irradiation following therapy (Al-Mefty, Kersh et al. 1990).

Malignant tumors grow and migrate fast and overwhelm healthy cells by seizing nutrients, space and blood. They can also spread to the other places of the body (DeAngelis 2001). In the United States, every year about 6 out of 1,000 people are affected by brain or nervous system tumors (Preston-Martin 1996, Fang, Kulldorff et al. 2004).

Brain tumors that commonly known are glioma, meningioma, vestibular schwannomas, pituitary adenoma and primitive neuroectodermal tumors (neuronal tumors). The most common malignant brain tumor is glioma, which begins with colloidal (supportive) tissue. Around 80 percent of all malignant brain tumors is glioma (Goodenberger and Jenkins 2012), it may grow anywhere in the brain or spinal cord. Glioma includes glioblastoma, astrocytoma, oligodendroglioma and ependymoma (Peter, Linet et al. 1995).

2.1.2 Causes of brain tumors

The exact causes of the formation of brain tumors are unclear. Like most other tumors, genetic factor and various environmental toxins can cause brain tumors, and head radiation and HIV infection are associated with brain tumors. The only widely accepted risk factor for brain tumors is ionizing radiation. The irradiation of the skull can increase the incidence of meningioma by a factor of 10 and the incidence of glioma by 3 to 7-times, even at low dose radiation (Pollak, Walach et al. 1998, Walter, Hancock et al. 1998).

Retroviruses may also be one of the reasons for brain tumors. A study based on fetal rat brain cells has demonstrated that microinjection of retroviral vectors into the brain within 20 days of birth, 7 of which develop malignant neuroectodermal tumors. One oligodendroglioma, two

hemangiomas and one malignant hemangioendothelioma were also observed (Radner, El-Shabrawi et al. 1993).

Genetic factors such as neurofibromatosis and tuberous sclerosis complexes are associated with glioma (Reuss and von Deimling 2009). Other rare syndromes that may cause glioma include Li-Fraumeni, melanoma-astrocytoma and Turcot syndrome.

With the proliferation of mobile phones, there is concern about the link between cell phone technology and the central nervous system (CNS) and intracranial tumors. Thus, researchers have investigated the trends in the incidence of such tumors during periods of dramatic increases in mobile phone usage. Researchers have investigated the long-term trends in the incidence rate of primary and central nervous system brains in Israel between 1990 and 2015, during which mobile phone technology became extremely common in Israel. The results didn't give the proof of the view that cell phone use rises brain cancer incidence (Keinan-Boker, Friedman et al. 2018).

2.1.3 Diagnosis of brain tumors

Brain tumors have many symptoms that are not only occur in brain tumors, which means they may be also caused by other diseases. Significant symptoms are not found in brain tumors, some are not usually found (e.g. pituitary tumors) unless CT scans or MRIs are performed for other reasons. Headache, weakness, clumsiness and seizures sometimes are the most common symptoms, other nonspecific symptoms and signs include loses in memory, attention or alertness, starting of nausea, vomiting, abnormalities in vision and others.

In most cases, the patient will have a CT scan of the brain. CT scan shows more detail in three dimensions, usually, contrast dyes are injected into the blood to highlight scan abnormalities. More commonly, MRI scans are used for suspected brain tumors (Young and Knopp 2006). This is because MRI has a higher sensitivity for detecting the presence or change of a tumor. However, most organizations still use CT scans as the first diagnostic test (Hochberg and Pruitt 1980). PET is another kind of testing way (Langleben and Segall 2000). Recently, fluciclovine was shown as a novel radiotracer using PET for meningioma, one kind of brain cancers (Nguyen, Amato et al. 2018). Routine laboratory analysis including blood, electrolytes, and liver function tests can be performed because people with brain tumors often have other medical problems.

2.1.4 Treatment of brain tumors

Treating brain tumors is often complicated and unsuccessful. The treatment of brain tumors depends on several factors: the age of a person, general health, the size, location and type of

the tumor. The treatment plan varies greatly depending on these factors and any other medical problems that the patient may have (Black 1991). The most widely used treatments are surgery, radiation therapy and chemotherapy. In general, comprehensive treatment is recommended, meaning surgery combined with radiotherapy and chemotherapy, which can delay recurrence and prolong survival.

2.1.4.1 Surgical treatment

The treatment of brain tumors (for example glioblastoma) mainly uses surgery, but because there is no obvious boundary between tumor and brain tissue, it is difficult to remove all tumor mass during resection. The invasive growth of tumors aggravates this problem unless it is an early small tumor and is located at an appropriate site. The principle of surgery is to remove the tumor as much as possible while retaining nerve function. When complete tumor resection is achieved, no further treatment is required and there is little recurrence (Watson, Kadota et al. 2001). Those with small early tumors should try to remove all tumors. Cerebral resection can be used for tumors located in the anterior or frontal temporal lobe, if the tumor involves the cerebral hemisphere, both brains have hemiplegia, but do not invade the basal ganglia, the thalamus and the contralateral side, cerebral hemisphere resection can also be used (Matsukado, MacCarty et al. 1961, Yeh, Kashiwagi et al. 1990). If the tumor is in a motor or speech area and there is no significant hemiplegia, patients with aphasia should maintain neurological function and avoid serious sequelae when undergoing surgery (Asthagiri, Pouratian et al. 2007). Advances in neurosurgery and neuroimaging techniques have made surgical resection of low-grade gliomas a safe choice for patients (Pouratian, Asthagiri et al. 2007).

Medical management is also essential. Effective medical management can reduce morbidity and mortality, as seizures, venous thromboembolism and edema around the tumor can complicate the treatment of tumor surgery (Drappatz, Schiff et al. 2007).

2.1.4.2 Radiation therapy

Different types of brain tumors have different sensitivities to radiation therapy. It is generally considered that a poorly differentiated tumor is superior to a well-differentiated tumor regarding radiation sensitivity (Brierley, Panzarella et al. 1997). Taking gliomas as examples: Medulloblastoma is most sensitive to radiotherapy, followed by ependymoma, polymorphic glioblastoma is only moderately sensitive, astrocytoma, pineal somatic tumors are less sensitive to radiotherapy (Martin, Moyal et al. 2013). Since medulloblastoma and ependymoma are easily spread with the cerebrospinal fluid, total spinal canal irradiation is generally used.

For several decades, a standard treatment for brain metastases is the whole-brain radiation therapy (Patchell, Tibbs et al. 1998, Kondziolka, Patel et al. 1999), then the focal aggressive therapy combined with whole-brain radiation therapy has been applied (Patchell, Tibbs et al. 1990).

2.1.4.3. Chemotherapy

When a chemotherapeutic drug kills a tumor cell, it also kills normal cells, causing damage to the healthy tissues and organs, and causing side effects such as nausea, vomiting, platelets, and leukopenia (Shah and Kochar 2018). Despite this, chemotherapy is still an important treatment for brain tumors. The chemotherapy kills cancer cells with its ability to halt cell division (Darzynkiewicz 2011). The chemotherapy will kill the cells more effeiciently when the cells are dividing fast. According to the structural formula and mechanism of action of tumor chemicals, they can be divided into six categories: alkylating agents, anti-metabolites, antibiotics, plant drugs, hormone drugs and others (DiPiro, Talbert et al. 2014). Some widely used chemotherapeutic agents are procarbazine, dacarbazine (DTIC) and temozolomide (TMZ), which transfer methyl groups to DNA.

2.2 Alkylating agents and the related DNA damage responses

Alkylating agents belong to the earliest and largest families of oncologic drugs. Since the application of nitrogen mustard in the treatment of malignant lymphoma in 1942, alkylating agents have become the most important class of drugs in cancer chemotherapy.

The main common feature of these drugs is the cytotoxic component of the molecular structure, that is, the molecule contains an alkyl group. These alkyl groups can usually be converted into electron-trapping intermediates that covalently bind to electron groups contained in the DNA, RNA or protein of the cell, causing alkylation reactions that make these cellular components useless in cell metabolism, resulting in cell death. This class of drugs rarely produces resistance compared with other antineoplastic agents. Commonly used alkylating agents are cyclophosphamide, nitrogen mustard, thiotepa, temozolomide, cyclohexyl nitrosourea, lomustine, procarbazine and others. In my project I was working with temozolomide and lomustine (CCNU).

2.2.1 Temozolomide

Temozolomide (TMZ) (Figure 1) is an alkylating agent which is used in the chemotherapy of

brain cancers, such as astrocytoma and glioblastoma. TMZ is a small molecule, its relative molecular mass is 194. Adjuvant TMZ after radiotherapy helps glioblastoma patients survive significantly longer, although the increase in median survival is only 3 months (Stupp, Mason et al. 2004).

TMZ can pass the blood-brain barrier (Newlands, Stevens et al. 1997). At physiological pH, it spontaneously hydrolysis to the active form 3-methyl-(triazen-1-yl) imidazole-4-carboxamide (MITC)(Kaina, Christmann et al. 2007). In the DNA, more than 10 targets were methylated by MITC. The main product is *N*7-methylguanine (*N*7MeG) while some of the minor products are *N*3-methyladenine (*N*3MeA), *N*3-methylguanine (*N*3MeG), and O^6-methylguanine (O^6-MeG). These DNA adducts show different stabilities. *N*3MeA and *N*3MeG are easily hydrolyzed, *N*7MeG is stable for longer times and can be repaired by base excision repair, so they are considered harmless at clinically relevant doses. O^6-MeG only takes up for about 6-8% of all induced DNA adducts by TMZ (Beranek 1990, Drabløs, Feyzi et al. 2004), while it is the most cytotoxic lesion due to its high mutagenic potential (Kaina, Christmann et al. 2007). For TMZ, it has been proved that apoptosis are caused by TMZ- induced DSBs (Roos, Nikolova et al. 2009), which is still not known for fotemustine yet. p53 has a critical dual function, so p53 proficient glioblastoma cells are more resistant to ACNU but more sensitive to TMZ than p53 deficient cells, which was explained by up-regulation of FAS-R or DNA repair after treatment (Batista, Roos et al. 2007, Roos, Batista et al. 2007).

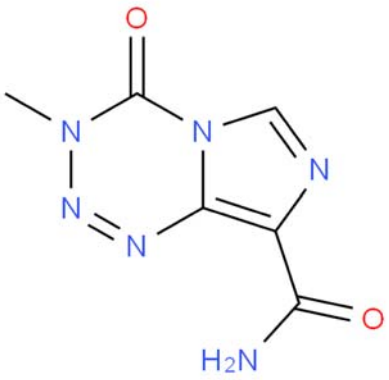

Figure 1 Structure of Temozolomide.
(http://www.chemspider.com/Chemical-Structure.5201.html).

2.2.2 O^6-methylguanine and MGMT

O^6-MeG is one of the methylation products caused by TMZ. It causes DNA double-strand breaks and triggers apoptosis (Kaina, Ziouta et al. 1997, Meikrantz, Bergom et al. 1998). O^6-MeG is repaired by the enzyme O^6-methylguanine-DNA methyltransferase (MGMT) in a stoichiometric damage reversal reaction that restores guanine in the DNA and inactivates

MGMT (Kaina, Christmann et al. 2007) (Figure 2). O^6-MeG stably persists in the DNA when the MGMT is absent (Pegg 2000). The expression of MGMT, and consequently the resistance of gliomas to TMZ based therapy, is governed by epigenetic modifications of CpG islands in its promotor (Esteller, Hamilton et al. 1999). If these CpG islands are methylated, *MGMT* is silenced and O^6-MeG persists in the DNA. Promoter methylation of MGMT has been shown to be prognostic for glioma therapy outcome, which supports the importance of O^6-MeG in glioma therapy (Esteller, Garcia-Foncillas et al. 2000, Hegi, Diserens et al. 2005).

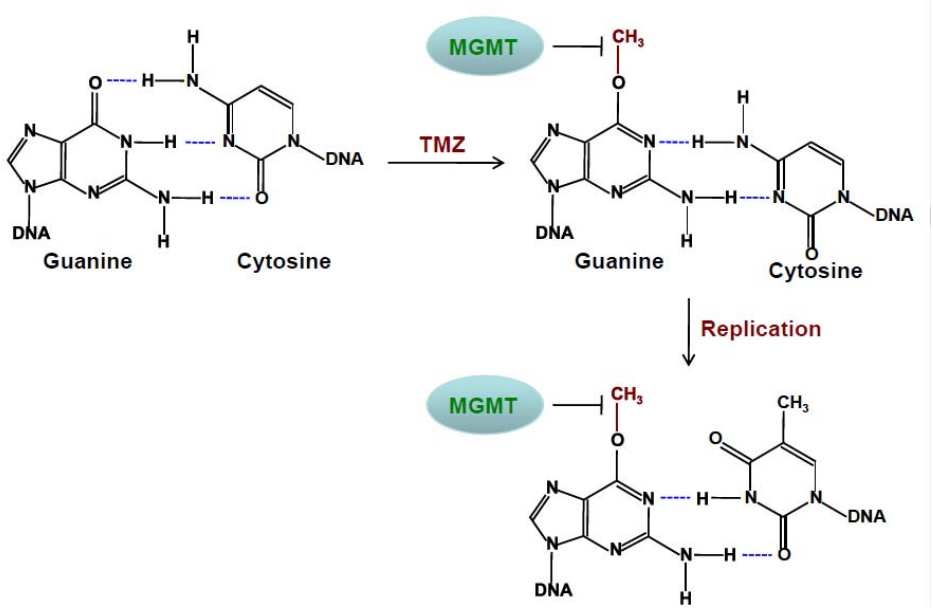

Figure 2 MGMT repairs O^6-MeG by removing the methyl group. (According to Kaina et al, DNA repair, 2007)

When O^6-MeG is induced by TMZ and MGMT is expressed, the repair protein recognizes O^6-MeG and removes the methyl group either before or after replication of DNA.

2.2.3 DSBs induced by O^6-methylguanine

DNA double-strand breaks (DSBs) are one of the most toxic lesions that are found in eukaryotic cells, they are able to harm the genome stability. DSBs occur because of DNA damage, either exogenous or endogenous, and occur during meiotic recombination. Homologous recombination (HR) repairs DSBs, it employs the sister chromatid in mitotic cells as a template, in meiotic cells, HR uses the homologous chromosome as a template for repair.

O^6-MeG is a cytotoxic lesion, the level of killing resistance is determined by the existing amount of MGMT in the cell and the rate of re-synthesize of it. In tumors such as

glioblastoma, the synthesis of the MGMT are prevents by epigenetic silencing of the MGMT gene. As a consequence, this kind of tumors has more probability to be killed by TMZ. O^6-MeG can not induce apoptosis itself, while with the help of mismatch repair (MMR) and DNA replication, it causes DNA double-strand breaks (DSBs) in cells, which are responsible for provoking apoptosis. Quiros' work has shown that the DNA damage response and cell death pathways only occur once cells have passed through two DNA synthesis cycles (Quiros, Roos et al. 2010). In MGMT depleted and MMR proficient cells, O^6-MeG induces DSBs and replication-blocking lesions that trigger the DNA damage response through ataxia-telangiectasia mutated (ATM), ataxia telangiectasia and Rad3 related (ATR), Chk1, Chk2 and p53 (Kaina, Christmann et al. 2007). Previous work done by our group (AG Kaina) has shown that ATR contributes more to the protection from O^6-MeG toxicity than ATM (Eich, Roos et al. 2013).

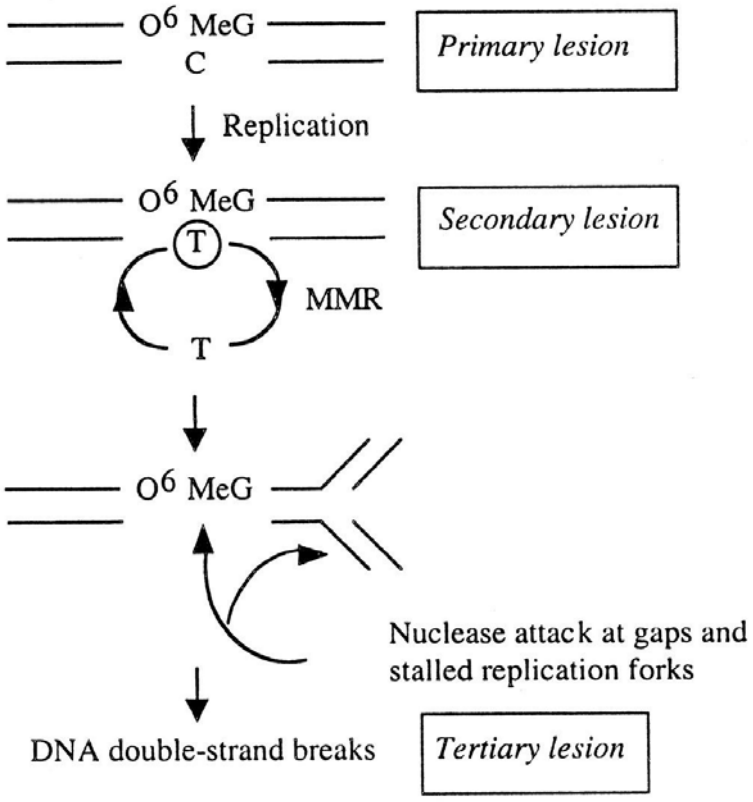

Figure 3 O^6-MeG induces double strand breaks with the help of mismatch repair and cell replication (Modified from Ochs and Kaina, Cancer Research, 2000)**.** In MGMT deficient cells, thymine is introduced to pair with O^6-MeG instead of cytosine, the MMR recognizes the wrong pairing while it introduces thymine again and again since the O^6-MeG cannot be recognized and repaired. And therefore, after the second DNA replication cycle cycle, DSBs are formed.

2.2.4 Lomustine (CCNU) and *O*^{6}-chloroethylguanine

Lomustine [1-(2-chloroethyl)-3-cyclohexyl-1-nitrosourea], as an alkylating antineoplastic drug, it inhibits cell cycle progression in S and G_2 phase (Agarwal, Jangir et al. 2014, Nikolova, Roos et al. 2017). It is often used in the chemotherapy of brain tumors, resistant or relapsed Hodgkin's disease, small cell lung cancer, lymphomas, malignant melanoma and various solid tumors (Agarwal, Jangir et al. 2014).

Lomustine (Figure 4) induces *O*^{6}-chloroethylguanine, which induces N1-guanine-N3-cytosine crosslinks. The molecular cell death pathways triggered by the *O*^{6}-chloroethylguanine are not predictable, the pathways depend on the different cellular background. In this case, the same DNA lesion can induce different responses, such as apoptosis, necrosis, senescence and growth arrest (Roos and Kaina 2006, Knizhnik, Roos et al. 2013), the reason for which is still unclear.

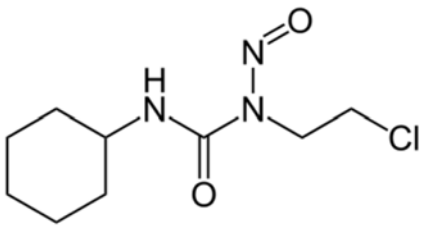

Figure 4 Chemical structure of lomustine. (from https://www.drugbank.ca)

2.3 p53 related repair and apoptosis pathways

2.3.1 Regulation of p53

The tumor suppressor protein p53 can be activated for a number of reasons, such as DNA damage induced by UV, chemical agents, oxidative stress (Han, Muller et al. 2008), osmotic shock and oncogene expression. After p53 is activated, the half-life of p53 increases very fast, which leads to the rapid accumulation of p53 protein. The p53 may also activate as a transcriptional regulator in cells. Phosphorylation of its N-terminal domain is the most critical step in p53 activation. The N-terminal domain is the major target of protein kinases that transduce stress signals because it contains many phosphorylation sites.

In unstressed cells, p53 has remained at a low level. MDM2 is an E3 ubiquitinated ligase (also known as HDM2 in humans) that covalently links ubiquitin to p53, thereby labeling p53 as proteasome degradation.

However, the ubiquitination of p53 can be reversed. The combination of MI-63 and MDM2 makes it possible to use p53 again (Canner, Sobo et al. 2009). The USP7 (or HAUSP), an ubiquitin-specific protease, is able to cleave ubiquitin on p53, protect p53 from the proteasome-dependent degradation. USP42 has also been proved to deubiquitinate p53 (Hock, Vigneron et al. 2011).

There are two groups of protein kinases that are broadly known to target the p53 transcriptional activation domain. The first group is the protein kinases from the MAPK family, which including JNK1-3, ERK1-2 and p38 MAPK. The second group contains ATM, ATR, CHK1 and CHK2, DNA-dependent protein kinase (DNA-PK), CDK-activating kinase (CAK) and TP53RK. The first group can cope with membrane damage, oxidative stress and similar factors. The second group is involved in the genomic integrity checkpoint and can detect and respond to several kinds of DNA damage induced by genotoxic lesions. Binding between Mdm2 and p53 is disrupted by the phosphorylation of the N-terminus of p53 by these protein kinase, some other proteins are also recruited to p53 and prevents MDM2 binding and p53 degradation, such as Pin1. Deacetylases, such as Sirt1 and Sirt7, are able to deacetylate p53, and inhibiting apoptosis (Vakhrusheva, Smolka et al. 2008).

2.3.2 Downstream signaling of p53

Following DNA damage and activation of p53, either survival or death pathways can be triggered with the participation of p53. Different downstream factors may be involved depending on the level of damage. One model says that repair and survival mechanisms will be triggered by low levels of DNA damage responses, while cell death triggered by high levels of damage. The survival pathway is supposed to be dependent on ATM/ATR-CHK1/2 to active p53, and the cell death pathway rests on the MDM2 negative regulation (Zhang, Liu et al. 2009, Roos, Thomas et al. 2016). That means, when simulations come, activated ATM or ATR initiates the p53 stabilization, the target downstream genes of p53 are selectively activated to lead to different cell fate. The activated p53 fosters the repair of minor DNA damage while inhibits the repair of severe DNA damage. At low DNA damage levels, a few p53 induces the expression of p21 (coded by *CDKN1A*), thereby evokes cell cycle arrest and promote survival of cells, while when high levels of damage occur, sustained p53 induces p53AIP1 and subsequently triggers apoptosis (Zhang, Liu et al. 2009, Nicol, Bray et al. 2013). The p53-p21 survival path also depends on p68 (Nicol, Bray et al. 2013) in mouse, while in human, the human cellular apoptosis susceptibility protein (hCAS/CSE1L) is related to p53 target promoters such as *PIG3* and *p53AIP1* in lung and breast cancer cells (Tanaka, Ohkubo et al. 2007). The regulation of p53 and the downstream factors that are involved probably differ in various cells types and cancers.

It is also reported that phosphorylations and acetylations of p53 can make the decision between survival and cell death (Ichwan, Yamada et al. 2006, Pietsch, Sykes et al. 2008, Loughery, Cox et al. 2014). Phosphorylations of p53 at Ser15, Ser20, Ser37 and Thr18 help p53 to get rid of its inhibitory MDM2 binding partner and assists p53 transcriptional activation, for example, ser15 is required for p53-mediated gene expression like CDKN1A (p21). It also supports the p53 protein to promote the expression of BAX and MDM2 by activating the corresponding promoters (Loughery, Cox et al. 2014). Phosphorylation of p53 at Ser46 specifically activates apoptosis (Mayo, Seo et al. 2005).

It is postulated that p53ser46 alters promoter selection and favours the expression of pro-apoptotic genes such as *NOXA* (also known as *PMAIP1*) (Ichwan, Yamada et al. 2006), *PTEN* (Mayo, Seo et al. 2005) and *TP53AIP1* (Oda, Arakawa et al. 2000), which cause apoptosis in response to different chemical agents and even physical stress. A number of kinases have been shown as candidates to interact with p53 and to phosphorylate p53 at Ser46, homeodomain-interacting protein kinase 2 (HIPK2) is one of them (Hofmann, Möller et al. 2002), others include p38 (Bulavin, Saito et al. 1999), protein kinase Cδ (PKCδ) (Yoshida, Liu et al. 2006), p53-dependent damage-inducible nuclear protein 1 (p53DINP1) (Okamura, Arakawa et al. 2001) and dual specificity tyrosine-phosphorylation-regulated kinase 2 (DYRK2) (Taira, Nihira et al. 2007). ATM and ATR are thought to signal upstream of p53ser46 phosphorylation (via XIAP-associated factor 1 (XAF1) (Lee, Han et al. 2014)) where they phosphorylate seven in absentia homologue 1 (SIAH1), an E3 ubiquitin ligase, at Ser19. This modification disrupts the HIPK2–SIAH1 complex to stabilize HIPK2 (Winter, Sombroek et al. 2008) and allows its association with promyelocytic leukemia protein (PML; a potent pro-apoptotic tumor suppressor), p300, CREB-binding protein (CBP) and p53 in nuclear PML bodies, with the effect for the upregulation of pro-apoptotic p53 targets (Guo, Salomoni et al. 2000, Conrad, Polonio-Vallon et al. 2016).

The dephosphorylation of p53 is believed to be dependent upon the p53-induced phosphatase WIP1 (Guo, Salomoni et al. 2000). Therefore, it may exists opposing feedbacks of p53 (Ser46) phosphorylation and dephosphorylation. An imbalance for HIPK2 stabilization, perhaps initiated by high and/or persistent levels of activated ATM and/or ATR (in situations of high levels of damage) may switch the cell to apoptosis. Nonetheless, it needs further study to understand how the cell fate decision is made between survival and death following DNA damage response.

2.4 HIPK2 and its function

2.4.1 Homeodomain-interacting protein kinase 2 (HIPK2) and diseases

Homeodomain-interacting protein kinase 2 (HIPK2) was discovered in 1998. It acts as a serine/threonine protein kinase and located in the nucleus (Kim, Choi et al. 1998). HIPK2 belongs to the HIPK family, HIPK family is involved in the occurrence of cancer and fibrosis.

HIPK2 is a tumor suppressor gene, mainly because it is activates by DNA damage repair, induces apoptosis and regulates cell proliferation. It is reported that HIPK2 lacking mice are more susceptible to chemical carcinogenesis of the skin (Wei, Ku et al. 2007). HIPK2 is proved to be down-regulated in breast and colon cancers (Pierantoni, Bulfone et al. 2002). HIPK2 is also involved in signaling pathways critical for the induction of renal and pulmonary fibrosis, such as TGF-β/SMAD3, WNT, Notch and p53.

2.4.2 Modification and regulation of HIPK2

The post-translational modification mechanism (PTM) of HIPK2 is a fast, sensitive, and versatile mechanism for regulating protein function and properties. They involve chemical factors such as acetylation, phosphorylation or biological factors such as small ubiquitin-like modifications (SUMO) and ubiquitin (de la Vega, Grishina et al. 2012). In addition, the increase in reactive oxygen species (ROS) contributes to HIPK2 deSUMOlyation and initiates its acetylation.

Three E3 ubiquitin ligases, WSB-1, Siah-1 and Siah-2, regulate HIPK2 at the protein level (Choi, Seo et al. 2008, Winter, Sombroek et al. 2008). HIPK2 binds to SIAH-1 in its C-terminal region, and multiple lysine residues may be ubiquitination targets (Winter, Sombroek et al. 2008). In addition to this, in the normal state and overexpression of HIPK2, it will co-localize in nuclear bodies (NB) with Siah-1, indicating that ubiquitination of HIPK2 may occur in inclusion bodies within the nucleus. Similarly, WSB-1 also bins HIPK2 and forms a complex, which triggers ubiquitination and degradation of HIPK2, whereas WSB-1 mediated HIPK2 degradation can be completely prevented by the DNA damaging agents doxorubicin and cisplatin. This explains why HIPK2 remains stable in the case of DNA damage. Reducing the expression of endogenous Siah-1, Siah-2 or WSB-1 may prolong the half-life of HIPK2 (Choi, Seo et al. 2008, Winter, Sombroek et al. 2008).

HIPK2 can be acetylated by CBP (CREB-binding protein), but not by PCAF (P300/CBP-associated factor). It cannot be acetylated by CPB without catalytic activity. Acetylated HIPK2 is primarily localized to the cytoplasm, and acetylation of HIPK2 does not interfere with its kinase activity. It has been reported that HIPK2 is recruited to PML-NBs where it localizes together with p53 and CBP(Hofmann, Möller et al. 2002).

There is also a SUMO modification in HIPK2. Like ubiquitination, SUMO reacts with any three of the amino groups of lysine residues by a cascade of enzymes, allowing SUMO to covalently bind to HIPK2. The SUMO site of mouse HIPK2 is Lys1189, and the SUMO site of human HIPK2 is Lys25. The interaction of HIPK2 with SUMO protein is critical for its precise localization, p53 activation and apoptosis (Sung, Lee et al. 2011). SUMOlyation keeps HIPK2 in the nuclear speckle (de la Vega, Fröbius et al. 2011). SUMOylation is a highly dynamic process, meanwhile, the binding of SUMO to HIPK2 is easily reversed by SUMT-specific proteases (SENPs). In addition, an increase in the concentration of active oxygen contributes to HIPK2 deSUMOlyation (de la Vega, Fröbius et al. 2011).

Although different modifications like SUMOylation, ubiquitination, acetylation, caspase cleavage, and interaction with scaffold proteins regulate HIPK2 activity (Sombroek and Hofmann 2009, de la Vega, Grishina et al. 2012), there is no uniform explanation for the catalytic activity of HIPK2. It has been found that the active ring Y354 of HIPK2 is phosphorylated in different cells, thereby making HIPK2 catalytically active. The catalytically active HIPK2 further phosphorylates the Ser/Thr site of the downstream target protein. The study found that HIPK2-Y354 phosphorylation is an autocatalytic process (Siepi, Gatti et al. 2013).

2.4.3 HIPK2 regulates the activity of p53

When cells are damaged, p53 protects the body by cell cycle arrest, senescence, DNA repair, differentiation and apoptosis, it promotes the repair, survival or clearance of damaged cells. It is the most important tumor suppressor gene known until now (Hofseth, Hussain et al. 2004).

It is shown that HIPK2 phosphorylates p53 at Ser46 in DNA damage response and provokes apoptosis (Hofmann, Möller et al. 2002). It was found that HPK2, p53, CBP (CREB-binding protein) and PML (promyelocytic leukemia), especially PML3, can bind to each other and localize to PML nuclear bodies (PMLNBs). HPK2 is stablized by ultraviolet (UV) irradiation to selectively phosphorylate serine (ser) at position 46 of p53, accelerates CBP acetylation of lysine at position 382 of p53, thereby enhancing p53 function. Blocking the HPK2 function attenuates UV-induced apoptosis level (D'Orazi, Cecchinelli et al. 2002, Hofmann, Möller et al. 2002). Low concentration of nitric oxide selectively blocked the phosphorylation of p53 at position 46, which reduced apoptosis in a p53 wild-type human colon tumor cell line following treatment with UV-light (Fukunaga-Takenaka, Fukunaga et al. 2003). It was also found that NK-3 homology domain transcription factor, HIPK2 and the co-suppressor Groucho are able to bind to each other. Groucho deacetylates the histones of the NK-3 target gene promoter by recruiting histone deacetylase HDAC1 and mSin3A,

thereby blocking transcription (Choi, Kim et al. 1999). HIPK2 also regulates the co-inhibitory activity of Groucho. In the absence of Groucho, HIPK2 can enhance the inhibitory activity of GAL-NK3, while in the presence of Groucho, HPK2 seems to attenuate the co-inhibitory activity of Groucho. HIPK2 can abrogate the transcriptional repression of p53 on the target gene collagenase and MDR1, while TSA blocking HDAC can reverse the transcriptional downregulation of p53 (Kim, Park et al. 2002).

In addition to phosphorylation of p53, overexpression of HPK2 also down-regulates the protein expression level of MDM2, which abolished the antagonism of MDM2 on p53, but had no effect on the transcription of MDM2 (Wang, Debatin et al. 2001, Di Stefano, Blandino et al. 2004).

Although there is already some understanding of HPK2, there are still many aspects that need further elucidation. Thus, although HIPK2 is highly conserved and phosphorylation of human p53 at position 46 serine plays an important role, it is striking that mouse p53 has no human corresponding 46-position serine. HIPK2 has at least four alternative splicing sites that are expressed in specific cells. What is their biological significance? Tumors generally have low expression of HIPK2, but individual tumors express HIPK2 at a high level. What is the difference and is there a physiological relevance behind? Are there relevant mutations in HIPK2 protein? Further research is necessary to identify HIPK2 as a potentional target for cancer therapy.

2.5 Aims of the study

A key question in understanding the mechanism of TMZ (and other methylating anticancer drugs) is how the small DNA damage O^6-MeG triggers cell death. Although there is evidence that O^6-MeG lesions induced by TMZ are converted into DSBs in a replication and mismatch repair (MMR) dependent way (Ochs and Kaina 2000, Roos, Baumgartner et al. 2004, Quiros, Roos et al. 2010, Happold, Roth et al. 2012), the cellular responses triggered by this tumor suppressor are crucial in understanding how glioblastoma cells respond to therapy.

It has been shown in cells exposed to ultraviolet light (D'Orazi, Cecchinelli et al. 2002, Winter, Sombroek et al. 2008), ionizing radiation (Dauth, Krüger et al. 2007), adriamycin and doxorubicin (Bitomsky, Conrad et al. 2013) and cisplatin (Di Stefano, Blandino et al. 2004) that p53Ser46 is a substrate of HIPK2 kinase, which can stimulate cell death. Since the reference studies referred to above were not done in glioblastoma cells, no conclusion can be drawn yet whether this also holds true in glioblastomas. Thus, it is unknown whether this pathway can be activated by alkylating agents like TMZ and nitrosoureas, which are used first and second-line in glioblastoma therapy. In addition, the question of whether HIKP2 stimulates p53

pro-apoptotic functions in glioblastoma cells has not been addressed yet. Since alkylating agents are not only being used for brain cancer therapy, the data are expected to bear implications also for other tumor entities treated with such drugs.

In summary, the following questions were addressed in this work:

1) Are there thresholds in the activation of TMZ-induced apoptosis and senescence?

2) Are there thresholds in the dose-response in the induction of DSBs following treatment with TMZ in glioblastoma cells?

3) Has downregulation of HIPK2 an effect on TMU and CCNU-induced cell death by apoptosis?

4) Is apoptosis enhanced in HIPK2 downregulated glioblastoma cells?

5) How does p53 work together with HIPK in this process?

6) What downstream factors of p53 activate cell death after TMZ treatment?

7) Are SIAH1 and SIAH2 involved in these processes?

3 Material and methods

3.1 Cell lines

The glioblastoma cell lines employed in this study are of human origin: the glioblastoma cell lines LN229 was from American Type Culture Collection (ATCC), LN229MGMT is LN229 cells with stable MGMT transfection, LN229 DN-FADD is LN229 cells with stable dominate negative FADD transfection. The human glioblastoma line LN308 was a generous gift from Prof. Dr. M. Weller (Laboratory of Molecular Neurooncology, University of Zurich, Switzerland) to Prof. Kaina. Two mouse embryonic fibroblast cells (MEF) and MEF SIAH1&2 knockout cells were kindly provided by Andreas Möller (QIMR Gerghofer, Australia).

3.2 Cell culture and preservation

3.2.1 LN229, LN308, MEF and MEF SIAH1&2 knockout cells culture

The human glioblastoma cells LN229 and LN308 were seeded onto cell culture dishes in Dulbecco's Modified Eagle Medium (DMEM) (Gibco, Life Technologies Corporation, Paisley, UK). The DMEM was supplemented with 10% FBS (Gibco, Life Technologies Corporation, Paisley, UK) and penicillin/streptomycin (PAA Laboratories, GmbH, Cölbe, Germany). Cells were cultured in an incubator with 5% CO_2, 37°C saturated humidity. Cells were passaged according to their proliferation rates specifically. 0.05% trypsin-EDTA (Sigma-Aldrich, Steinheim, Germany) was used for detaching the cells. Every two months the mycoplasma test was performed. Mouse embryonal fibroblasts (MEF) and MEF SIAH1&2 knockout cells were cultured in the same way as LN229 and LN308.

3.2.2 LN229MGMT and LN229 DN-FADD cell culture

The LN229 cells stably overexpressing MGMT (LN229MGMT) has been established in our group previously (Quiros, Roos et al. 2011). The LN229 DN-FADD cells were also generated in our group previously. For the generation of LN229 cells that stably overexpressing a dominant-negative form of FADD (DN-FADD), LN229 cells were transfected with the plasmid pcDNA3-DN-FADD (Tewari and Dixit 1995) using the Effecting transfection reagent (Qiagen, Hilden, Germany). G418-resistant clones were picked, expanded and tested for MGMT expression by Western blot. Positive clones were cultured in DMEM medium containing G418

(Sigma-Aldrich, Munich, Germany), which was omitted during the experiments process.

LN229MGMT and LN229 DN-FADD cells cultured in DMEM supplemented with 10% fetal bovine serum). Cells were cultured in an incubator with 5% CO_2, 37°C saturated humidity. When cells were passaged, G418 was added into new dishes to select the stably transfected cells, the final concentration of G418 in DMEM was 1.5mg/ml. Every two months the mycoplasma test was performed.

3.2.3 Cell cryopreservation

For the cryopreservation of cells, cells were suspended in 92.5% full DMEM medium with 7.5% dimethylsulfoxide (DMSO) and transferred into cryo-tubes, these tubes were moved into a passive freeze container filled with isopropanol and placed at -80°C overnight. Cells were then transferred into a liquid nitrogen tank for longer preservation.

3.3 Cell treatments

3.3.1 *O*^{6}-benzylguanine (*O*^{6}-BG) and TMZ treatments

The MGMT inhibitor *O*^{6}-benzylguanine (*O*^{6}-BG, Sigma-Aldrich, Steinheim, Germany) was dissolved in DMSO at a stock concentration of 10 mM, aliquoted and stored at -20^{o}C. To inactivate all residual MGMT, one hour before the addition of TMZ or CCNU, O^6-BG was added to the medium of LN229. The final concentration of O^6-BG in DMEM was 10 µM.

TMZ (from Dr. Geoff Margison, The University of Manchester, UK) stocks were dissolved in dimethyl sulfoxide (DMSO, Carl Roth GmbH, Karlsruhe, Germany), diluted in approximately two parts sterile dH_2O to a concentration of 35 mM, aliquoted and stored at -80^{o}C until use. The stock was thawed and sonicated for 10 seconds to dissolve any TMZ precipitate before use. Cells were exposed to TMZ at different concentrations by adding the drug to the medium.

3.3.2 CCNU treatment

CCNU (lomustine, Sigma-Aldrich, Steinheim, Germany) was dissolved in pure ethanol to a stock concentration of 10 mM, aliquoted and stored at -80^{o}C. When treated with 30 µM CCNU, 30 µl of CCNU stock solution was added once into 10 ml DMEM.

3.3.3 RI-1 treatment

The Rad51 inhibitor RI-1 (Sigma-Aldrich, Steinheim, Germany) was dissolved in the DMSO to get a 25 mM stock solution and stored in -80 °C. Ri-1 was added two hours after TMZ treatment. For 5 μM RI-1 treatment: 1μl Ri-1 stock solution was added once into 5 ml DMEM.

3.3.4 Pifithrin-α treatment

The p53 inhibitor pifithrin-α (Sigma-Aldrich, Steinheim, Germany) was dissolved in the DMSO to a final stock solution of 30 mM, aliquoted and stored at -80 °C. For the inhibition of p53, pifithrin-α (20 μM) was added to the medium 24h after TMZ exposure.

3.4 Cell seeding and growth

Cells were seeded 24 h to settle down before any treatment, to get ready for knockdown and treatments. According to the cell growing rate observed in my experiments, in order to get enough cell for further test and at the same time keep the cells in plates from overfull, the average seeding number and growing time were as follows:

Growing time (h)	Cell seeding number in a 10 cm dish	Cell seeding number in a 6 cm dish
0	1500000	500000
24	500000	300000
48	300000	200000
72	200000	100000
96	150000	60000
120	100000	40000
144	80000	20000

3.5 HIPK2, SIAH1 and SIAH2 knockdown

A certain number of cells was seeded according to different treatments time as described in 3.4. When cells were 60% confluence, the medium was changed according to the transfection

system before knockdown. Lipofectamine® RNAimax Reagent (ThermoFisher Scientific, Darmstadt, Germany) was diluted in Opti-MEM® Medium (Gibco, Life Technologies Corporation, Paisley, UK) and mixed gently, HIPK2 siRNAs were diluted in the same way. Diluted HIPK2 siRNAs were added into diluted reagent at 1:1 ratio, incubated at the room temperature for 5 minutes, then the mixture of siRNA and Opti-MEM® Medium was added to cell culture dishes carefully. RNase free tips were used for all steps during the knockdown. For RNAi mediated knockdown of HIPK2, siRNAs with the following sequences were used: siHIPK2-1 (5'-CCAGGTGAACATGACGACAGA-3') and siHIPK2-2 (AAGCGTCGGGTGAATATGTAT) were from QIAGEN (Hilden, Germany). For knockdown of SIAH1 and SIAH2, siRNAs for SIAH1 were from Dharmacon (Lafayette, USA) custom siRNA (GATAGGAACACGCAAGCAA) and SIAH2 siRNA was from Dharmacon siGenome SMARTpool. The negative control siRNA was from QIAGEN.

3.6 Apoptosis/ necrosis detection by flow cytometry using Annexin V/PI double-staining

For the determination of apoptosis induced by TMZ or CCNU in LN229, LN229MGMT, LN308, LN229DN-FADD and MEFs knocked out for SIAH1&2, the annexin V/propidium iodide (PI) assay with flow cytometry analysis was used. Annexin V is a phospholipid-binding protein, itt binds to the membrane of early apoptotic cells. Membrane phosphatidylserine (PS) flips from the inside of the membrane of plasma to the outside when apoptosis occurs in the cell. Annexin V has a high affinity for phosphatidylserine since the onset of phosphatidylserine valgus occurs earlier than changes in the nucleus at the onset of apoptosis, apoptotic cells can be detected earlier using Annexin V compared to DNA fragmentation assays. Phosphatidylserine valgus also occurs during cell necrosis, Annexin V is often used in combination with a nucleic acid dye (for example PI) to tell apoptotic cells and necrotic cells.

Following knockdown of either HIPK2, SIAH1 and/or SIAH2, TMZ or CCNU exposure and incubation time, the cells in the supernatant were collected in a 15 ml tube. The supernatant samples were washed twice with PBS and digested with trypsin, the digested cells were transferred to the tube which contains the supernatant from the same sample, centrifuged at 1000 r/min for 4 minutes, then PBS washing step and centrifugation were applied once again, the supernatants were discarded. 50 µl 1x binding buffer and 2.5 µl Annexin V/FITC (Miltenyi Biotec GmbH, Bergisch Gladbach, Germany) were added to every sample, 15 min incubation in the dark and on ice, 430 µl 1x binding buffer and 1 µg/ml PI (Sigma-Aldrich, Steinheim, Germany) were added to the cells. Data acquisition was done by using a FACS Canto II flow cytometer (Becton Dickinson GmbH, Heidelberg, Germany). Annexin V positive cells were

classified as apoptotic while annexin V and PI double-positive cells were classified as necrotic/late-apoptotic. The raw data were analyzed with the BD FACSDiva software.

Annexin V Binding Buffer was prepared as a 10-fold concentration solution, stored at 4 °C. It was diluted at a 1:10 ratio with distilled water before use. The 10-fold Annexin V Binding Buffer was made according to this recipe: 100 μM Hepes, 1.4 M NaCl, 25 $CaCl_2$, 1% BSA.

3.7 Colony formation assay

Colony formation assay is to test if a cancer therapy drug or method is able to help reduce the colony formation of tumor cells, or the efficiency of cytotoxic agents (Franken, Rodermond et al. 2006). LN229 cells were cultured in DMEM with 10% FBS. Before seeding, the medium was discarded and the dishes were rinsed with PBS. 1 ml trypsin-EDTA was added to a 10 cm dish (or 0.5 ml trypsin-EDTA was added to a 6 cm dish) for detaching the cells. After 1-3 min, 5-10 ml medium with 10% FBS was added according to the confluence of the cells, and the clumps were broken up by pipetting carefully, then the medium with cells was transferred to a sterile 15 ml tube. All cell masses were disseminated into individual cells by pipetting again, the cell number was counted by using a hemocytometer, and diluted to the desired concentration. Serial dilutions with different numbers of cells were prepared according to the increasing concentrations of TMZ or CCNU. LN229 cells were seeded in 6 cm dishes and distributed evenly at appropriate cell numbers to form approximately 100 surviving colonies after TMZ or CCNU exposure, the dishes were marked with cell type, treatment, cell number and date, and were put into the CO_2 incubator at 37 °C to let the cells settle down.

After 2-3 weeks, the colonies were checked with a microscope, the assay was stopped when most of the colonies in the untreated sample contains more than 50 cells. Cell medium was removed, and the assay was stopped by adding fixation solution (Acetic acid: Methanol: Distilled water=1:1:8) for 1 h, the fix solution was discarded and the dishes were allowed to dry thoroughly. The samples were stained with colony satin solution (1.25% Giemsa, 0.125% crystal violet) for 1 h. The dishes were washed softly with flowing water to remove the residual dye and were left open until dry. The colony numbers were counted and the plating efficiency and surviving fractions were calculated by the following formulas: Plating efficiency = number of colonies formed in the control sample/ number of cells seeded in the control sample x 100% Surviving fraction = number of colonies after treatment/ number of cells seeded x PE. Colonies containing more than 50 cells were scored, colony numbers were adjusted for the cell line's plating efficiency and the surviving fractions were plotted on the graphs.

3.8 Protein detection and analysis

3.8.1 Whole-cell protein extracts

The samples were harvested on ice with pre-cooled buffer to prevent protein degradation. The medium for cell culture was removed, cells were washed with PBS twice after PBS was thoroughly removed, 300-600ul RIPA buffer was added to every sample, accordingly, attached cells were scraped off and transferred to pre-cooled tubes, vortexed and put on ice. Sonication was employed to help to break cells (3x10 pulses), then the samples were centrifuged 10 minutes at 4 °C, 14000rpm, the supernatant in a tube was protein extracts. The protein concentration was determined by Bradford. The RIPA buffer recipe is:

RIPA buffer: 50 mM Tris (pH 8), 150 mM NaCl, 1 mM EDTA，1% NP-40, 0.5% sodium deoxycholate, 0.1% SDS, store at 4 °C. Before use, take 835μl RIPA buffer stock, add freshly PMSF 100mM stock 10 μl, Na_3VO_4 200 mM stock 10 μl, DTT 1 M stock 2 μl, 7x protease inhibitor 142.9 μl to get a 1 ml full RIPA buffer.

3.8.2 Membrane extracts

For FAS-R detection, the membrane proteins extracts were employed.

3.8.2.1 Preparation of cell pellets

For every sample, 5x10 cm^2 semi-confluent culture dishes were prepared in order to obtain enough protein. After rinsing with PBS, the cells were harvested with trypsin-EDTA, transferred to15 ml tubes and centrifuged at 1000 rpm for 4 min. Supernatant of samples were removed, pelleted cells were suspended in 1 ml cold PBS and transferred to a 1.5 ml Eppendorf. PBS was removed after centrifuging at 4000 rpm for 5 min. The cell pellets can be flash frozen with liquid nitrogen and stored at -80 °C till needed.

3.8.2.2 Protein extracts

Thawed cell pellets were suspended in 50-200 μl fractionation butter A, depending on pellet size. Cells were lysed by freeze-thaw-vortex circle: first the cells suspension was frozen in liquid nitrogen, then it was heated to 37 °C, as soon as it thawed, the suspension was vortexed for 5 seconds and put back into liquid nitrogen, the process was repeated three times. The lysate was centrifuged at 700 g (4 °C) for 10 min. The pellet (Pellet I) contained the nuclei, while the supernatant contained the cytoplasmic proteins and mitochondria and membranes. The supernatant was transferred to a new Eppendorf cap and centrifuged at 700 g for 10 min at 4 °C. The pellet (Pellet II) contained the mitochondria and membranes, while the

supernatant contains the cytoplasmic proteins. Pellet II, containing the mitochondria and membranes, was suspended in 20-50 µl Fractionation butter B depending on pellet size. Pellet I, containing the nuclei and cell fragments, was suspended in 50-100 µl Fractionation butter C depending on pellet size. Sonication was used to homogenize the suspension. The samples were centrifuged for 10 min at 10 000 rpm. The supernatant contained the nuclear proteins and the pellet (Pellet III) contains the membrane fragments. The supernatant that contains the nuclear protein fraction was transferred to a new Eppendorf cap. Pellet III (membrane pellet) was suspended in Fractionation buffer B and combined with a suspension of pellet II for having all the membrane proteins. Protein concentrations of samples were determined by the Bradford method (Bradford 1976).

The fractionation butter recipes were as follows:

Fractionation butter A	10 mM Hepes-KOH pH 7.4 1 mM EGTA 0.1 mM EDTA 250 mM sucrose 1 µM Na_3VO_4 0.5 mM PMSF 10 mM DTT The Na_3VO_4, PMSF and DTT were added freshly before use.
Fractionation buffer B	20 mM Tris 1 mM EDTA 1 mM beta-Mercaptoethanol 5% Glycerin pH 8.5 with HCl 1% Triton X-100 0.5 mM PMSF The PMFS and 1% Triton X-100 were added from stocks to the buffer just before use
Fractionation buffer C	20 mM Tris 1 mM EDTA 1 mM beta-Mercaptoethanol 5% Glycerin pH 8.5 with HCl 1 µM Na_3VO_4 0.5 mM PMSF 10 mM DTT The Na_3VO_4, PMSF and DTT were added freshly before use.

3.8.3 Protein concentrations determination with the Bradford method

Bradford assay was developed by Marion McKinley Bradford to determine the protein concentration. This method ueses the spectroscopy absorption shift of Coomassie Brilliant Blue G250. The maximum absorption of unbound Coomassie Brilliant Blue G250 is at 465nm when it's bound to the protein, the maximum absorption changes to 595 nm.

To set the standard curve with different BSA concentrations (0, 0.5, 1, 2, 3, 4 and 5 µg/µl), the protein samples to be tested were prepared in two different dilutions: one 1:1 dilution, the other 1:10 dilution. The standard BSA samples were loaded into a 96-well plate (the top or bottom was avoided touching with fingers, because stains on the plate may affect the assay results), with three replicates per well for every concentration. The tested samples were added to the

alternative areas in the same plate, three replicates per sample for both 1:1 and 1:10 dilutions. The plate was protected from light, 200 µl of the Bradford assay reagent (8.5 % phosphoric acid, 4.75 % ethanol, 0.01% Coomassie Brilliant Blue G250) were added per well, after 10 minutes incubation in the dark, fluorescence intensities were measured at absorption 595 nm.

Data analysis: The standard curve was drawn depending on 0-5 µg/µl BSA concentrations. The samples' data was compared with the standard BSA curve, the appropriate dilution was chosen (if the sample's fluorescence intensity value was higher than the maximal BSA value, then choose the 1:10 dilution values), and samples' concentrations were calculated accordingly.

3.8.4 Western blot

Western blot is the protein detection technique that transfers proteins from the gel to the NC membrane or PVDF membrane after the electrophoresis, information on the expression of specific proteins in the cells or tissues analyzed is obtained by analyzing the position and depth of the coloration. Before the experiment, SDS gels were prepared according to the following:

Separating gels for 1 mm glass plates (x2)

Separating Gel	15%	12%	10%	7.5%	5%
dH_2O	4.3 ml	5.1 ml	5.7 ml	6.5 ml	7.2 ml
Tris 1.5M (pH8.8)	3 ml	3 ml	3 ml	3 ml	3 ml
SDS 20%	60 µl	60 µl	60 µl	60 µl	60 µl
(Bis-) Acrylamide 40% (37.5:1)	4.5 ml	3.6 ml	3 ml	2.3 ml	1.5 ml
TEMED (Tetramethylethylenediamine)	6 µl	6 µl	6 µl	6 µl	6 µl
APS (Ammonium persulphate) 10%	60 µl	60 µl	60 µl	60 µl	60 µl

Separating gels for 1.5 mm glass plates (x2)

Separating Gel	15%	12%	10%	7.5%	5%
dH_2O	6.45 ml	7.65 ml	8.55 ml	9.75 ml	10.8 ml
Tris 1.5 M (pH 8.8)	4.5 ml	4.5 ml	4.5 ml	4.5 ml	4.5 ml
SDS 20%	90 µl	90 µl	90 µl	90 µl	90 µl
(Bis-) Acrylamide 40% (37.5:1)	6.75 ml	5.4 ml	4.5 ml	3.45 ml	2.25 ml
TEMED	9 µl	9 µl	9 µl	9 µl	9 µl
APS 10%	90 µl	90 µl	90 µl	90 µl	90 µl

For separating gels, the ingredients were inverted gently 2-3 times before adding TEMED and APS. The liquid was poured immediately into the caster, sealed with 1ml isopropanol until polymerized (about 30-45 min). The gels were rinsed with dH_2O 5 times after pouring off isopropanol.

Stacking Gels:

Stacking Gel	for 1.5 mm glass plates	For 1 mm glass plates
dH_2O	4.95 ml	3.3 ml
Tris 1.5 M, pH 8.8	855 µl	570 µl
SDS 20%	67.5 µl	45 µl
(Bis-) Acrylamide 40% (37.5:1)	855 µl	570 µl
TEMED	6.75 µl	4.5 µl
APS 10%	67.5 µl	45 µl

For stacking gels, the ingredients were inverted gently 2-3 times before adding TEMED and APS. Afterwards, combs were inserted carefully, and gels were left to polymerize (around 5 min). Gels were placed to the electrophoresis chamber and pressed tightly until no gap between the gels and the plastic board. SDS-PAGE electrode buffer was poured into the tank, combs were removed and every well was washed with the buffer. Samples (usually 30 µg samples per well) were loaded avoiding any leakage and mixing. Protein marker (VWR, Darmstadt, Germany) was loaded before samples to show protein sizes.

In order to activate the positive groups on the membrane, the membrane was cut to the size of the gel and immersed into 1xblotting buffer 30 min before the SDS-PAGE gel finish. The upper gel part was discarded, the activated membrane was handled with tweezers, gel and membrane were pressed together (gel was put next to the negative electrode and membrane next to the positive electrode) and transferred with 100 mA electric current constantly overnight. The membrane was washed with TBST, then blocked with milk-TBST (5%) or BSA-TBST (5%) for 1 h. After blocking, the memberane was incubated in primary antibody overnight at 4 °C, then washed 3 times with TBST, and incubated with secondary antibody at room temperature for 3 h in the dark.

The antibodies were used are: Anti-β-actin, anti-HSP90, anti-p53, anti-FAS, anti-BAX, all from Santa Cruz Biotechnology (Heidelberg, Germany), anti-phospho-p53 (Ser15), anti-phospho-p53 (Ser46), anti-PTEN, anti-PUMA all from Cell Signalling Technology (Frankfurt, Germany), anti-NOXA and anti-FADD from Calbiochem (Merck/Millipore, Billerica, USA), anti-MGMT from Chemicon International Inc. and anti-HIPK2, which are privately-produced antibodies already reported on (Winter, Sombroek et al. 2008). Proteins were detected by the Odyssey 9120 Infrared Imaging System (Li-Cor Biosciences, Lincoln, Nebraska, USA).

The membrane was dried in the dark and scanned with the Odyssey system.

The SDS-PAGE electrode buffer and blotting buffer were prepared with the following recipes:

SDS-PAGE electrode buffer	200 ml 5x Laemmli stock 5 ml 20% SDS 1 L total volume with dH_2O
1xblotting buffer	100 ml Laemmli stock (5x) 200 ml Methanol 700 ml distilled water

3.9 Autophagy detection

Autophagy is a process for cells to break down its own cytoplasmic proteins or organelles, forming autophagy lysosomes, to degrade the contents within, and help cell metabolism and renew certain organelles. Cyto-ID kit (ENZO life sciences, Lörrach, Germany) was used in this test. Before the assay, the reagents were diluted. 1 µl Cyto-ID dye was diluted in 1 ml DMEM (without phenol red) containing 5% FBS. 1 ml 10x Assay buffer was added into 9 ml ddH_2O. The cells were seeded in 6 cm dishes at proper concentrations to prevent confluence when harvesting.

When the assay started, the supernatant from one sample was transferred to a 15 ml tube, cells were rinsed with PBS, trypsinized with 1 ml Trypsin-EDTA and after 2 minutes 1 ml fresh medium was added to every dish to suspend the cells. The medium with cells was transferred in a 15 ml tube for centrifugation (250 g, 5 min). The supernatant was discarded, the pellet was suspended in 2 ml PBS. The supernatant was discarded after centrifugation (250 g, 5 min).

For staining of the cells, every cell pellet was suspended in 0.25 ml DMEM with 5% FBS without phenol red, each sample was added with 0.25 ml diluted Cyto-ID solution and after resuspension, the samples were incubated in the dark for 30 min at 37 °C. After centrifugation (1500 rpm, 5 min), the supernatant of samples was discarded, and every pellet was suspended in the 1 ml 1x Assay buffer. Samples were centrifuged at 1500 rpm for 5 min and suspended in 0.5 ml 1x Assay buffer, transferred into pre-cooled FACS tubes. FACS Canto was employed for the measurement. The data were analyzed using the BD FACSDiva software.

3.10 Analysis of DNA double-strand breaks

For quantification of DNA double-strand breaks, the γH2AX foci method was employed. The cells were seeded in 6 cm dishes. Coverslips were stored in 75% ethanol. Before seeding, coverslips were taken out and rinsed by PBS for 3 times to get rid of ethanol. Two coverslips

were put onto one 6 cm dish without any overlapping by sterilized tweezers. An appropriate concentration of cells was plated in the dishes, 24 h later, the samples were treated. When harvesting, the medium for cells was discarded, and the samples were washed with PBS twice. Fix solution (Methanol: Acetone=7:3, store at -20 °C) was added in the dishes and kept in room temperature for exactly 9 minutes. The fix solution was discarded, and samples were rinsed 3 times with PBS. PBS (2 ml) was added to every dish to keep the coverslips moist. One cover slip from every sample was put onto a 3 cm dish (the cells side up), blocked with blocking buffer (5% BSA in PBS that contains 0.3% Triton X-100) for 1 h, the other coverslip was stored at 4 °C as a backup. The blocking buffer was removed, 50 µl of γH2AX antibody (1:1000 dilution of γH2AX in PBS that contains 0.3% Triton X-100) was added on the coverslip for overnight incubation at 4 °C. After 3 times PBS washing, 50 µl Alexa Fluor® 488 secondary antibody (rabbit green, 1:500 of Alexa Fluor® 488 in PBS that contains 0.3% Triton X-100) was added to the coverslip, and incubated at room temperature in the dark for 2 h. Three times of PBS washing was performed when the incubation finished. The secondary Alexa Fluor® 488 antibody was from LifeTechnologies, Carlsbad, USA. DAPI-Vectashield (Vector Laboratories, Burlingame, USA) solution (1.5 µl of 1 mg/ml DAPI was added in 1 ml Vectashield mounting medium, vortex thoroughly) was prepared freshly for staining. The object slides were marked with cell lines, treatments and date for every sample, 20 µl of the DAPI-Vectashield solution was dropped on the center of one slide, the coverslip was put on the DAPI-Vectashield solution (avoid any bubble) and sealed by nail varnish. The slides were kept in the dark for 10 minutes to let them dry. The γH2AX foci numbers were quantified using Metasystem finder version 3.1.

3.11 Senescence detection

Two methods were employed to determine the senescence ratio, one was C_{12}FDG staining, another X-gal staining was employed in experiments that had less than 8 samples. Pre-experiments showed that the results from the two methods are consistent with each other.

3.11.1 Senescence detection with C_{12}FDG staining

C_{12}FDG is a β-galactosidase substrate. When C_{12}FDG enters the cell, the substrate is cleaved by β-galactosidase and produces green fluorescence, which can be detected by FACS. Bafilomycin A1 inhibits vacuolar-type H+-ATPase, it blocks lysosomal acidification, also increases the pH of lysosomes (Bayer, Schober et al. 1998). Bafilomycin A1 (Sigma-Aldrich, Steinheim, Germany) was dissolved in pure DMSO to get a 0.1 mM stock solution, protected from light and stored at -20 °C. The working concentration was 100 nM (1 µl stock solution was

added to 1ml medium). C_{12}FDG (Sigma-Aldrich, Steinheim, Germany) was also dissolved in the DMSO to get a 20 mM stock solution, aliquoted, protected from light and stored at -20 ° C. The stock solution was diluted 1:10 with fresh medium to get a 2 mM working solution. Cells were seeded and treated 96 h before the detection. The cells were incubated for 1 h with 100 nM Bafilomycin A1, afterward, incubated for 2 h with 33 μM C_{12}FDG. All the procedures after C_{12}FDG incubation were operated avoiding light. The samples were rinsed 3 times with PBS, 30s per time, and harvested with trypsin-EDTA, suspended in DMEM with 10% FBS and the supernatant of the dish was added in the suspension. The cells were centrifuged at 4 °C, 100-250 g for 5 min. The pellet of every sample was suspended in 0.4-0.5 ml PBS (4°C) to get the final cell concentration of around $1x10^6$ /ml. Results were obtained by using the FACS Canto flow cytometer.

3.11.2 Senescence detection with X-gal staining

Cells were seeded in the 6-well plate, to get rid of the influence of contact inhibition, they were not confluent when harvesting. The Senescence Detection Kit (Abcam, Cambridge, UK) was employed. The 10x fixing solution (8.1 ml 37% formaldehyde, 0.6 ml 50% glutaraldehyde, 6 ml 25 x PBS, 0.3 ml distilled water, mixed and stored at -20 °C) was diluted 1:10 with distilled water before use. Plates were get out from the incubator, every well was washed with PBS twice, 1 ml diluted fixing solution was added to each well, after 5 min incubation, plates were washed with PBS twice and the plates could be stored at 4 °C in PBS covering the cells. The X-gal solution was prepared as follows: 20 mg X-gal were dissolved in 1 ml DMSO to prepare a 20x stock solution and stored at -20°C. While the cells were in the fixative solution, the staining solution mix was prepared in a polypropylene plastic tube, for every well to be stained, enough solution was prepared. For every well, the staining solution mix contained staining solution 470 μl, 5 μl staining supplement, 20 mg/ml X-gal in DMSO 25 μl. When staining, PBS was discarded and 1 ml staining solution was added to each well, samples were incubated at 37 °C overnight in an incubator without CO_2 (5–10% CO_2 in normal incubator makes the pH of the buffer lower thereby affects the color development). Positive blue cells and negative cells were quantified using an Axiover 35 light microscope from Zeiss.

3.12 Caspase activity assays

Mammalian caspases are divided into three groups: Caspase-2, -8, -9 and -10 are seen as initiator caspases, Caspase-3, -6 and -7 are executioner caspases, and Caspase-1, -4, -5, -11 and -12 are inflammatory caspases. The first two groups are responsible for the initiation and execution of apoptosis.

3.12.1 Caspase-3 activity assay

In this assay, the caspase-3 assay kit (Abcam, Cambridge, UK) was employed to determine the caspase-3 activity. Protease inhibitors in the sample preparation step were avoided. The substrate was strictly kept from light. Cells were treated with TMZ and harvested, 1-5 x 10^6 cells were pelleted and suspended in 50 µl of cooled Cell Lysis Buffer from the kit and the suspension was incubated on ice for 15 minutes. After 1 minute centrifugation at 10,000 x g, the supernatant (cytosolic extract) was transferred to a new tube and placed on ice. Protein concentrations were determined by the Bradford Assay. 100 µg of protein was diluted in 50 µl Lysis Buffer for each well, in a 96 well plate with a clear flat bottom. The DTT was added into 2x Reaction Buffer freshly to get a final concentration of 10 mM and each sample was added 50 µl of 2 x Reaction Buffer (containing 10 mM DTT). The DEVD-p-NA substrate (200 µM final concentration) was added into each well. Samples were incubated at 37 °C for 120 minutes and measured on a microplate reader at 400 nm. The summary of the caspase-3 activity assay is:

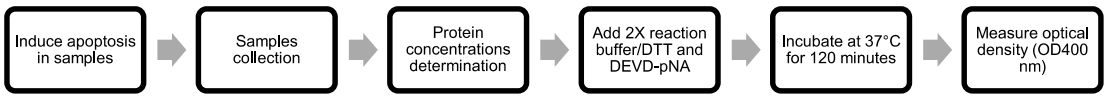

Figure 5 Workflow of caspase 3 activity test.

3.12.2 Caspase-8 and -9 activity assays

The procedures of caspase-8 and caspase-9 activity assays were basically the same as caspase-3 activity assay, the substrate of caspase-8 activity assay was IETD-pNA, and substrate of caspase-9 activity assay was LEHD- pNA. The kits for caspase-8 and -9 detections were from Abcam Cambridge, UK. For all the experiments, the substrates were protected from light.

3.13 RNA analysis

3.13.1 RNA extraction

Invitrogen™ TRIzol™ Reagent (ThermoFisher Scientific, Darmstadt, Germany) was employed to extract RNA. Samples were washed with PBS, each dish was added 1 ml TRIzol reagent by pipetting, after 5 minutes incubation, the cells were lysed, the mixture of cell lysates and TRIzol reagent was transferred into a DNase/RNase free tube and was kept on ice during the extraction steps. 0.2 ml Chloroform was added to every 1 ml TRIzol extract tube, the samples were shaken for 15 seconds by hand vigorously. After 3 minutes incubation in room temperature, they were centrifuged 12000x g for 15 minutes at 4 °C, RNA stays in the upper aqueous phase.

The extraction was done with Direct-zol™ RNA MiniPrep Kit (Zymo Research, Irvine, USA). A same volume of ethanol (95-100%) was mixed with every sample in RNA Lysis Buffer (1:1). Two volumes of the buffer/ethanol were added to an RNA sample. The mixture was transferred to the Zymo-Spin™ IIC Column in a collection tube and centrifuged for 30 seconds, the flow-through liquid was discarded, the column was loaded on a new collection tube. For each sample to be tested, a mixture of DNase I (5 µl) and DNA Digestion Buffer (75 µl) was prepared and added directly to the column matrix. After 15 minutes incubation at room temperature (20-30 °C), samples were centrifuged for 30 seconds. For each column, 400 µl Direct-zol RNA PreWash was added in, then centrifuged for 30 seconds, the step was repeated once. 700 µl RNA Wash Buffer was added to each column and centrifuge for 30 seconds. Columns were transferred carefully into RNase-free tubes. 50 µl DNase/RNase free water was added directly to each column matrix and centrifuge for 30 seconds. The eluted RNAs were ready for used or can be stored at -70 °C. The RNA concentrations of the samples were measured by NanoDrop™ 2000/2000c from ThermoFisher Scientific.

3.13.2 cDNA Synthesis

The Thermo Scientific Verso cDNA Kit (ThermoFisher Scientific, Waltham, MA, USA) was employed to generate high yields of full-length cDNA. Six ingredients were included: Verso™ Enzyme Mix, 5x cDNA Synthesis Buffer, Anchored Oligo dT primers, Random Hexamer, dNTP Mix and RT Enhancer. The reagents were thawed on ice, the reaction system is 20 µl in total (5x cDNA Synthesis Buffer 4 µl, dNTP Mix 2 µl, RT Enhancer 1 µl, Verso™ Enzyme Mix 1 µl, RNA Primer 1 µl, Template 1-5 µl, and nuclease-free water was added to make the final volume 20 µl). The cDNA synthesis was finished with T100™ Thermo cycle from BIO-RAD,

reverse transcription cycling program was set as 42 °C 60 min, 95 °C 2 min.

3.13.3 Real-time polymerase chain reaction (Real-Time PCR)

The real-time PCR is a method for detecting the quantitative relationship between the pre- and post-PCR products of the target, earlier detection of the specified fluorescence value indicates more target genomes. Before the real-time PCR, all synthesized cDNA samples were diluted to 5 ng/μl concentration, one reaction system was 20 μl (SYBR Green 10 μl, primer forward and reverse mix 1 μl, RNase free water 7 μl, cDNA 2 μl). The temperature cycles are 50 °C 2 min, 95 °C 10 min, (95 °C 10 s, 55 °C 20 s, 72 °C 20 s)-44 cycles, 95 °C 10 s, 65 °C 5 s, 95 °C 50 s. Every sample was done with 3 repeats, one internal control primer was prepared and run with the program at the same time to make the starting quantity of different samples equal.

These primers were used: *HIPK2*-up: 5'-AGGAAGAGTAAGCAGCACCAG-3', *HIPK2*-low: 5'-TGCTGATGGTGATGACACTGA-3'; *FAS*-up: 5'-TTATCTGATGTTGACTTGAGTAA-3', *FAS*-low: 5'-GGCTTCATTGACACCATT-3'; *PTEN*-up: 5'-TGCTAACGATCTCTTTGATGATG-3', *PTEN*-low: 5'-CTACCGCCAAGTCCAGAG-3'; *BBC3*-up: 5'-TTCAGTTTCTCATTGTTAC-3', *BBC3*-low: 5'-TAAGGATGGAAAGTGTAG-3'; *PMAIP1*-up: 5'-CCAACAGGAACACATTGAAT-3', *PMAIP1*-low: 5'-TCTTCGGTCACTACACAAC-3'; *BAX*-up: 5'-CAGAAGGCACTAATCAAG-3', *BAX*-low: 5'-ATCAGATGTGGTCTATAATG-3'; *ACTINB*-up: 5'- GCTACGAGCTGCCTGACG-3', *ACTINB*-low: 5'-GGCTGGAAGAGTGCCTCA-3';*GAPDH*-up: 5'-CCCCTCTGGAAAGCTGTGGCGTGAT-3', *GAPDH*-low: 5'-GGTGGAAGAGTCGGAGTTGCTGTTGA-3'.

The data were analyzed by the Bio-Rad CFX manager software, and results were shown in fold change compared with control samples.

3.14 Microarray dataset

A microarray dataset describing the differences in gene expression between samples obtained from 23 patients suffering from epilepsy, 42 patients suffering from grade II oligodendroglioma and astrocytoma, 31 patients suffering from grade III oligodendroglioma and astrocytoma and 81 patients suffering from grade IV glioblastoma was downloaded from ArrayExpress (https:/www.ebi.ac.uk/arrayexpress). This dataset, namely E-GEOD-4290, was reported on in (Sun, Hui et al. 2006). The intensity values for SIAH1 (NM_003031), SIAH2 (NM_005067) and HIPK2 (NM_022740) were extracted from the dataset and plotted in the graph.

3.15 Chromatin immunoprecipitation and promoter binding experiments (ChIP)

ChIP is used to study the interaction of DNA and protein in cells, specifically to determine whether a specific protein (such as a transcription factor) binds to a specific genomic region (such as a promoter or other DNA binding site), it is also used to identify specific sites on the genome that are associated with histone modifications.

Cells were added 1% formaldehyde for 10 min at room temperature for fixation, and the fixation was stopped by glycine (125 mM). Cells were lysed with lysis buffer (5 mM PIPES pH 8.0, 85 mM KCl, 0.5% NP40, 1 x protease inhibitor) for 10 min at 4 ℃. The nuclei were suspended in pre-cooled nuclear lysis buffer (50 mM Tris-HCl pH 8.0, 10 mM EDTA, 0.8% SDS, 1 x protease inhibitor) for 10 min on ice. Samples were sonicated (20 x 30 sec), lysates were centrifuged and the supernatants were collected and pre-cleaned by ChIP-Grade Protein G Magnetic Beads (Cell signaling technology, Danvers, MA, USA) in dilution buffer (10 mM Tris-HCl pH 8.0, 0.5 mM EGTA, 140 mM NaCl, 0.1% Na-deoxycholate, 1% Triton X-100, 1 x protease inhibitor) for 1 h at 4 ℃. The pre-cleaned lysates were aliquoted equally and incubated with the p-p53ser46 antibody (Becton Dickinson, USA) overnight at 4 ℃. Saturated protein G magnetic beads were added into each sample and incubated for 2 h at 4 ℃. The beads were washed with TSE I (10 mM Tris-HCl pH 8.0, 1 mM EDTA, 0.5 mM EGTA, 140 mM NaCl, 0.1% SDS, 1% Triton X-100), TSE II (20 mM Tris-HCl pH 8.0, 2 mM EDTA, 500 mM NaCl, 0.1% SDS, 1% Triton X-100), buffer LiCl (10 mM Tris-HCl pH 8.0, 1 mM EDTA, 0.25 M LiCl, 0.5% Na-deoxycholate, 0.5% NP40), and buffer TE (10 mM Tris-HCl pH 8.0, 1 mM EDTA), sequentially. The binding components were eluted in 1% SDS and 0.1 M $NaHCO_3$ and reverse cross-linkage was performed at 65 ℃ overnight. DNA was extracted using the PCR purification Kit (Qiagen, Hilden, Germany). Real-time PCR was employed to detect relative enrichment of the target protein in mRNA level. The primers used were *FAS-R* -up: 5'-TGAAGCGGAAGTCTGGGAAG-3', *FAS-R*-low: 5'-GACCTTTGGCTTGGCTTGTC-3'.

3.16 Immunofluorescence microscopy

LN229 and LN229 knockdown for HIPK2, for γH2AX foci, or LN229, for FAS-L expression, were plated onto glass microscope cover slips. Following exposure to 50 μM TMZ and either 120 h incubation for γH2AX foci or 72 h for FAS-L expression, cells were fixed in either ice cold (-20°C) methanol: acetone (7:3) for 9 min at -20°C for γH2AX foci or 1% formaldehyde for 30 min for FAS-L expression. The first antibodies used were anti-γH2AX (ser139, #9718s) from Cell Signalling Technology (Frankfurt, Germany) and anti-FAS-L (F37720) from Transduction

Labs. The second antibodies, coupled to Alexa Fluor® 488, were from Invitrogen (ThermoFisher Scientific, Darmstadt, Germany). DNA was counterstained with 1 µM TO-PRO-3 (Invitrogen, ThermoFisher Scientific, Darmstadt, Germany). Slides were mounted in Vectashield antifade mounting medium (Vector Laboratories, Burlingame, CA, USA). Microphotographs were got by laser scanning microscopy (LSM710, Carl Zeiss Micro Imaging).

3.17 Others

3.17.1 Chemicals and Consumables

If not stated otherwise, other chemicals that were used for this project were from Carl Roth GmbH & CoKG (Karlsruhe, Germany) or Sigma-Aldrich (Steinheim, Germany). Plasticware was bought from Greiner BioOne GmbH (Frickenhausen, Germany) and Eppendorf AG (Hamburg, Germany). Cell culture reagents were obtained from Gibco/ThermoFisherScientific (Waltham, MA, USA).

3.17.2 Antibodies list

Primary antibodies:

Name	Company	Product No.	Dilution	Host
p53ser46	Becton Dickinson	558245	1:1000	Mouse
p53ser15	Cell Signaling Technology	9284	1:1000	Rabbit
p53	Santa Cruz	sc-126	1:2000	Mouse
HIPK2	From Prof. Hofmann	Aa824	1:1000	Rabbit
NOXA	Merck Millipore	Op180	1:1000	Mouse
PUMA	Cell Signaling Technology	12450s(D30C10)	1:1000	Rabbit
BAX	Santa Cruz	Sc-7480	1:1000	Mouse
FAS-R	Santa Cruz	Sc-8009	1:1000	Mouse
MGMT	Sigma-Aldrich	HPA032136	1:1000	Rabbit

HSP90	Cell Signaling Technology	4874	1:1000	Rabbit
β-Actin	Abcam	Ab8227	1:2000	Rabbit
γH2AX (ser139)	Cell Signaling Technology	9718s	1:1000	Rabbit

Secondary antibodies:

Name	Company	Product No.	Dilution	Host
IRDye anti mouse IgG 800CW	LI-COR	926-32213	1:10000	Donkey
IRDye anti rabbit IgG 800CW	LI-COR	926-32212	1:10000	Donkey
IRDye anti mouse IgG 680RD	LI-COR	925-69072	1:10000	Donkey
IRDye anti rabbit IgG 680RD	LI-COR	926-68073	1:10000	Donkey

3.17.3 Equipments list

Function	Commercial name	Company/Supplier
CO_2 incubator	HeraCell	Thermo Fisher Scientific
Incubator without CO_2	Heraeus D6450	Thermo Fisher Scientific
Hepatocyte Counter	Tiefe depth profondeur 0.100 mm	Marinfeld
Digital circulating water bath	GFL water bath	Labotec Wiesbaden
Alcohol burner	IBS fireboy plus	Integra
Flow cytometer	FACS CANTO II	BD Biosciences
Centrifuge	Biofuge	Heraeus Instrument
Centrifuge 4 ℃	Refrigerated Microcentrifuge 5402	Eppendorf
Centrifuge for 96 well plate	Heraeus Megafuge1.0	Thermo Fisher Scientific
Centrifuge	Microcentrifuge Sprout	Heathrow Scientific
Membrane scanner/ Imaging system	Odyssey 9120	LI-COR

Electron microscopy	Axiovert 35	Carl Zeiss
Inverse microscope	Wilovert A	Hund, Germany
Analytical balance	Sartorius analytical	Sartorius
pH Meter	Hanna pH211 microprocessor pH meter	Sigma-Aldrich
magnetic stirrer	IKAMAG®-RCT	Sigma-Aldrich
Microwave	Micromaxx	Medion Micromaxx
Electrophoresis glasses	Mini PROTECAN® glasses 1.5 mm/1.0 mm	Bio-Rad
Heating block	Thermostat 5320	Eppendorf
Cell disruptor	Branson sonifier 250	Branson Ultrasonics
Laminar flow cabinet	Herasafe	Thermo Fisher Scientific
Laminar flow cabinet	Nuaire	NuAire
Pipetting boy	Pipet-Lite XLS	RAININ
Blotting chamber	TransBlot Cell	Bio-Rad
Shaker	Certomat TC2	Sartorius
PCR Amplifier	C1000 Thermal cycle	Bio-Rad
Ultra-low Temperature Freezer	Forma 900	Thermo Fisher Scientific
cDNA synthesizer	BioRad T100 Thermal cycle	Bio-Rad
Refrigerator	Premium NoFrost	Liebherr
Vortex	Vortex-Genie	Bender Hobein AG
Electrophoresis chamber	Tetra Vertical Electrophoresis Cell	Bio-Rad
Transfer chamber	Trans-blot cell	Bio-Rad
Freezer	ProfiLine 7082-577-00	Liebherr
Roller mixer	STUART SRT9	Sigma-Aldrich

Laser scanning microscope	LSM 710	Carl Zeiss
Microplate reader	TECAN sunrise microplate reader	TECAN
Metafar system	Axio imager M1	Carl Zeiss
RNA work space	CCI contamination control safety hood	Kahlden GmbH
Power bank	powerpac HC	Bio-Rad
Gel imaging system	InGenius syngene bio imaging	Syngene
Ultrasound water bath	Sonorex super RK 1034	Bandelin
Safety cabinet	Safety cabinet for storage	Dueperthal
RNA concentration determination	Nanodrop 2000	Thermo Fisher Scientific

3.17.4 Softwares

Name	Company/Supplier
Ascent Software Version 2.6	Thermo Fisher Scientific
Cell^A	Olympus Soft Imaging Solutions
CFX Manager software	Bio-Rad
BD FACSDIVA SOFTWARE	BD Biosciences
PRISM 6	Graphpad software
ImageJ V1.49	Wayne Rasband, http://imagej.nih.gov
Zen 2012 (blue edition)	Carl Zeiss
EndNote (Version 9.0.0)	Thomson Reuters
Flowing Software (Version 2.5.1)	Perttu Terho, http://www.flowingsoftware.com
Metasystem Finder V3.1	MetaSystems
Magellan V7.2	Tecan Diagnostics

3.18 Statistics

All experiments, including Western blots, were repeated at least two times, i.e. three independent experiments were performed. If not clarified specifically, data points show the means of at least three independent experiments, the standard deviation from mean was used as error bars. For comparison, two-way ANOVA was employed, the calculated *p*-values are displayed: *p*-value<0.05*, *p*-value<0.005**, *p*-value<0.001***, *p*-value<0.0001****. For statistical analysis and graph plotting GraphPad Prism software was used.

4 Results

4.1 Are there thresholds for the activation of the TMZ-induced DDR and glioblastoma cell death?

Temozolomide (TMZ) is an anti-cancer drug used in the treatment of glioblastoma multiforme. O^6-methylguanine (O^6-MeG) is one of the DNA adducts induced by TMZ. In MGMT depleted cells, O^6-MeG induce DSBs that trigger apoptosis via ATM, ATR, CHK1, CHK2, p53 or p73. As the dual function of p53 regulates both cell death and cell survival mechanisms, we focus in this part on the switch between p53 regulated apoptosis and DNA repair and try to find possible thresholds for the TMZ-induced DDR in glioblastoma cells.

4.1.1 Pro-survival and pro-death factors are induced by O^6-MeG

To determine whether p53, p-p53ser15 and/or p-p53ser46 are involved in the TMZ-induced DNA damage response (p-p53ser15 was considered as a pro-survival factor while p-p53ser46 a pro-death factor), the glioblastoma cell lines LN229 and LN229MGMT (LN229 with stable MGMT expression) were used. To inactivate any residual MGMT activity, LN229 cells were treated with O^6-BG 1 h before TMZ exposure. LN229 and LN229MGMT were exposed to different doses of TMZ (0 μM, 12.5 μM, 25 μM, 50 μM, 75 μM, 100 μM, 125 μM) and harvested at different time points (24 h and 72 h). Thereafter protein expression of p53, phosphorylation levels of p53ser15 and p53ser46 were detected by Western blot and quantified by Image J software.

The results showed that total p53 and p53ser15 protein levels went up with increasing TMZ doses after 24 h treatment in LN229 cells, while p53ser46 protein expression levels did not change. After 125 μM TMZ treatment, total p53 reached 3.7 times the protein expression of the control group (Figure 6 A), meaning that p53 accumulated upon the damage induced by TMZ. The expression levels of p-p53ser15 also increased with increasing dose of TMZ compared with control while they showed more increases than total p53 at the same dose of TMZ treatment. When p53ser15 reached 10.9 times expression level upon 125 μM TMZ treatment comparing with the control sample (Figure 6 A), the p-p53ser46 levels stayed the same as control at 24 h (Figure 6 A and Figure 6 E). This suggested that the pro-survival factor p-p53ser15 started work already at the early time point after TMZ treatment. Total p53 also started accumulation at the same time, pro-death factor p-p53ser46 was not provoked by TMZ induced damage after 24 h. LN229MGMT did not show any significant increase in p53,

p53ser15 or p53ser46, which proved when MGMT expresses, cells were protected and no further response occurred, the damage induced by TMZ in LN229 cells was due to the O^6-MeG lesion (Figure 6 B).

After 72 h TMZ treatment, LN229 cells showed sharply increasing signals of p53 and p-p53ser46 (Figure 6 C), p-p53ser15 also increased than control while the increases weren't as strong as p53 and p-p53ser46 (Figure 6 C and Figure 6 E and F). The total p53 accumulated 13.1 times protein level compared with control after 125 μM TMZ treatment (Figure 6 C). The pro-death factor p53ser46 reached 8.9 times to the expression level of untreated sample (Figure 6 C), p-p53ser15 expression level at 72 h also went up 5.2 times as control after TMZ treatment, when considering the time points 24 and 72 h together, p-p53ser15 expression level at 72 h (5.2 times of control) did not increase as obviously as 24 h (10.9 times of control) after TMZ treatment. Compared to LN229 cells, the expression levels of p53, p-p53ser15 and p-p53ser46 in LN229MGMT cells were attenuated (Figure 6 B and Figure 6 D). Collectively, these data show that when the damage occurred, the pro-survival factor p-p53ser15 was phosphorylated at the early time point, while the pro-death factor p-p53ser46 was phosphorylated at the late time point.

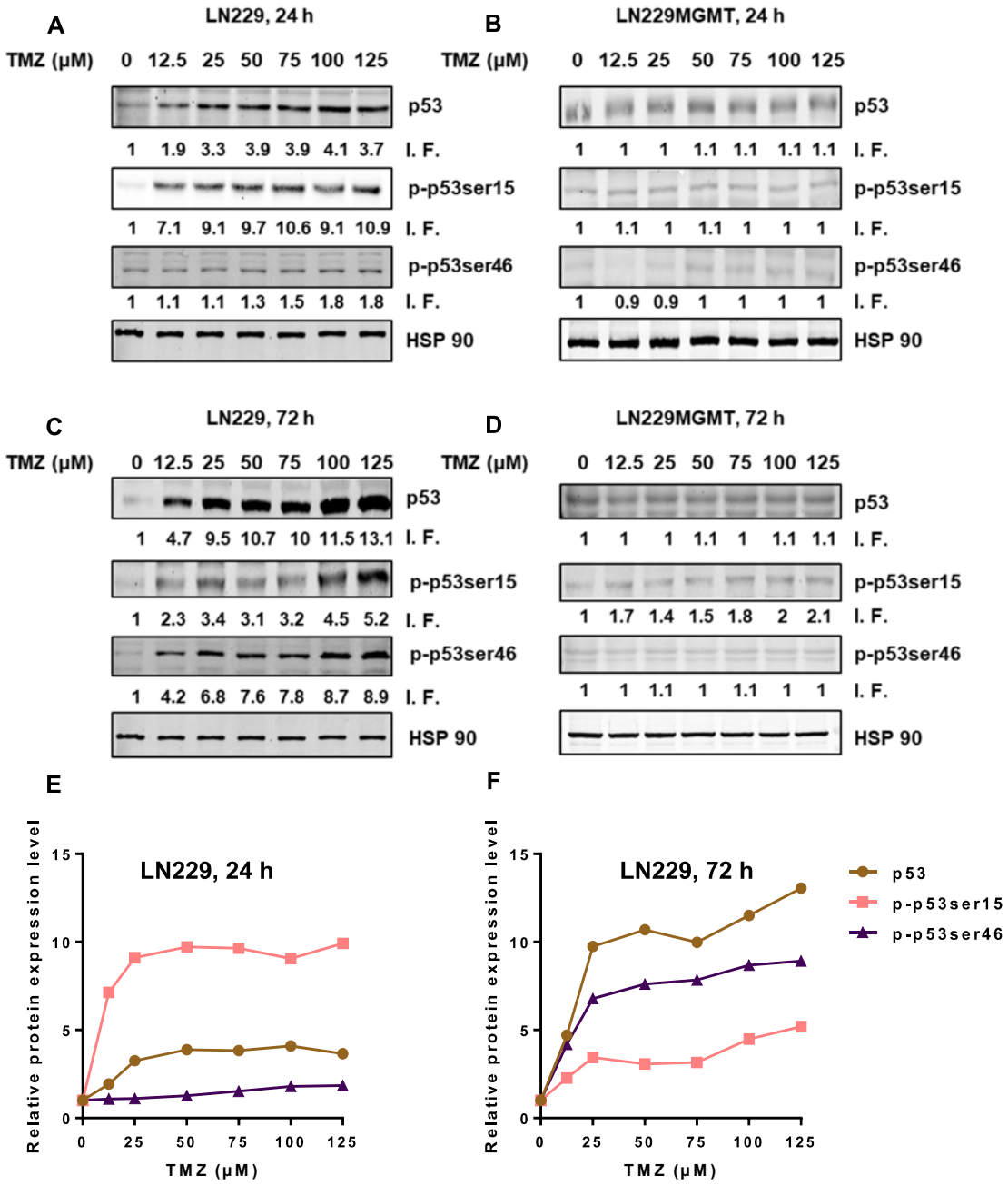

Figure 6 p53 expression and phosphorylation levels of p-p53ser15 and p-p53ser46 in LN229 and LN229MGMT cells treated with doses of TMZ. LN229 (**A**) and LN229MGMT (**B**) cells were exposed to different doses of TMZ (0 μM-125 μM), 24 h later protein extracts were collected, p53 protein expression, phosphorylation levels of p53ser15 and p53ser46 (p-p53ser15 and p-p53ser46) were detected by Western blot. LN229 (**C**) and LN229MGMT (**D**) cells were treated by different doses of TMZ (0 μM-125 μM), 72 h later p53 protein expression, phosphorylation levels of p53ser15 and p53ser46 were detected by Western blot. HSP90 was used as the loading control. I.F. means induction factor. Relative expression levels of p53, p-p53ser15 and p-p53ser46 in LN229 cells after 24 h (**E**) and 72 h (**F**) TMZ treatment were quantified with ImageJ software and plotted on a linear scale.

4.1.2 O^6-MeG triggers apoptosis at late time points

Since the pro-death factor p-p53ser46 increased after two cell cycle, which is also consistent with the study that TMZ induces DNA damage response after two cell cycles with the help of MMR during DNA replication (Quiros, Roos et al. 2010), the apoptosis and necrosis levels of LN229 and LN229MGMT after TMZ treatment were determined by the annexin V/PI double-staining and FACS Canto II flow cytometer analysis.

Although the p-p53ser46 increased at 72 h, the apoptosis level in LN229 stayed low and did not show any significant difference compared to the control (Figure 7 A). The apoptosis levels in LN229 started to increase at 96 h after TMZ exposure and reached its maximum after 120 and 144 h (Figure 7 A), revealing that O^6-MeG triggers apoptosis at late time points. Considering all the time points and the apoptosis/necrosis levels, 120 h was chosen for the subsequent apoptosis detection experiments. In LN229MGMT cells, the results (Figure 7 B) showed there is no significant apoptosis was induced, it had the same tendency as the p-p53ser46 expression level in Western blot in LN229MGMT cells, which again indicates MGMT prevented cells from undergoing TMZ-induced apoptosis.

The necrosis levels of LN229 and LN229MGMT didn't go up much after TMZ treatment (Figure 7 C and D), meaning O^6-MeG induces mainly apoptosis but not necrosis. After the high dose range of TMZ treatment, up to 125 μM, no threshold was observed in O^6-MeG triggered apoptosis in LN229 cells.

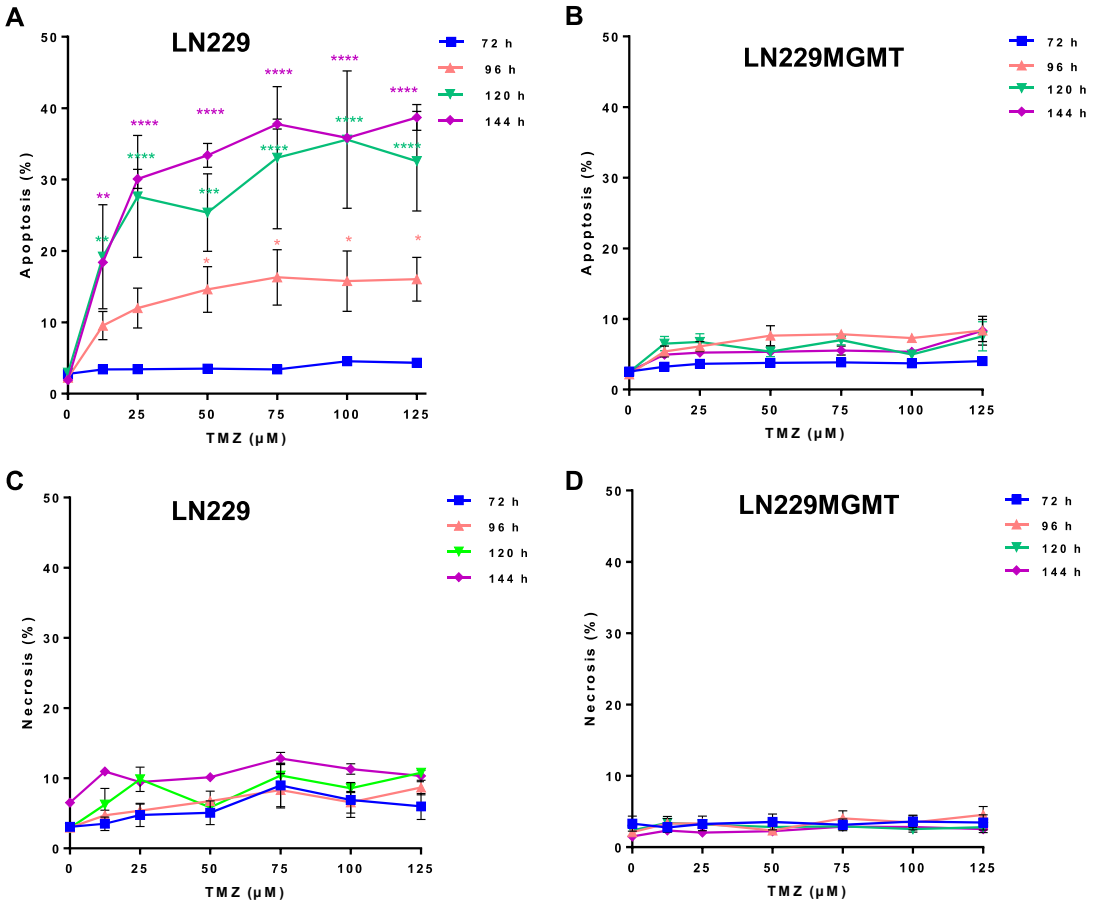

Figure 7 Apoptosis and necrosis levels of LN229 and LN229MGMT cells after TMZ treatment. Apoptosis induced by TMZ in LN229 (**A**) and LN229MGMT (**B**) cells were detected by the annexin V/PI double-staining and FACS Canto II flow cytometer analysis, 72, 96, 120 and 144 h after TMZ exposure. Necrosis induced by TMZ in LN229 (**C**) and LN229MGMT(**D**) cells were detected after TMZ exposure. For all these four figures, the data were analyzed with BD FACSDiva and the Prism software. p-values of < 0.05 are marked as *, p < 0.01 as *, p-values of < 0.001 as *** and < 0.0001 as ****.

4.1.3 O^6-MeG triggers p53 accumulation, phosphorylation of p53ser15 and p53ser46 in a dose and time-dependent manner

It has been shown that there is no threshold in the high dose range of the TMZ-induced (up to 125 μM) DNA damage response in LN229 cells, while a sharp increasing line was observed at the region lower than 25 μM, so the next question arose: is there a threshold in DNA damage response caused by low doses of TMZ (0– 20 μM)?

In this case, the LN229 cells were treated with O^6-BG 1 h before the TMZ treatment, in order to deplete any residual MGMT activity. LN229 and LN229MGMT were treated with different doses of TMZ (0 μM, 1 μM, 2 μM, 3 μM, 4 μM, 5 μM, 10 μM, 15 μM, 20 μM) and protein extracts of p53, phosphorylation levels of p53ser15 and p53ser46 were harvest at different time points (24 h and 72 h), protein expression levels were detected by Western blot.

The Western blot results showed that after 24 h TMZ exposure, p-p53ser15 level increased with increasing dose, total p53 also accumulated, p-p53ser46 expression stayed comparable to control level (Figure 8 A). However, after 72 h TMZ exposure, the p-p53ser46 level increased, total p53 showed stronger signals than 24 h and p-p53ser15 increased (Figure 8 A and C). Relative expression levels of p53, p-p53ser15 and p-p53ser46 in LN229 cells after 24 and 72 h TMZ treatment were shown in Figure 8 E and F. In LN229MGMT, where MGMT is expressed, the DNA damage response induced by TMZ was not observed (Figure 8 B and D). These results indicated that after low dose TMZ treatment, O^6-MeG triggers p53 accumulation, phosphorylation of p53ser15 and p53ser46 in a dose and time-dependent manner, the pro-survival factor p-p53ser15 is phosphorylated earlier to induce cell cycle block, when it doesn't work, then the pro-death factor p-p53ser46 starts to work that leads to apoptosis.

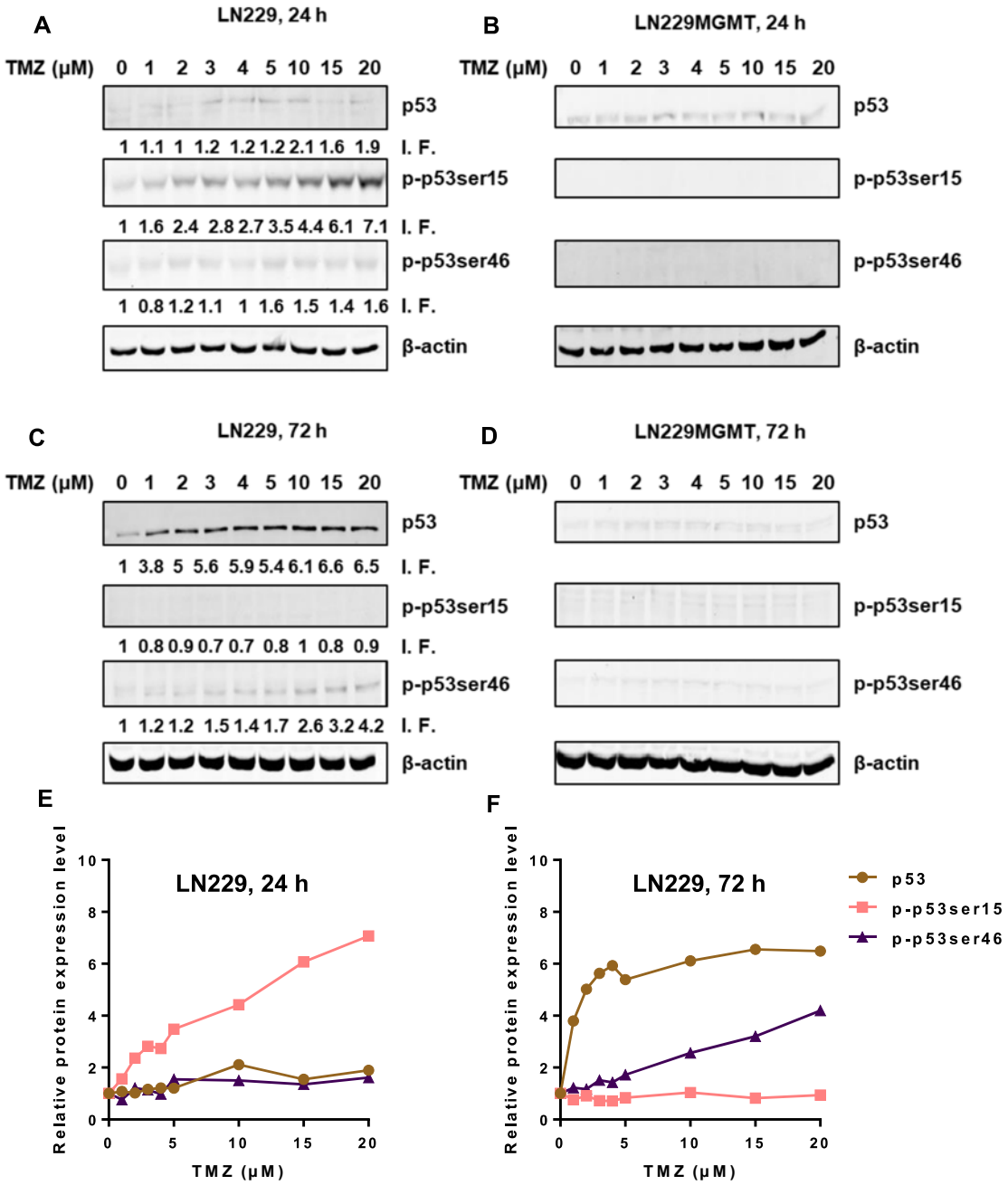

Figure 8 p53 expression and phosphorylation levels of p53ser15 and p53ser46 in LN229 and LN229MGMT cells treated with low doses of TMZ. LN229 and LN229MGMT cells were exposed to TMZ (0 μM-20 μM), 24 h later protein extracts were collected, p53 protein expression, phosphorylation levels of p53ser15 and p53ser46 of LN229 (**A**) and LN229MGMT (**B**) were detected by Western blot. 72 h after exposed to different doses of TMZ (0 μM-20 μM), p53 protein expression, phosphorylation levels of p53ser15 and p53ser46 of LN229 (**C**) and LN229MGMT (**D**) cells were detected with Western blot. β-actin was used as the loading control. I.F. means induction factor. Relative expression levels of p53, p-p53ser15 and p-p53ser46 in LN229 cells after 24 h (**E**) and 72 h (**F**) TMZ treatment were quantified with ImageJ software and plotted on a linear scale.

4.1.4 A survival threshold was observed in LN308, but not in LN229 cells, after low doses of TMZ treatment

To further explore the possible threshold, another glioblastoma cell line, namely LN308, was introduced in this step since no threshold of protein expression was observed in LN229 after low doses TMZ treatment. First LN229 and LN308 cells were exposed to TMZ 100 μM, 72 h later, the p53 expression levels of these two cell lines were determined by Western blot. The Western blot results confirmed that LN308 expresses no p53 protein even after TMZ treatment, it showed a small amount of p53 signal in control sample and a strong induction of p53 expression after TMZ treatment in LN229 cells, while in LN308 no signal was detected in control and TMZ treated samples (Figure 9 A). In the apoptosis and necrosis detection experiments, LN229, LN229MGMT and LN308 cells were exposed to TMZ up to 20 μM, the apoptosis/necrosis levels were determined at 120 h after TMZ treatment. The results showed that LN229 cells had an increasing apoptosis level depending on TMZ doses. The Lowest Observed Adverse Effect Level (LOAEL) was 3 μM (Figure 9 B), while no obvious necrosis was detected (Figure 9 C). LN229MGMT was protected from apoptosis and necrosis after TMZ treatment (Figure 9 B and C). LN308 cells only showed a significant increase in apoptosis at relatively high TMZ doses (15 μM, 20 μM) when compared to the untreated sample (Figure 9 B), indicating that p53 deficient LN308 cells are more resistant than p53 wild-type LN229 cells.

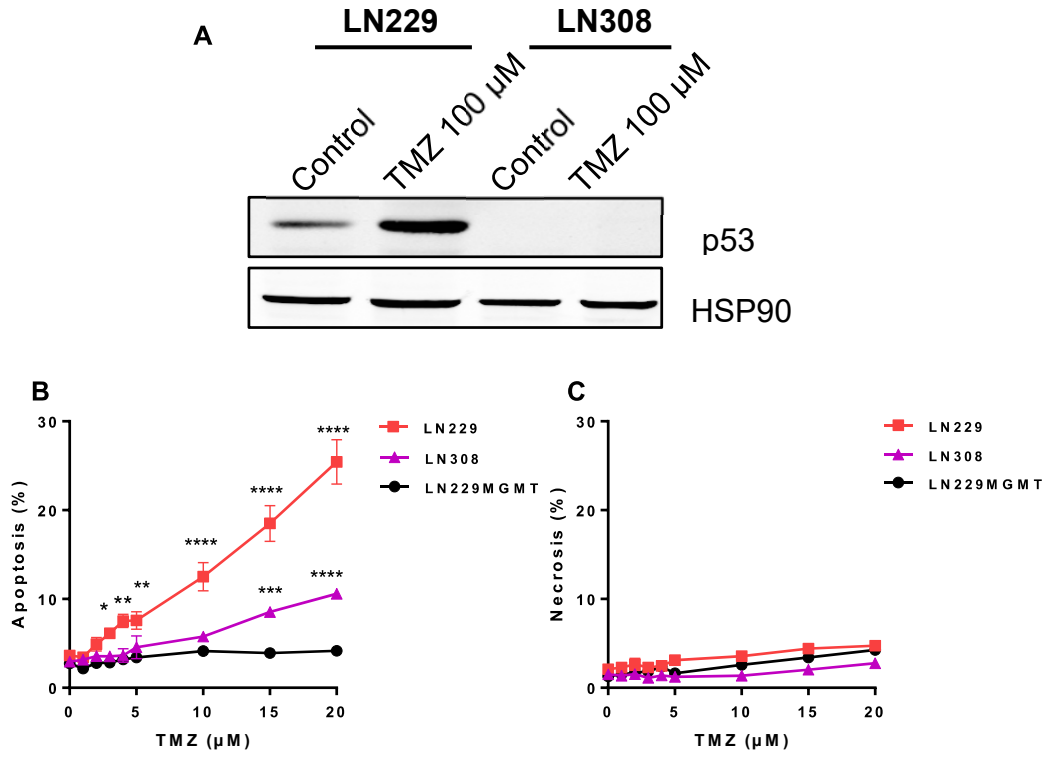

Figure 9 TMZ-induced apoptosis and necrosis as a function of TMZ dose in LN229, LN229MGMT and p53 lacking LN308 cells. (**A**) LN229 and LN308 cells were exposed to TMZ 100 µM, 72 h later protein extracts were collected and the p53 protein levels were detected by Western blot. HSP90 was used as loading control. Apoptosis (**B**) and necrosis (**C**) levels of LN229, LN229MGMT and LN308 cells, 120 h after TMZ exposure, were measured by annexin V/PI double staining and flow cytometry analysis. For (**B**) and (**C**), the data were analyzed with BD FACSDiva and the Prism software. p-values of < 0.05 are marked as *, p < 0.01 as *, p-values of < 0.001 as *** and < 0.0001 as ****.

To test if thresholds exist in cell death, colony formation assay was employed. After exposing LN229, LN229MGMT and LN308 cells to TMZ and allowing them to grow for at least two weeks, the surviving colonies were counted. TMZ-induced cell death in LN229 and LN308 were dose-dependent. For LN229 cells, the survival curves did not show a shoulder (Figure 10

A), indicating that there is no threshold for the induction of cell death in this cell line. LN229MGMT cells were protected by MGMT expression from TMZ-induced cell death (Figure 10 A). For LN308 cells, the survival rate did not decline until 10 μM TMZ treatment, and the survival curve did show a shoulder (Figure 10 B). The LOAEL in LN229 was 3 μM while in LN308 it was 10 μM (Figure 10 A and B). The colony formation results showed that a threshold in LN308 in TMZ induced cell death, which is consistent with the apoptosis results. As a threshold exists in LN308, but not in LN229 cells, it gave a hints that a threshold may depend on p53 status in these cells when responding to DNA damage.

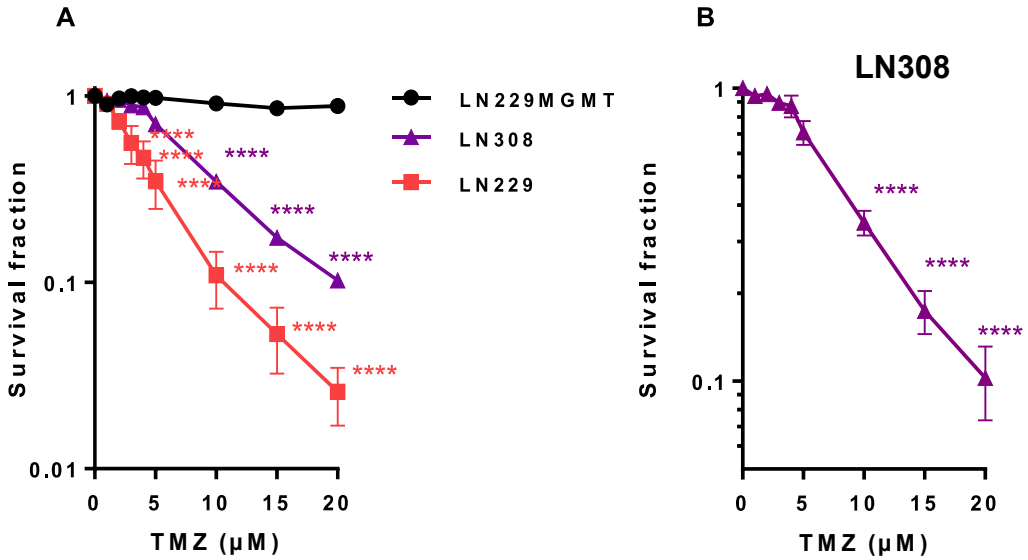

Figure 10 A survival threshold was observed in LN308 after low doses of TMZ treatment. (**A**) Colony survival assay of LN229, LN229MGMT and LN308 cells exposed to different concentrations of TMZ, survival fraction of each cell line was shown compared with control samples. (**B**) LN308 colony survival assay was also plotted separately on the right. for (**A**) and (**B**), the data were analyzed using the Prism software. p-values of < 0.05 are marked as *, p < 0.01 as *, p-values of < 0.001 as *** and < 0.0001 as ****.

4.1.5 TMZ induces senescence and autophagy in a dose-dependent manner

Previous work of our group showed that TMZ induces not only apoptosis but also senescence and autophagy in LN229 cells (Knizhnik, Roos et al. 2013). Consequently, it is also necessary to know if there is a threshold in TMZ induced senescence and autophagy in LN229 cells. At the same time, senescence and autophagy in p53 deficient cells LN308 were also determined. The results displayed that TMZ induced increasing amount of senescence with increasing TMZ doses in LN229 cells (Figure 11 A). The senescence curve was linear and the dose-response curves showed no threshold. A LOAEL of 3 μM was calculated for LN229 from the curve (Figure 11 A). Similar to the apoptosis data, MGMT protected LN229 cells from TMZ-induced senescence (Figure 11 A). In LN308 cells, the slope of the senescence curve was gentler than for LN229 cells, only relatively high doses of TMZ induced senescence significantly.

The autophagy of these three cell lines was similar as the senescence response. TMZ induced more autophagy in LN229 cells than in LN308 cells, while LN229MGMT showed no response since MGMT protected LN229 cells from the DNA damage triggered by TMZ (Figure 11 B). Together with the apoptosis data, all these results indicate that p53 proficient LN229 cells are more sensitive than p53 deficient LN308 cells.

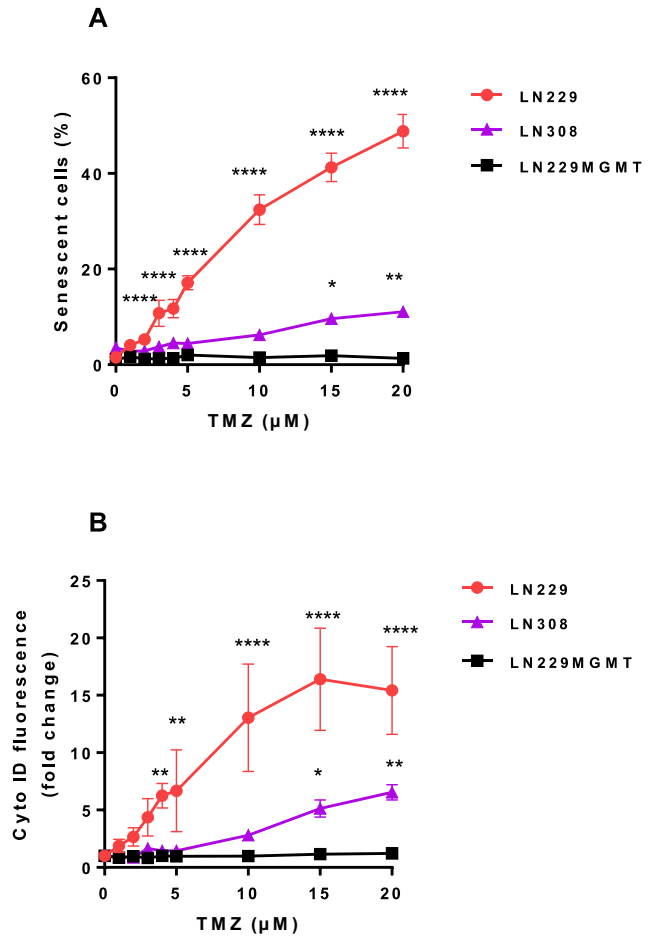

Figure 11 TMZ-induced senescence and autophagy in LN229, LN229MGMT and LN308 cells. (**A**) LN229, LN229MGMT and LN308 cells were exposed 0-20 μM TMZ, 96 h later cells were collected, stained with C_{12}FDG, and detected with flow cytometry in 15 minutes. (**B**) Autophagy levels were measured in LN229, LN229MGMT and LN308 cells 96 h after TMZ exposure with flow cytometry. The results were shown by Cyto ID fluorescence fold change compared with control samples. Control samples in the three cell lines were set as 1. For (**A**) and (**B**), the data were analyzed with BD FACSDiva and Prism software. p-values of < 0.05 are marked as *, p < 0.01 as *, p-values of < 0.001 as *** and < 0.0001 as ****.

4.1.6 TMZ induces DNA double-strand breaks in LN229 and LN308 cells in a dose-dependent manner

The p53 proficient LN229 cells showed more sensitivity than p53 deficient LN308 cells in TMZ-induced apoptosis, senescence and autophagy, while it's still unknown that in these cell lines whether there is any difference in the amount of DSBs caused by TMZ. For this reason, γH2AX foci were used to quantify the numbers of DSBs induced by TMZ. LN229, LN229MGMT and LN308 cells were treated by 0-20 μM TMZ, after 72 h γH2AX foci were determined and quantified by Metafar system. For each sample, more than 120 cells were tested. Cells that were not in focus or were stained improperly were excluded from analysis. After three repeats, at least 300 cells for every treatment condition were quantified. The γH2AX foci in LN229 showed a linear increase with increasing TMZ dose (Figure 12 A), indicating no threshold in TMZ-induced DSBs in LN229 cells. Most of the DSBs was eliminated in LN229MGMT cells (Figure 12 B). In LN308 cells, surprisingly, the tendency of γH2AX foci numbers went up linearly (Figure 12 C), which was very similar to LN229 cells. To have a more intuitive comparison of the γH2AX foci numbers between LN229 and LN308, an integrated figure12 D was displayed (also with LN229MGMT). No threshold in the γH2AX foci numbers was observed after each dose of TMZ. The LOAEL in both cell lines is 3 μM (Figure 12 A and C). DSBs numbers in these two cell lines proved that TMZ induces DSBs in LN229 and LN308 in a dose-dependent manner, and the tendency and DSBs amount were the same in the two cell lines. It needs to be further studied that why LN308 and LN229 cells display the same amount of DSBs after TMZ exposure, while they show a different response to TMZ-induced cell death and apoptosis, preliminary results are shown in supplementary 7.2.

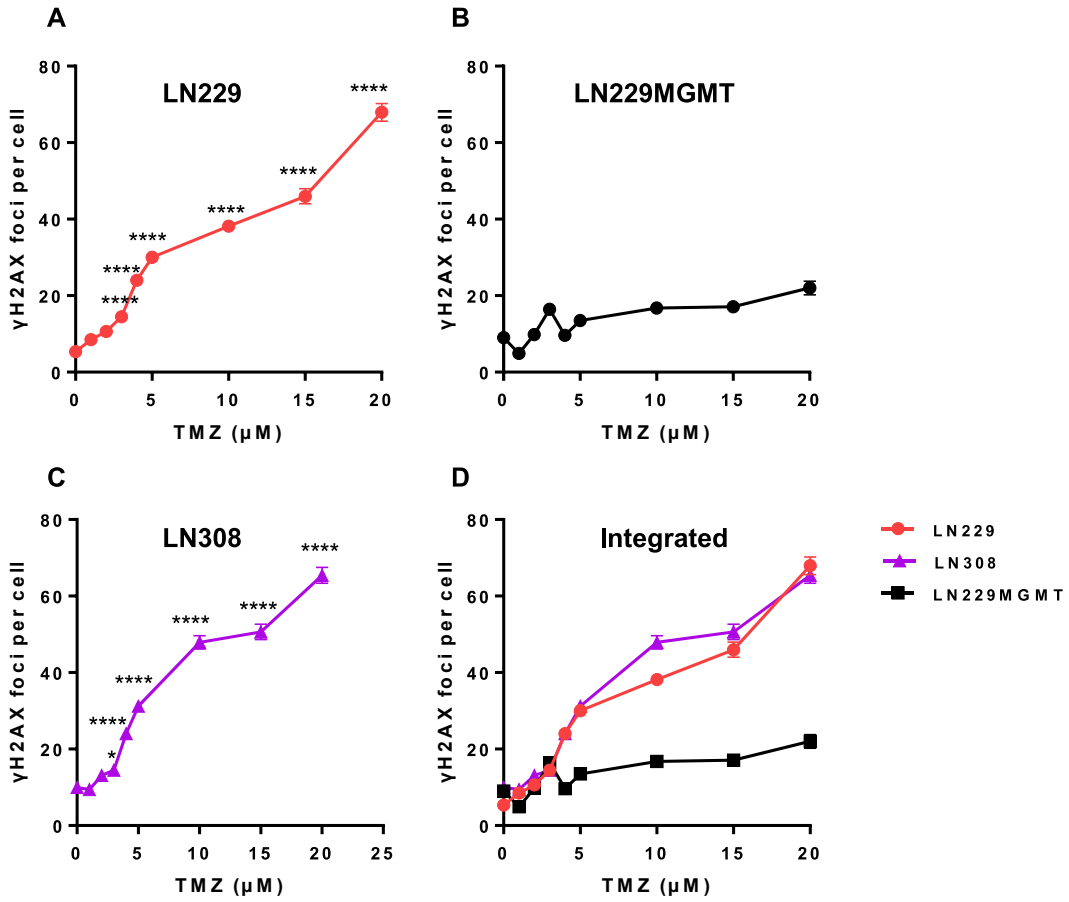

Figure 12 TMZ-induced γH2AX foci in LN229, LN229MGMT and LN308 cells. Cells were treated with TMZ 0-20 μM, 72 h later cells were fixed, γH2AX foci quantified by Metafar system in LN229, LN229MGMT and LN308 cells. Dose-dependent γH2AX foci numbers per cell were shown in LN229 (**A**), LN229MGMT (**B**) and LN308 (**C**), an integrated figure of LN229, LN229MGMT and LN308 cells were shown in (**D**). For (**A**), (**B**) and (**C**), n>300, data were analyzed using the Prism software. p-values of < 0.05 are marked as *, p < 0.01 as *, p-values of < 0.001 as *** and < 0.0001 as ****.

4.2 Exploring the SIAH1-HIPK2-p53 regulated cell death pathways induced by TMZ and CCNU

4.2.1 HIPK2 is involved in the TMZ-induced DNA damage response

To determine the possible role of HIPK2 in glioblastoma cell death upon TMZ treatment, the conditions for its knockdown had to be established. To this aim, LN229 cells were treated with TMZ and the amount of HIPK2 was monitored by Western blot. HIPK2 was expressed in LN229 cells and upon TMZ exposure, the increased protein level of HIPK2 indicated that TMZ induces HIPK2 accumulation, presumably through HIPK2 stabilization as described previously for DNA damaging conditions (Dauth, Krüger et al. 2007, Winter, Sombroek et al. 2008, Crone, Glas et al. 2011). Using siRNAs that target two different sequences of HIPK2 mRNA (siHIPK2-1 and siHIPK2-2), LN229 cells were exposed to TMZ following HIPK2 knockdown. Both siHIPK2-1 and siHIPK2-2 abolished the TMZ-induced stabilization of HIPK2 (Figure 13). As siHIPK2-2 was more efficient in knocking down HIPK2 upon TMZ exposure, this siRNA was used in the subsequent experiments.

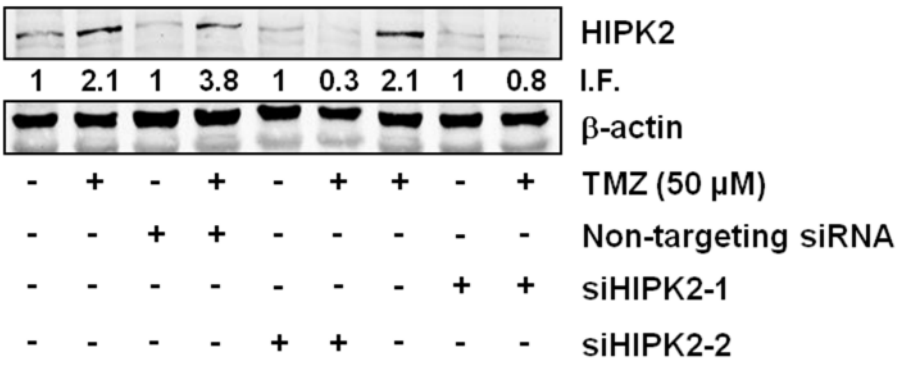

Figure 13 HIPK2 protein expression levels after TMZ treatment and HIPK2 knockdown. Western blot result of RNA interference-mediated knockdown of HIPK2 in LN229 cells 96 h after 50 μM TMZ exposure. Two siRNAs that target different sequences of HIPK2 mRNA was employed and non-targeting siRNA was used for control. β-actin was used as the loading control.

4.2.2 TMZ induces the phosphorylation of p-p53ser46 and the expression of two pro-apoptotic proteins in a HIPK2-dependent manner

It has been proved that upon exposure of cells to DNA damaging agents such as ultraviolet light, HIPK2 specifically phosphorylates p53 at serine 46 (D'Orazi, Cecchinelli et al. 2002). To determine if this is also the case for the chemotherapeutic TMZ, LN229 cells were exposed to TMZ in the presence and absence of HIPK2 knockdown. As shown in the following figure, TMZ treatment gives rise to p53 stabilization and its phosphorylation at serine 15 and serine 46. While knockdown of HIPK2 had no effect on the p53 stabilization and on TMZ-induced p-p53Ser15, HIPK2 depletion strongly reduced the levels of p-p53ser46 (Figure 14). These data show that HIPK2 plays an essential role in phosphorylation of p53 at serine 46 upon TMZ exposure, while not affecting the stabilization of p53 nor its phosphorylation at serine 15.

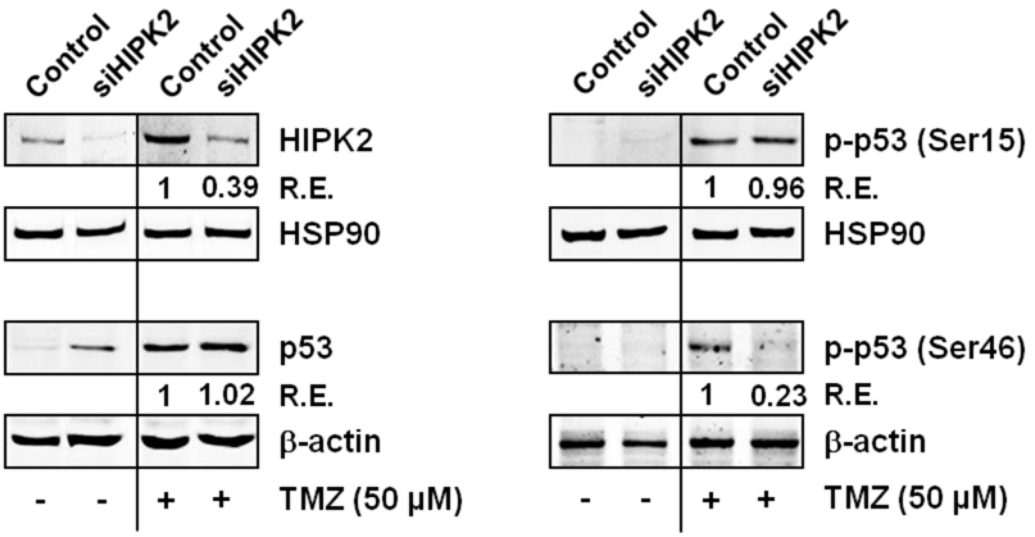

Figure 14 p53 expression, phosphorylation of p53 at serine 15 and serine 46 in LN229 cells upon HIPK2 knockdown and TMZ exposure. Western blot analysis of HIPK2, p53, phosphorylated p53 at serine 15 and phosphorylated p53 at serine 46 upon HIPK2 knockdown, 96 h after 50 μM TMZ exposure. Control samples were transfected with non-targeting siRNA. HSP90 and β-actin were used as loading control. R.E. relative expression compared to control.

4.2.3 HIPK2 sensitizes glioblastoma cells to the DNA lesion *O*^{6}-MeG by stimulating the apoptotic response

In the next experimental series, the influence of HIPK2 and the phosphorylation of p53 at ser46 on TMZ-induced apoptosis were elucidated. LN229 cells, which lack MGMT, and LN229 stably expressing MGMT (LN229MGMT) (Figure 15 A) were employed(Quiros, Roos et al. 2011).

Upon treatment with 50 µM TMZ, about 40% of LN229 cells were tested as apoptotic (annexin V positive) cells while in the LN229 HIPK2 knockdown the level was markedly reduced to 20% (Figure 15 B), which indicated that HIPK2 sensitizes glioblastoma cells to the *O*^{6}-MeG. HIPK2 knockdown didn't attenuated the apoptosis levels induced by TMZ in LN229MGMT (Figure 15 C), showing that the effects observed in LN229 cells that lack MGMT, in the presence or absence of HIPK2, were brought about by the specific DNA lesion *O*^{6}-MeG. A small amount of necrosis (annexin V/PI double-positive cells) was induced by TMZ in LN229 (Figure 15 D), the necrosis levels of LN229MGMT did not differ between HIPK2 knockdown and control cells upon TMZ treatment (Figure 15 E). which is in line with previous results demonstrating that TMZ induces cell death in glioblastoma cells mainly by apoptosis (Roos, Batista et al. 2007).

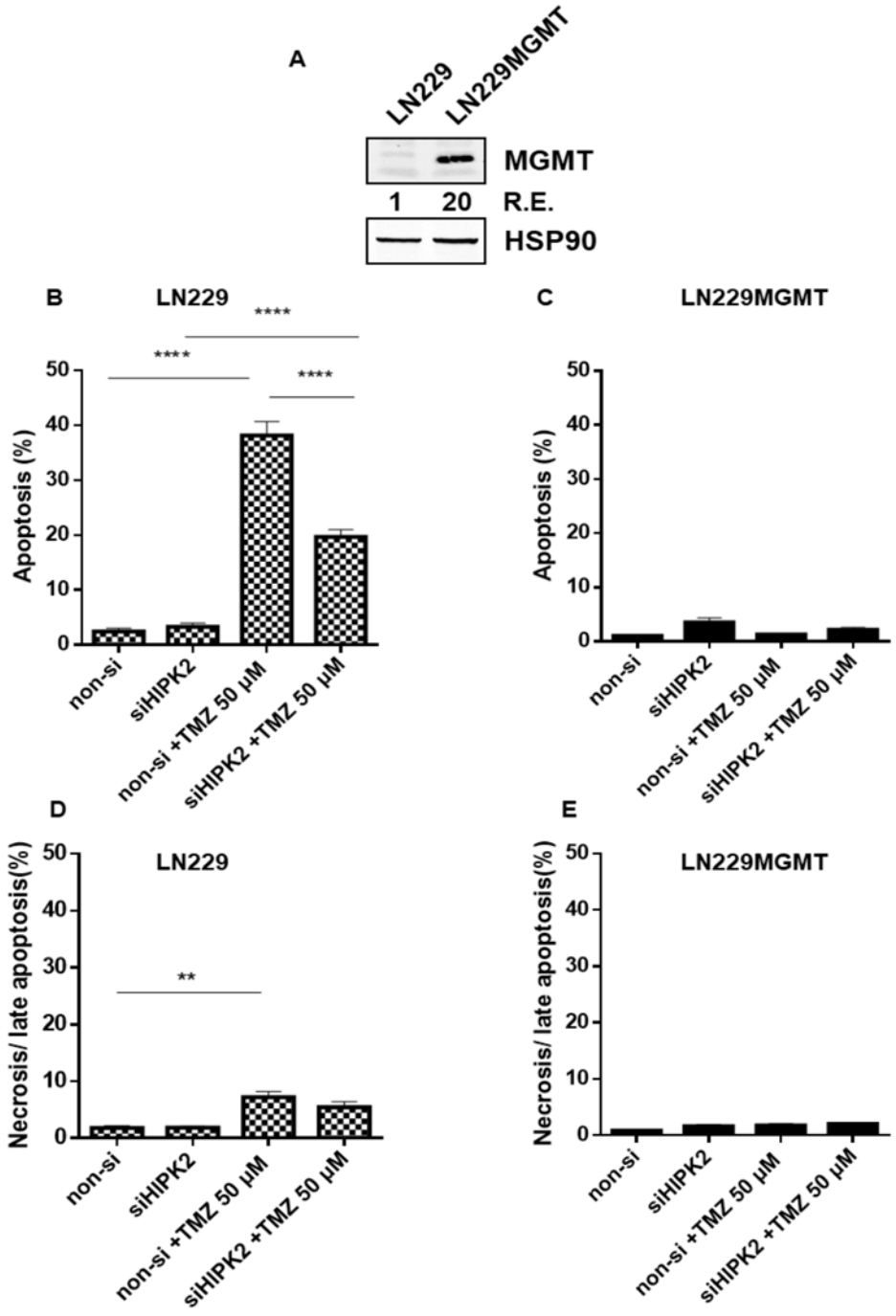

Figure 15 Apoptosis and necrosis triggered by the TMZ-induced DNA lesion O^6-MeG after HIPK2 knockdown in glioblastoma cell lines. (**A**) Western blot results of MGMT in LN229 and LN229MGMT lines. HSP90 was used as loading control. R.E. relative expression compared to control. Apoptosis and necrosis induced by TMZ in LN229 (**B**, **D**) and LN229MGMT (**C**, **E**) cells following HIPK2 knockdown, 144 h after TMZ exposure. Control samples were transfected with non-targeting siRNA and p-values of < 0.005 are marked as **, p-values of < 0.001 as *** and < 0.0001 as ****.

The gain of resistance to TMZ following HIPK2 downregulation was confirmed in TMZ-induced cell death. As shown by colony-forming experiments (Figure 16), LN229MGMT cells were completely resistant to TMZ whereas LN229 failed to resist the damage induced by TMZ, as expected, in a dose-dependent manner. Knockdown of HIPK2 in LN229 increased the resistance of LN229 cells to the cell death induced by TMZ compared to the LN229 cells without knockdown.

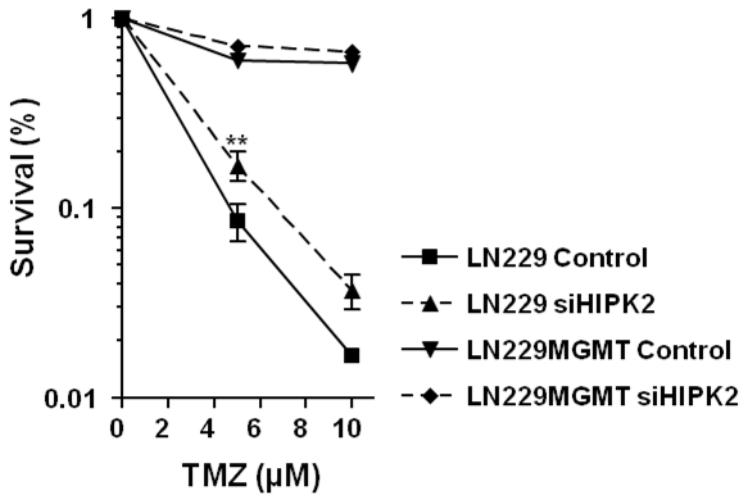

Figure 16 Cell death triggered by the TMZ-induced DNA lesion O^6-MeG after HIPK2 knockdown in glioblastoma cell lines. Colony survival assay of LN229 and LN229 stably expressing MGMT (LN229MGMT) exposed to the indicated concentrations of TMZ upon HIPK2 knockdown. Control samples were transfected with non-targeting siRNA and p-values of < 0.005 are marked as **.

4.2.4 HIPK2 knockdown does not influence senescence induced by TMZ

TMZ has also been shown to be effective in inducing, in the same time frame, apoptosis and senescence (Knizhnik, Roos et al. 2013). The induction of senescence by TMZ was quantified by senescence-associated β-galactosidase (SA-β-Gal) activity staining. The results showed TMZ induced senescence (blue cells) in LN229 cells after TMZ treatment. In the treated sample without HIPK2 knockdown the induced senescence was 27% on average; the HIPK2 knockdown samples had 23% induced senescence, however, there was no significant difference between them (Figure 17). The senescence percentage after TMZ treatment was not affected by HIPK2 downregulation. Thus, HIPK2 specifically regulates TMZ-induced cell death.

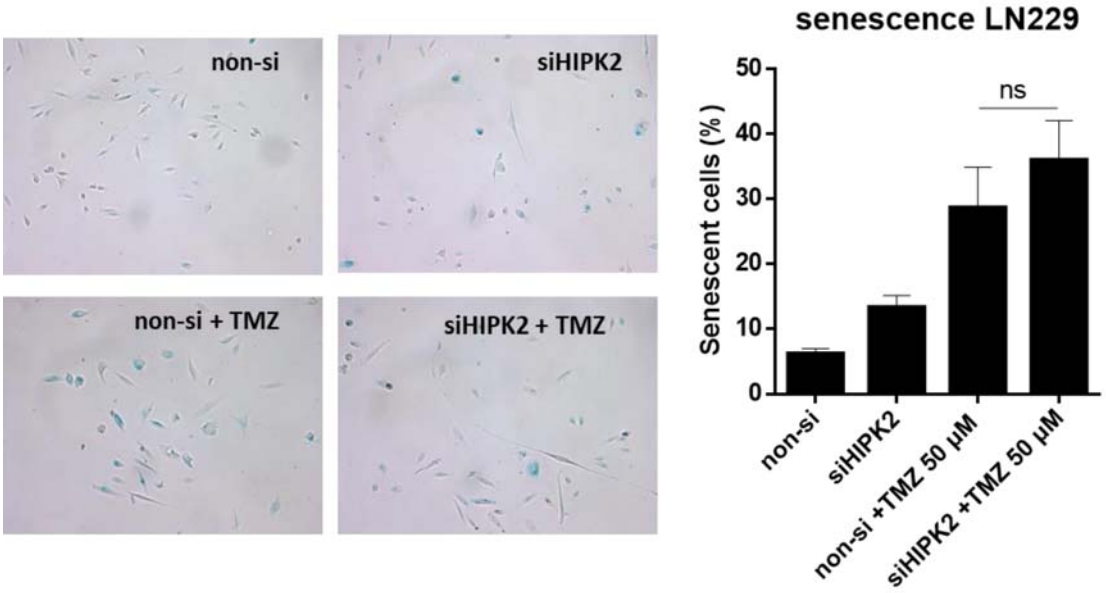

Figure 17 TMZ-induced senescence after HIPK2 knockdown. Senescence-associated β-galactosidase activity determination in LN229 cells 96 h after 50 µM TMZ exposure and HIPK2 knockdown. Representative micrographs (left) and quantification of SA-β-gal stained LN229 cells (right) following 50 µM TMZ exposure and HIPK2 knockdown. Control samples were transfected with non-targeting siRNA.

4.2.5 HIPK2 knockdown does not affect the amount of DNA double-strand breaks induced by TMZ

HIPK2 is a kinase activated by the DNA damage response, downstream from ATM and ATR (Dauth, Krüger et al. 2007, Winter, Sombroek et al. 2008). To exclude whether the downregulation of HIPK2 has an impact on DNA damage detection and the activation of the DNA damage response, notably in the presence of DSBs, the extent of γH2AX foci formation was quantified. Upon treatment with 50 µM TMZ, the average number of γH2AX foci that was contained in LN229 cells did not significantly change following HIPK2 knockdown (Figure 18). This indicates that HIPK2 has no impact on DSBs formation upon TMZ exposure, but works downstream from the ATM and ATR mediated, DNA damage response.

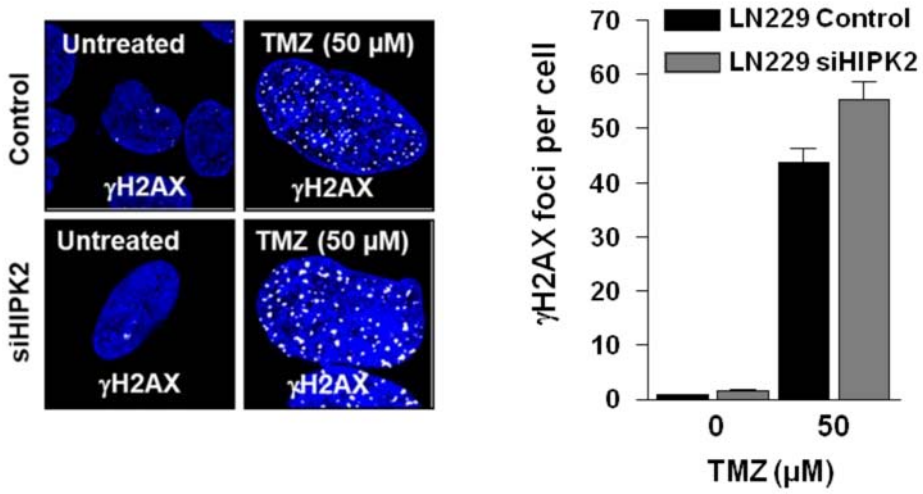

Figure 18 HIPK2 promotes TMZ-induced apoptosis without effecting TMZ-induced DSB formation. γH2AX foci quantified by fluorescence microscopy in LN229 cells exposed to 50 µM TMZ upon HIPK2 knockdown. Representative micrographs showing TMZ-induced γH2AX foci in white and nuclear staining in blue (left). Quantification of γH2AX foci was shown on the right. Control samples were transfected with non-targeting siRNA. This experiment was performed by Dr. Roos.

4.2.6 HIPK2 causes glioblastoma cell sensitization to TMZ-induced apoptosis in a p53 dependent manner

Since HIPK2 was shown to target p53 (D'Orazi, Cecchinelli et al. 2002), its role in TMZ-induced apoptosis was assessed next. It is not clear if p53 is the main target of HIPK2 in TMZ induced apoptosis, although the knockdown of HIPK2 down-regulated the p-p53ser46 expression. The p53 deficient LN308 cells were treated with TMZ following HIPK2 knockdown. Hypothetically, if the sensitization to TMZ-induced apoptosis by HIPK2 is mainly dependent on p53, then glioblastoma cells like LN308 that lack p53 should not differ in their apoptosis response upon HIPK2 knockdown. This was, in fact, the case as the p53 deficient LN308 cell line did not differ in its TMZ-induced apoptosis response following HIPK2 knockdown (Figure 19 A).

To substantiate the p53 dependent action of HIPK2 for the sensitization of glioblastoma cells to TMZ, p53 was inhibited with pifithrin-α in LN229 cells. Inhibition of p53 protected LN229 cells from TMZ-induced apoptosis (Figure 19 B), showing that p53 stimulates apoptosis induced by TMZ. Simultaneously inhibiting p53 and knocking down HIPK2 had no additional effects on TMZ-induced apoptosis compared to p53 inhibition or HIPK2 knockdown on their own (Figure 19 B). These data support the conclusion that HIPK2 stimulated TMZ-induced apoptosis in glioblastoma cells LN229 is dependent on p53.

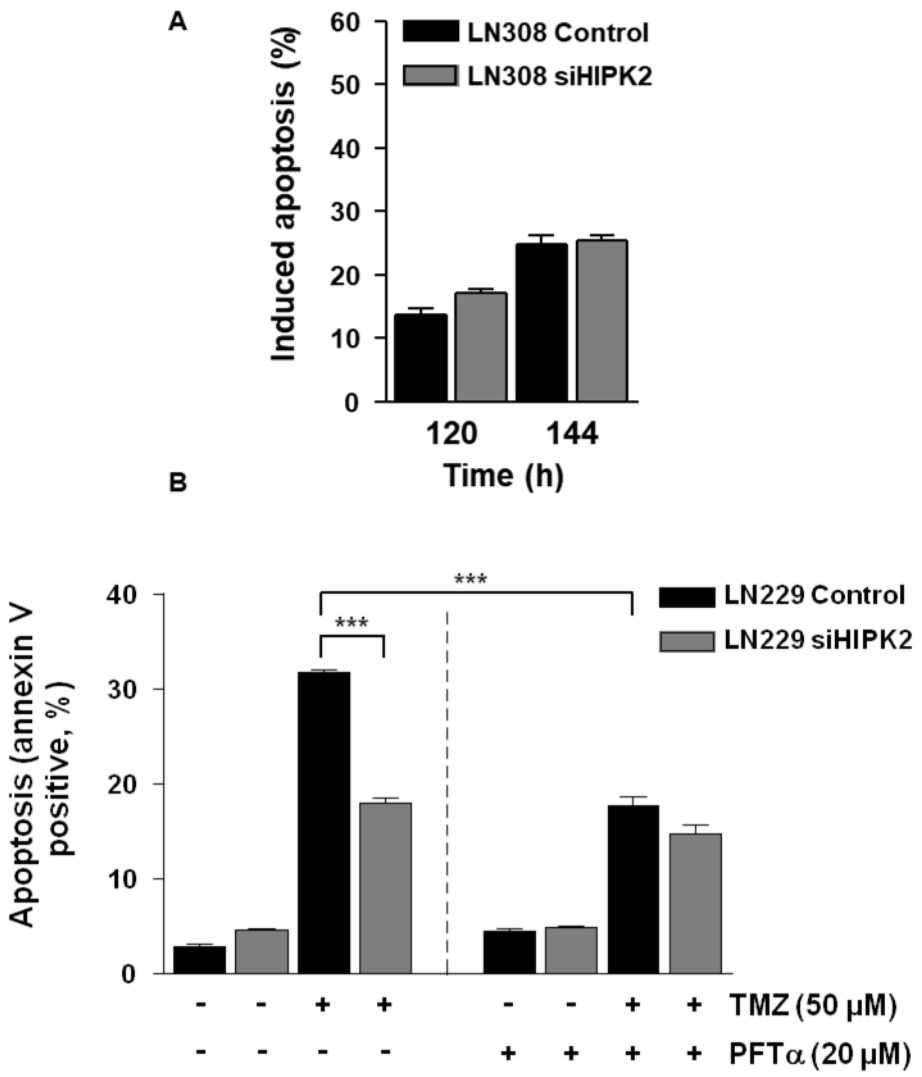

Figure 19 HIPK2 promotes TMZ-induced apoptosis in a p53 dependent manner. (**A**) Apoptosis induced by 50 µM TMZ in LN308 cells upon HIPK2 knockdown. (**B**) Inhibition of p53 by pifithrin-α (PFTα) in LN229 cells upon 50 µM TMZ exposure and HIPK2 knockdown. The assay was performed at 144 h after TMZ exposure. For all figures, control samples were transfected with non-targeting siRNA, p-Values of < 0.001 are marked as ***.

4.2.7 HIPK2 stimulates gene expression of the death receptor FAS upon TMZ exposure

Having shown that HIPK2 sensitizes glioblastoma cells in a p53 dependent manner upon TMZ, the question was addressed whether HIPK2 is able to activate a specific p53 dependent apoptosis pathway. As shown previously, TMZ induced the accumulation of p53 and p53 phosphorylation at ser15 and ser46. The downregulation of HIPK2 had an impact on TMZ-induced p-p53ser46, which is thought to regulate pro-apoptotic genes. Therefore, the expression profiles of a set of related genes were measured. As shown in Figure 20 A, HIPK2 knockdown caused a significant reduction in HIPK2 mRNA (as expected) and the level of TMZ-induced FAS (alias CD95/APO1) mRNA. For *PTEN*, *BBC3* (PUMA), *PMAIP1* (NOXA), and *BAX*, HIPK2 knockdown had no effect on mRNA level in non-treated and TMZ treated cells. These results suggest the death receptor FAS is the main target of p-p53ser46 that becomes activated by TMZ-induced DNA lesions. Since the pro-survival factor p-p53ser15 was taken for comparison with p-p53ser46, the expression levels of its potential downstream candidates *CDKN1A, RAD51, DDB2, pol H* were also checked. The results showed HIPK2 knockdown does not have a obvious impact on the expression of pro-survival factors induced by TMZ (Figure 20 B). This is compatible with the previous results that HIPK2 does not influence the TMZ induced p-p53ser15 level.

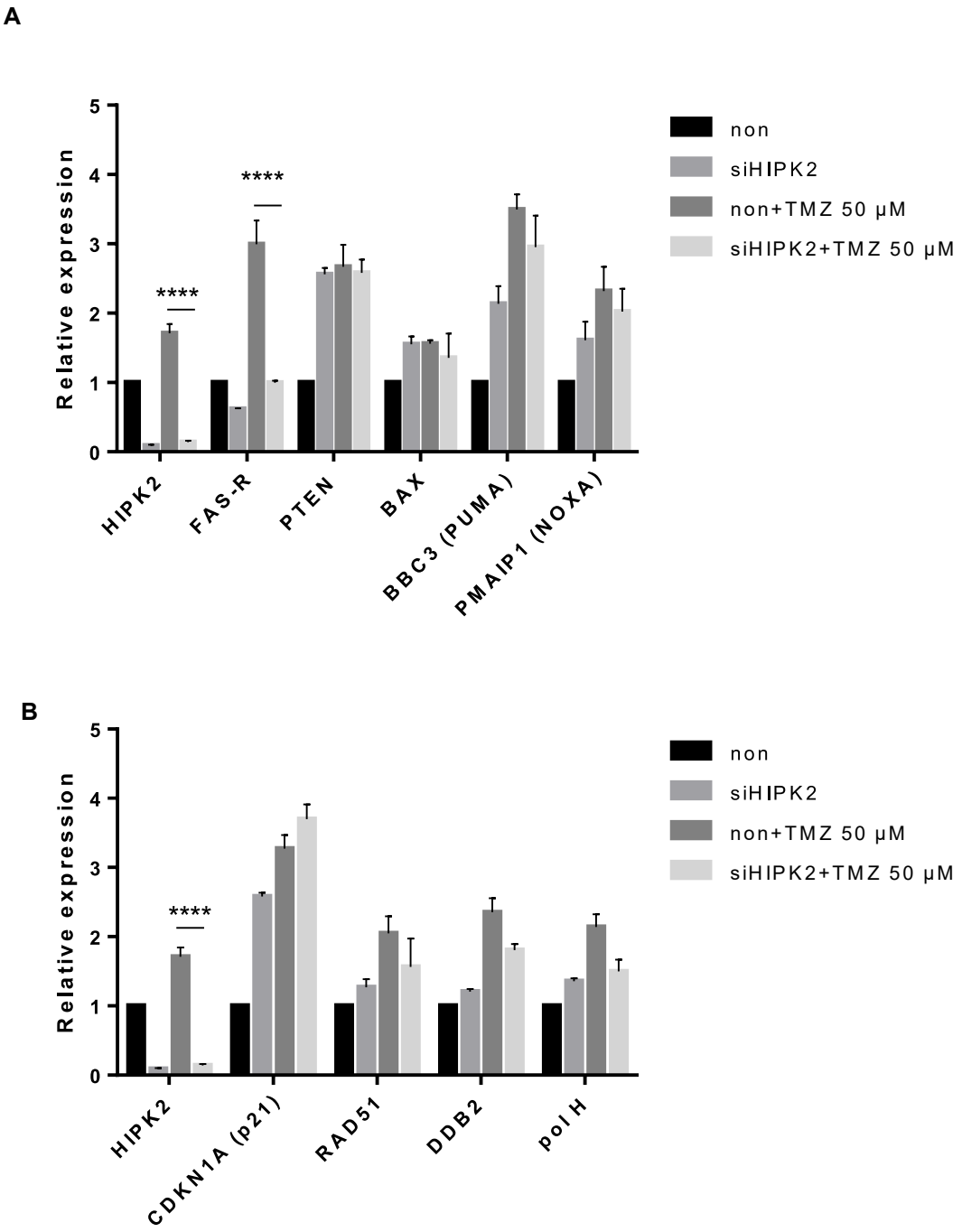

Figure 20 Gene expression levels of potential candidates of p53 in the TMZ-induced DNA damage response after HIPK2 knockdown. (**A**) Analysis of *HIPK2*, *FAS*, *PTEN*, *BBC3* (PUMA), *PMAIP1* (NOXA) and *BAX* gene expression by RT-PCR in LN229 cells 72 h after 50 µM TMZ exposure and HIPK2 knockdown. (**B**) Analysis of *HIPK2*, *CDKN1A* (p21), *RAD51, DDB2* and *pol H* gene expression by RT-PCR in LN229 cells 72 h after 50 µM TMZ exposure and HIPK2 knockdown. p-values of < 0.005 are marked as ** and < 0.001 as ***.

4.2.8 HIPK2 ameliorates TMZ-induced FAS-R expression in a p53ser46 dependent manner

Until now it was shown that HIPK2 stimulates FAS-R gene expression. This notion was confirmed by Western blot experiments, which showed that FAS is clearly upregulated following treatment with TMZ and this upregulation is abrogated by HIPK2 knockdown (Figure 21 A). In addition, there was a slight effect on PTEN expression, whereas the protein levels of PUMA, NOXA and BAX remained unaffected following TMZ when HIPK2 was downregulated (Figure 21 A).

The regulation of *FAS* through HIPK2 via the p53 pathway was substantiated using chromatin immunoprecipitation (ChIP) experiments. The results showed that following TMZ treatment, binding of p-p53ser46 to a p53 consensus binding site at the FAS promoter was substantially increased (Figure 21 B). In cells treated with 50 µM TMZ and HIPK2 siRNA significant less p-p53ser46 was found in the chromatin containing the FAS promoter sequence. Collectively, these results indicate a critical role for HIPK2 in regulating p-p53ser46-driven Fas expression in response to TMZ treatment.

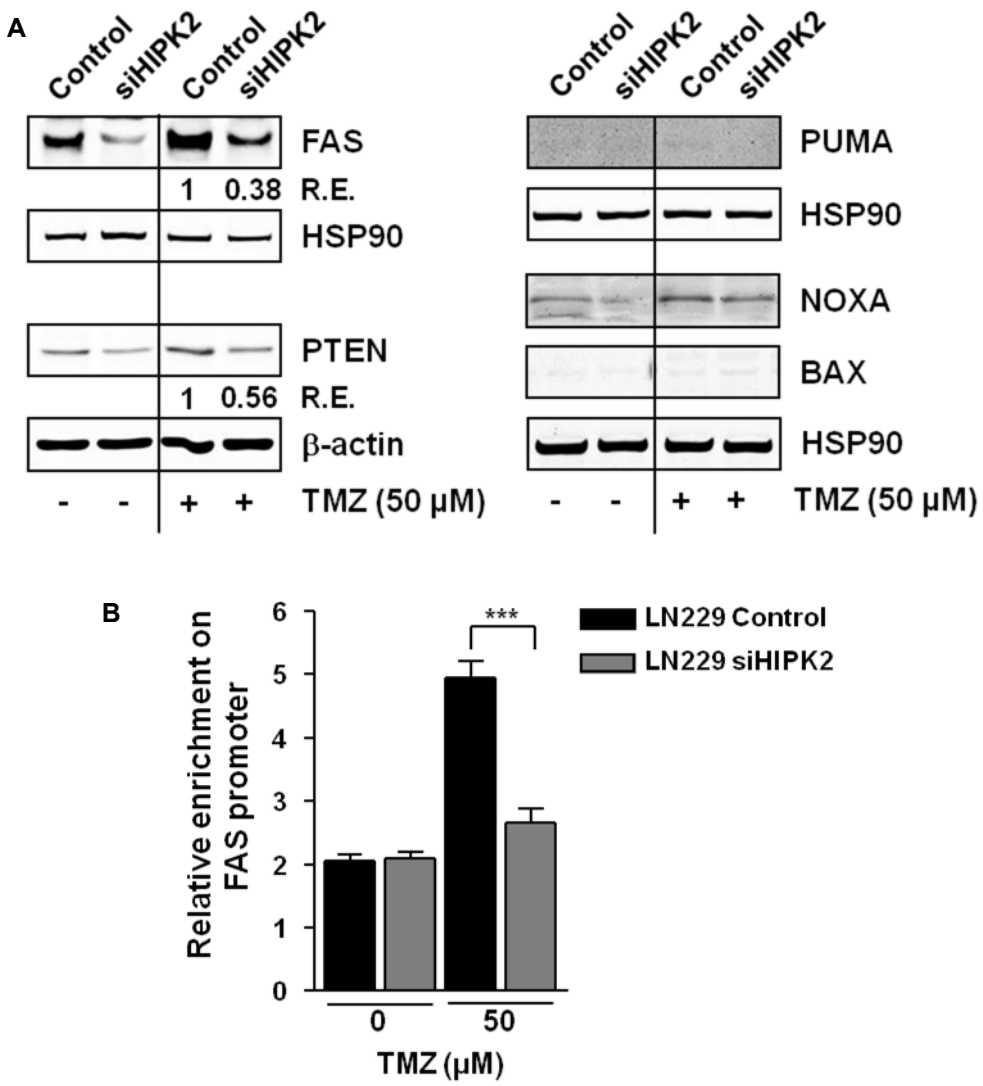

Figure 21 HIPK2 sensitize TMZ-induced FAS-R in a p53ser46 dependent manner. (**A**) Western blot analysis of FAS, PTEN, PUMA, NOXA and BAX protein level 96 h after 50 µM TMZ exposure and HIPK2 knockdown. HSP90 and β-actin were used as loading control. R.E. relative expression compared to control. (**B**) Binding amount of p-p53ser46 on chromatin that contains the FAS promoter. The ChIP experiment was performed by Qianchao Wu from our cooperation group AG Hofmann. The outcome is expressed in relation to LN229 control extract precipitated with IgG antibody, which was set to 1.

4.2.9 HIPK2 stimulates TMZ-induced caspase activity

As HIPK2 knockdown countered the expression levels of the p53 target gene *FAS*, the function of this death receptor pathway upon TMZ exposure of glioblastoma cells was examined more closely. To this end, the influence of HIPK2 knockdown on TMZ triggered caspase activity was determined. Upon exposure of LN229 cells to TMZ, caspase-8 and caspase-3, but not caspase-9, became activated (Figure 22) indicating that TMZ triggers the death receptor-dependent apoptosis pathway. These results are compatible with our previously published findings (Roos, Batista et al. 2007). HIPK2 knockdown decreased both the activation of caspase-8 and -3 following TMZ, supporting that HIPK2 works in the stimulation of TMZ-induced death receptor activation.

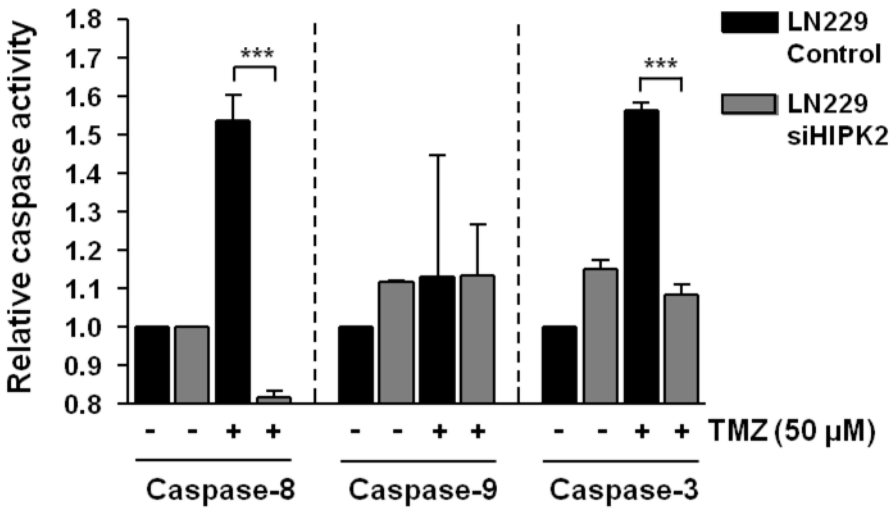

Figure 22 Relative caspase-8, caspase-9 and caspase-3 activity after HIPK2 knockdown and TMZ treatment. Relative caspase-8, -9 and -3 activity 96 h after 50 µM TMZ exposure and HIPK2 knockdown in LN229 cells, the fluorescence was detected by microplate reader. Control samples were transfected with non-targeting siRNA and p-values of < 0.005 are marked as ** and < 0.001 as ***.

4.2.10 HIPK2 stimulates TMZ-induced apoptosis in a death receptor-dependent manner

To test if FAS-R is the key factor in HIPK2 sensitized apoptosis induced by TMZ, LN229 cells were created that are defective in the activation of the death receptor downstream signaling. This was accomplished by stably overexpressing a truncated, dominant-negative FADD (DN-FADD) in LN229 cells (Figure 23 A). Expression of DN-FADD protected LN229 cells from TMZ-induced apoptosis, further proving the role of this death receptor in TMZ-induced apoptosis (Figure 23 B). Knockdown of HIPK2 had no influence on apoptosis in the DN-FADD expressing LN229 cells, showing that HIPK2 is unable to sensitize glioblastoma cells if death receptor signaling is non-functional.

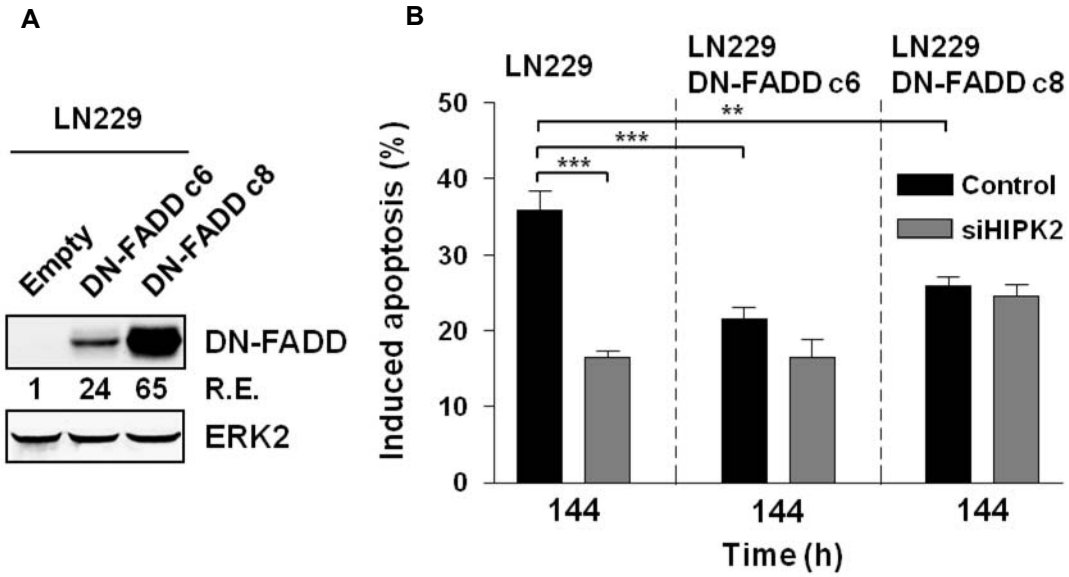

Figure 23 The apoptosis and necrosis in LN229DN-FADD after HIPK2 knockdown and TMZ exposure. (**A**) Apoptosis induced by 50 µM TMZ in LN229 stably overexpression dominant-negative FADD. Western blot analysis of DN-FADD in LN229, LN229DN-FADDc6 and LN229DN-FADDc8 cells (from Dr. Roos). ERK2 was used as the loading control. R.E. relative expression. (**B**) Quantification of induced apoptosis in the DN-FADD expression cells following 50 µM TMZ exposure and HIPK2 knockdown at the indicated time-point. Control samples were transfected with non-targeting siRNA, p values of < 0.005 are marked as ** and < 0.001 as ***.

The question of whether TMZ is able to induce the expression of FAS ligand (FAS-L) was also addressed. Upon exposure of LN229 cells to TMZ, the cells exhibited a robust increase in FAS-L levels (Figure 24).

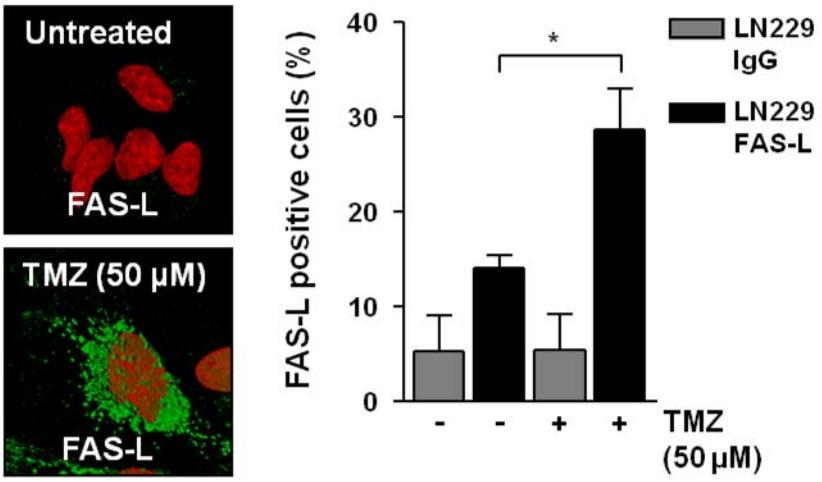

Figure 24 The expression of FAS-L in LN229 cells after TMZ treatment. Representative micrograms of FAS-L 72 h after 50 µM TMZ exposure in LN229 cells (left) determined by fluorescence microscopy, and percentage of FAS-L positive cells 72 h after 50 µM TMZ exposure in LN229 cells (right) quantified by flow cytometry, done by Dr. Roos, p values of < 0.05 are marked as *.

4.2.11 HIPK2 sensitizes CCNU-induced p53 protein accumulation, FAS-R and PTEN expression

A 2nd line drug in glioblastoma therapy is CCNU (lomustine), which is a chloroethylating agent forming secondary DNA crosslinks. Western blot results showed that neither total p53 nor p-p53ser15 were affected by HIPK2 knockdown. TMZ induced p-p53ser46 level and PTEN expression level decreased after HIPK2 knockdown compared to the treated sample without HIPK2 knockdown, while FAS-R didn't show a significant increase after CCNU treatment, although it had less signal after HIPK2 knockdown. The expression of PUMA, NOXA and BAX didn't change obviously after HIPK2 knockdown and CCNU treatment (Figure 25 A), which means PTEN and FAS-R may be involved in CCNU-induced HIPK2-p53 regulated DNA damage response. In LN229MGMT cells, as expected, MGMT strongly reduced the killing effect of CCNU (Figure 25 B) due to its ability to repair O^6-chloroethylguanine adducts (Nikolova, Roos et al. 2017).

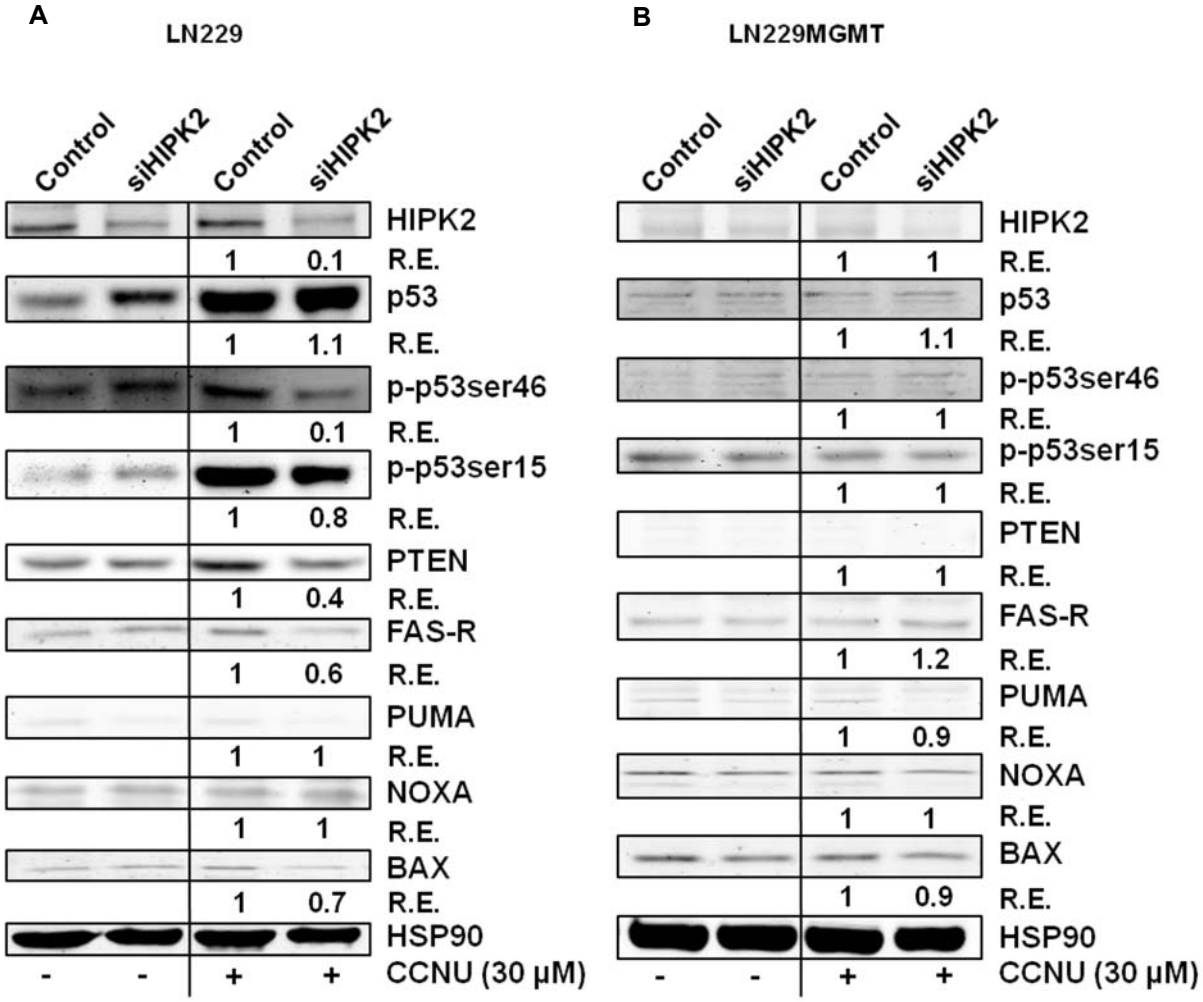

Figure 25 HIPK2 does not contribute to CCNU-induced apoptosis. Western blot analysis of HIPK2, p53, p-p53ser46, p-p53ser15, PTEN, FAS, PUMA, NOXA and BAX protein level in LN229 (**A**) and LN229MGMT (**B**) 96 h after CCNU exposure and HIPK2 knockdown. HSP90 was used as the loading control. Control samples were transfected with non-targeting siRNA.

4.2.12 CCNU-induced apoptosis is not affected by the knockdown of HIPK2

Now that we had results hinting that HIPK2 was also involved in CCNU induced DNA damage response. Since PTEN and FAS-R were affected after HIPK2 knockdown, it's necessary to know if these proteins increase the apoptosis level and cell death. As shown by apoptosis experiments, LN229MGMT cells were completely resistant to CCNU whereas LN229 was not. HIPK2 downregulation had a significant effect on TMZ-induced cell death, while knockdown of HIPK2 in LN229 didn't increase the resistance of LN229 cells to CCNU-induced cell death compared to the control LN229 (Figure 26 A,). Upon treatment with 50 µM TMZ, about 42% of LN229 cells were apoptotic (annexin V positive cells). Interestingly, in the LN229 HIPK2 knockdown the level was not reduced. Necrosis (annexin V/PI double-positive cells) was not much induced by CCNU (Figure 26 B), which is similar to TMZ, which barely induces necrosis. In LN229MGMT cells, as expected, MGMT strongly reduced the killing effect of CCNU (Figure 26 A and B) due to its ability to repair O^6-chloroethylguanine adducts (Nikolova, Roos et al. 2017), showing that the effects observed in LN229 cells that lack MGMT were brought about by O^6-chloroethylguanine, both in the presence and absence of HIPK2.

These results were confirmed by colony formation assays. After the knockdown of HIPK2, the cell survival rate stayed the same in control treated samples (Figure 27). Collectively, the data show that HIPK2 didn't sensitize glioblastoma cells to the CCNU-induced DNA damage response by stimulating apoptosis.

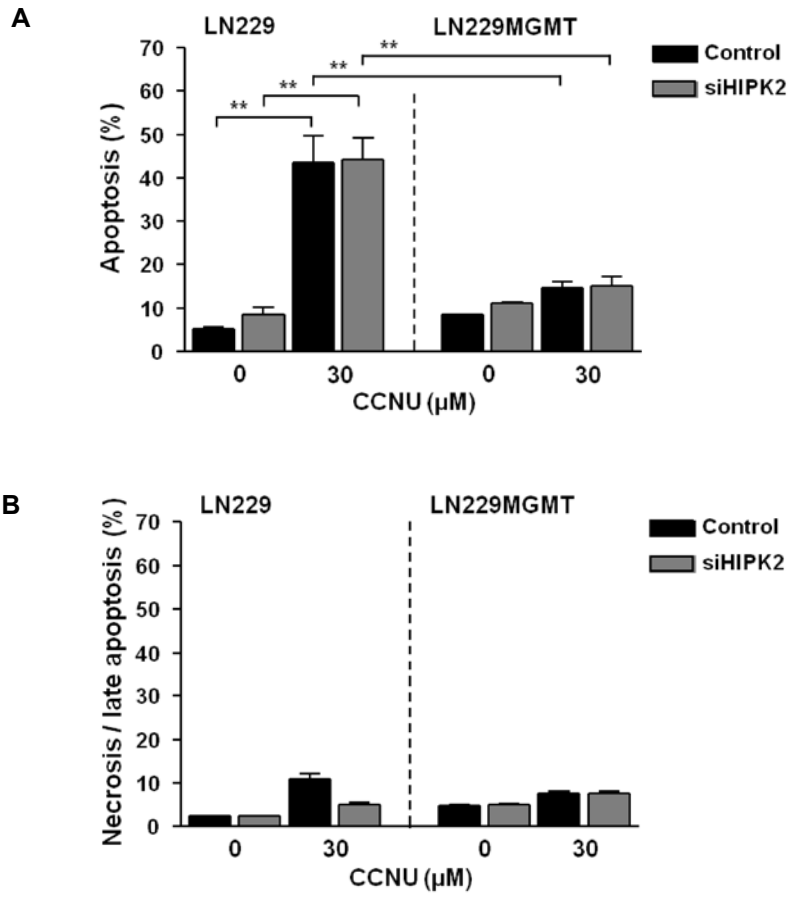

Figure 26 HIPK2 does not contribute to CCNU-induced apoptosis. Apoptosis (**A**) and necrosis (**B**) were induced 144 h after 30 µM CCNU exposure in LN229 and LN229MGMT cells following HIPK2 knockdown.

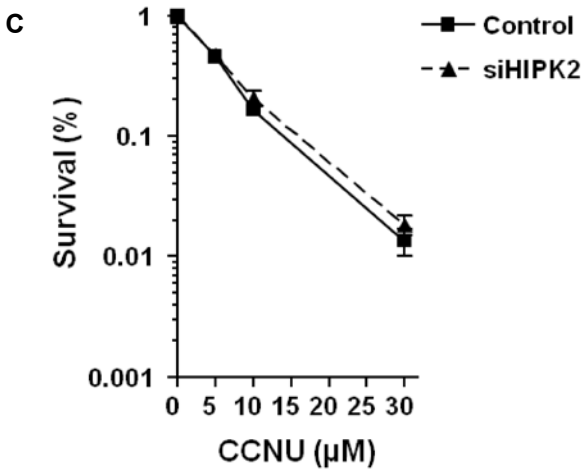

Figure 27 HIPK2 does not contribute to CCNU-induced cell death. Colony survival assay of LN229 cells exposed to the indicated concentrations of CCNU upon HIPK2 knockdown. Control samples were transfected with non-targeting siRNA.

4.2.13 Role of SIAH1 in the activation of HIPK2 in glioblastoma cells following TMZ treatment

A reported player in the regulation of HIPK2 stabilization is the E3 ubiquitin-protein ligase SIAH1 (Winter, Sombroek et al. 2008). For UV light it has been shown that following phosphorylation, SIAH1 is released from HIPK2 and the HIPK2 protein accumulates. In view of this scenario, the influence of SIAH1 on TMZ-induced apoptosis was determined by downregulating SIAH1, SIAH2 or SIAH1 and 2. As shown in Figure 28, TMZ induced HIPK2 stabilization, which was enhanced in the presence of SIAH1 or SIAH1 and 2 knockdowns, but not when exclusively SIAH2 was reduced. Accordingly, TMZ-induced apoptosis was significantly improved when SIAH1 or SIAH1 and 2 were knocked down (Figure 29). The sensitization observed with SIAH1 knockdown was not observed for SIAH2 knockdown. The results indicate that SIAH1 plays a critical role in apoptosis regulation in TMZ-treated glioblastoma cells, it negatively regulates TMZ-induced apoptosis by impact the function of HIPK2.

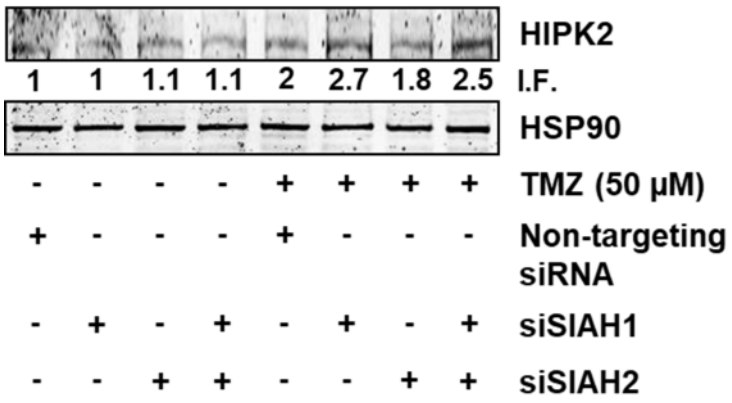

Figure 28 SIAH1 negatively impacts the expression of HIPK2 after TMZ exposure. Western blot analysis of HIPK2 in LN229 cells after 50 µM TMZ exposure, knocked-down for SIAH1, SIAH2 or SIAH1 and SIAH2. HSP90 was used as loading control. I.F. induction factor.

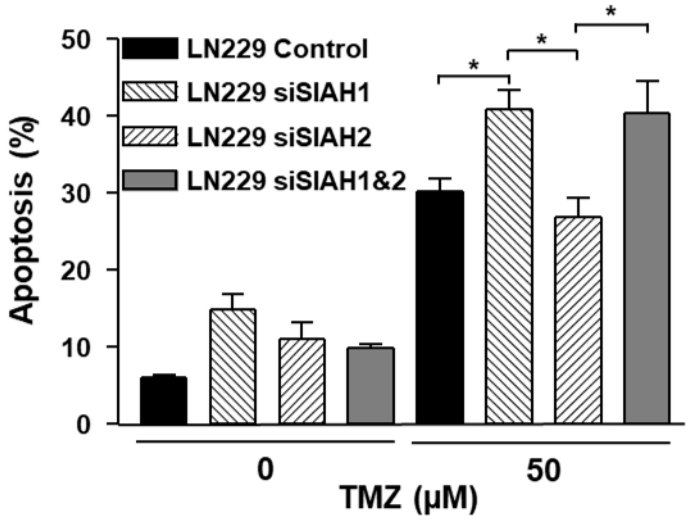

Figure 29 SIAH1 negatively impacts the function of HIPK2 in TMZ-induced apoptosis. Apoptosis levels of LN229 cells 144 h after 50 µM TMZ exposure, knocked-down for SIAH1, SIAH2 or SIAH1 and SIAH2. p-values of < 0.05 are marked as *, < 0.005 as ** and < 0.001 as ***.

4.2.14 HIPK2 and SIAH1 high expression in brain cancer tumors are more common than SIAH2

An in silico search for expression levels revealed that HIPK2 is expressed in glioblastomas *in situ* at about the same level as in normal brain and low-grade gliomas. The same is true for SIAH2. In contrast, SIAH1 is frequently overexpressed in gliomas, including glioblastoma multiforme (WHO grade IV) (Figure 30). Since SIAH1 is an inhibitor of HIPK2, whose activity is required to enhance the killing effect of TMZ in p53 wt glioblastoma cells, the data bear a significant impact on glioblastoma therapy as tumors with high SIAH1 expression may have a low therapeutic response.

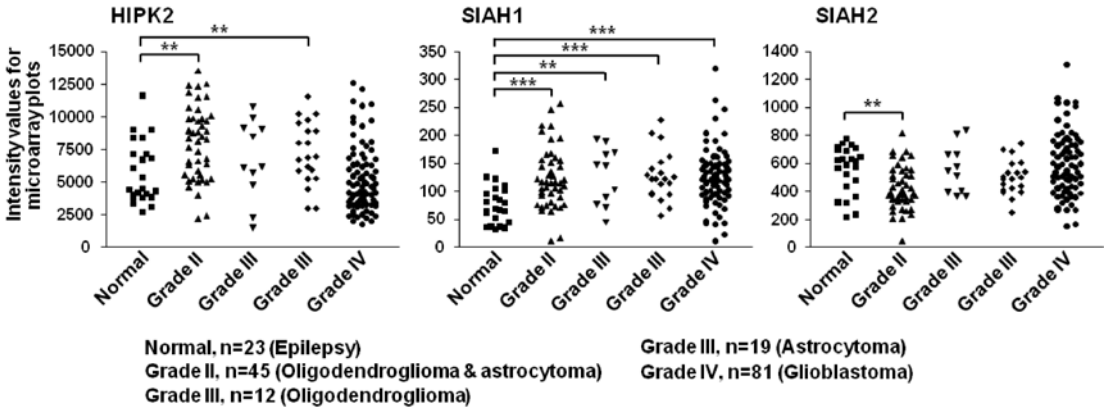

Figure 30 HIPK2, SIAH1 and SIAH2 expression in glioblastoma tumors. Using a public available microarray database the expression of HIPK2 (NM_022740), SIAH1 (NM_003031) and SIAH2 (NM_005067) was analysed in brain tissue from 23 epilepsy patients as well as tumour tissue from 45 grade II oligodendroglioma and astrocytoma patients, 12 grade III Oligodendroglioma patients, 19 grade III astrocytoma and 81 glioblastoma patients. Data are with kind permission from Dr. Roos. For the figure, p-values of < 0.05 are marked as *, < 0.005 as ** and < 0.001 as ***.

5 Discussion

Around 176,000 cases of central nervous system (CNS) cancer are diagnosed every year, the estimated annual mortality rate of 128,000 (Parkin 2001). Glioma is the most common intracranial tumor, accounting for approximate 50% of primary brain tumors. Glioblastoma is by far the most aggressive tumor (Davis, Freels et al. 1998). Currently, standard RT enrollment and temozolomide adjuvant chemotherapy after surgery are the standard treatment for patients with glioblastoma age <70 years, but the prognosis is still poor, with a average survival length of 12-15 months(Stupp 2005). Clearly, there is an urgent need to provide patients with more effective treatments (Minniti, Muni et al. 2009).

The reason for brain cancer is unclear. Although it has been discovered that several genetic abnormalities are associated with specific malignant diseases (Legler et al. 1999), until now only about 5% of primary brain cancers and genetic factors have been identified (Bondy 1994). Families with the excessive disease may have some genetic predispositions or they may be affected by environmental factors.

The only identified environmental risk factor for brain cancer is high dose of ionizing radiation (Ron et al. 1988). It has been reported that exposure to N-nitroso compounds, pesticides, polycyclic aromatic hydrocarbons or organic solvents may also increase the occurance risk of brain cancers (Inskip et al. 1995; Thomas and Inskip, 1996). The incidence of brain cancer is higher in the refining, rubber manufacturing (Kuijten and Bunin 1993; Marsh et al. 1991) and the farmers' industry (Brownson et al. 1990; Musicco et al. 1988).

Treatment of malignant brain cancer is a real challenge. The aim of both the threshold project and the HIPK2-p53 signaling project was to elucidate mechanisms of drug action that sensitize glioblastoma cells to TMZ and increase the potential chemotherapy effects of this agent.

5.1 Threshold in glioblastoma cells

In the threshold project, the aim was to find a possible threshold in LN229 and the mechanism behind a possible threshold. The working hypothesis was: at low doses, cells are tolerant of DNA damage caused by TMZ, p53 is phosphorylated at ser15 initially which induces the cell cycle arrested to keep cells from dying; when the TMZ doses increased beyond the cell's tolerance level, p53 will be phosphorylated at ser46, which start the apoptosis process. Similar experiments have been performed in RKO and LNCaP cells, where the nutlin-3 was used to induce p53 in order to mimic p53 activation in wild-type p53 tumors, after treatment with low doses (3 μM) of nutlin-3. Both cell lines showed growth arrest, while after higher doses (20 μM) of nutlin-3 treatment, RKO and LNCaP cells first went into arrest and then into the apoptosis pathway (Kracikova, Akiri et al. 2013).

In the threshold experiments with glioblastoma cells after TMZ treatment, we got unexpected results. The data show that the p53 level and its phosphorylated form p53ser15 and p53ser46 changed in a dynamic way, depending on the cell lines, replication cycles and doses of TMZ. In LN229 cells, the total p53 started accumulation if cells were treated with TMZ. The protein expression of p53 went up with increasing dose and time. The total p53 accumulation was dependent on the DNA damage. Importantly, the p53ser15 was not only expressed in cells following low dose TMZ treatment but also expressed in cells with high doses of TMZ. However, its protein expression declined at the second cell cycle. p-p53ser46 expression levels after TMZ treatment increased at 72 h. In this study, it was shown that the triggering of the DNA damage response and cell death pathways occur once cells have passed through two DNA replication cycles (Quiros, Roos et al. 2010).

TMZ induced DNA damage response start after two cell cycles with the help of cell replication and mismatch repair. A lack of a threshold was shown in LN229 cells, which can be explained by the lesions induced by TMZ. TMZ methylates DNA at different positions, inducing 13 different lesions (Kaina, Christmann et al. 2007). The main product is *N*7-methylguanine (*N*7MeG) while minor products are *N*3-methyladenine (*N*3MeA), *N*3-methylguanine (*N*3MeG), and O^6-methylguanine (O^6-MeG). These DNA adducts show different stabilities. *N*3MeA and *N*3MeG are easily hydrolyzed, *N*7MeG is stable for longer times and can be repaired by base excision repair. O^6-MeG is stable and persists in DNA in the absence of O^6-methylguanine-DNA methyltransferase (MGMT) (Pegg 2000). In MGMT depleted and MMR proficient LN229 cells, O^6-MeG induces DSBs and replication-blocking lesions that trigger the DNA damage response via ATM, ATR, CHK1, CHK2 and p53 (Kaina, Christmann et al. 2007). It has been shown that ATR contributes more to the protection against O^6-MeG toxicity than ATM (Eich, Roos et al. 2013).

A possible explanation for the threshold might be the p53 status differences of the cell lines, as p53 is majorly involved in apoptosis induction (Haupt, Berger et al. 2003). Comparing LN229 and the weak-responding cell line LN308 by western blot analysis showed that LN229 expresses wild-type p53 while LN308 does not. A172 was shown to express wild-type p53 as well (Park, Widi et al. 2006), showing that p53 might be involved in sensitizing both cell lines. However, the glioma cell line D-247, also expressing wild-type p53 did not show sensitization to TMZ-induced apoptosis after combination treatment thus suggesting a more complex signal cascade responsible for the observed effects which might yet be p53 dependent. It worth further study for the threshold and sensitivity to TMZ in glioblastoma cells.

5.2 Possible roles of p53ser15

Ser15 is an important target for p53 protein phosphorylation. Ser15 phosphorylation is

essential for the p53 transcription and also for its function. A investigation has proved that the PANDAR-binding protein SFRS2, a negative factor for regulating p53 and its phosphorylation at Serine 15, help the PANDAR-reduced cisplatin sensitivity, this leads to a reduction of p53-related pro-apoptotic genes, such as PUMA (Scheers, Palermo et al. 2018). In the first project, the results showed that the p53ser15 is induced by TMZ in glioblastoma LN229 cells at the early time point (24 h), when DSBs were induced by TMZ in the second cell cycle in LN229, p53ser15 was not as strongly induced as in the early time point. For another situation, it has been shown that inhibition of the Wip1 rescued p38 activation induced by hypoxia, while significantly compromised p53-Mdm2 binding, p-p53Ser15 was increased in this process (Tan, Tong et al. 2019).

Another research proved that p53ser15 is involved in the senescence pathway together with p-ATMser1981 and other downstream factors (Sakai, Kurokawa et al. 2019), p53ser15 is also shown works in ROS-mediated DNA damage (Wu, Fu et al. 2019). The phosphorylated p53ser15 levels are markedly induced in human epithelial cells 96 h after IR treatment, which is shown correlates with miR-34a transcription induced by IR and p38 MAPK signaling pathway (Wang, Li et al. 2013). ROP16 phosphorylates p53 at ser15/37 to mediate partially apoptosis and cell cycle arrest in SH-SY5Y cells (Chang, Shan et al. 2015).

5.3 Possible roles of p53ser46 and its relationship with HIPK2

Different factors causing p53 phosphorylation, resulting in different p53 phosphorylation sites, leading to different functions after p53 phosphorylation. Ser46 is another phosphorylation site other than ser15.

In the threshold project, p53ser46 showed clear relation with glioblastoma cell apoptosis after TMZ treatment. The apoptosis started when p53ser46 accumulation reached high amount (at least three times as control) in the glioblastoma cells, the apoptosis effect came relatively later after TMZ treatment than UV irradiation, this again consist with the finding that TMZ induces DNA DSBs in the second cell cycle.

P53 has a special role in TMZ induced apoptosis in glioblastoma cells, although there is no threshold found in p53 proficient LN229 cells, the p53 mutant LN308 cells showed strong resistance to apoptosis than LN229 with the similar level of DSBs formation after TMZ treatment. As a direct downstream factor of p53, p53ser46 is the essential factor in the TMZ triggered apoptosis process and the following cell death.

We confirmed the pro-apoptosis function of p53ser46 and explored HIPK2-p53ser46 related pathway in TMZ induced cell death. HIPK2 has been reported as a novel regulator of p53 function. HIPK2 phosphorylates Ser46 of p53, accelerating CBP acetylation of Lys382 of p53

(Hofmann, Möller et al. 2002). Phosphorylation of Ser46 by p53 and acetylation of Lys382 can induce the pro-apoptotic genes expression such as PUMA, BAX and p53AIP1, and also activate the exogenous death receptor pathway. When DNA damage or oxidative stress occurs, HIPK2 phosphorylates Ser46 of p53, promotes acetylation of Lys382, and activates the tumor suppressor gene p53, thereby promoting apoptosis. HIPK2 regulates p53 function in a variety of ways, including antagonizing the p53 inhibitor MDM2 (murine double minute 2), phosphorylating the 397 threonine residue of the p53 family member ΔNp63α to promote its degradation. Inhibition of HIPK2 strongly impairs the activity of p53, promotes tumor development, and promotes angiogenesis (Zhang, Yoshimatsu et al. 2003, Puca, Nardinocchi et al. 2009).

5.4 Interaction of HIPK2-p53 with DNA damage response factors

The main issue of the second project is to explore the role of HIPK2 and its negative regulating p53ser46 in the regulation of apoptosis triggered by *O*^{6}-MeG. This DNA damage is induced by methylating agents, including TMZ, which is the first-line chemotherapeutic for the treatment of malignant gliomas. Like other S_N1 methylating agents, TMZ induces many different kinds of DNA lesions, including *O*- and *N*-alkylations. Although produced in small amounts (~ 7% of total alkylation products), *O*^{6}-MeG is responsible for the majority of killing effects if TMZ is administered at low dose, i.e. <100 µM, which is relevant in the therapeutic situation (Newlands, Stevens et al. 1997, Mayo, Seo et al. 2005).

TMZ at dose levels below 100 µM induces mainly apoptosis. The pathway of *O*^{6}-MeG triggered apoptosis has been elucidated in detail (Roos, Batista et al. 2007). It can be split up into two sections, an upstream genotoxic and a downstream execution pathway. Upstream is characterized by the transforming *O*^{6}-MeG lesions into DSBs. It is generally accepted that this requires DNA replication and MMR operating on *O*^{6}-MeG/T mismatches. It was hypothesized (Karran and Bignami 1992) and experimentally verified (Branch, Aquilina et al. 1993) that MMR through MSH2, MSH6, PMS2, MLH1 and ExoIII generates, following removal of thymine on *O*^{6}MeG/T mismatches, long stretches of the single-stranded DNA (Mojas, Lopes et al. 2007), which strongly interfere with DNA replication in the 2_{nd} replication cycle giving rise to transient and, if not properly repaired, persistent DSBs (Ochs and Kaina 2000, Quiros, Roos et al. 2011). The block in replication, resulting from futile MMR cycles, and DSBs resulting from the collapse of replication forks, are key activators of the downstream DDR evoked by the primary lesion *O*^{6}MeG.

In the *O*^{6}-MeG triggered DDR following TMZ treatment, ATR and CHK1 activation are the

primary response players, followed later on by ATM/CHK2 activation (Eich, Roos et al. 2013). Experiments with pharmacological inhibitors confirmed that ATR/CHK1 is the key player in preventing the activation of the downstream killing response through apoptosis (Eich, Roos et al. 2013). Both ATR and ATM can phosphorylate p53 at serine 15, leading to its stabilization (Nakagawa, Taya et al. 1999, Hammond, Denko et al. 2002) and transcriptional activation of p21 (Loughery, Cox et al. 2014). The protective function of the p53-dependent cell cycle arrest observed in glioma cells exposed to TMZ (Hirose, Berger et al. 2001) can, therefore, be traced back to the activation of ATR and ATM. Paralleling this protective effect of p53, p53 was also identified as the trigger for the death receptor FAS (alias CD95/APO1) stimulated apoptosis pathway (Roos, Batista et al. 2007). In addition, p53wt glioma cells are more sensitive to TMZ, responding with a higher apoptosis frequency compared to glioma cells mutated for p53 (Roos, Batista et al. 2007), and thus it was reasonable to conclude that the apoptotic FAS pathway is more responsive than the mitochondrial apoptosis pathway (Roos, Batista et al. 2007).

In view of the dichotomic character of p53, we wished to know in more detail how p53 is able to make the switch from cell survival to death. Upon DNA damage, p53 is phosphorylated at several sites, including Ser15 and Ser46. Unlike p53Ser15, the phosphorylation at Ser46 was shown to be mediated by the kinase HIPK2 (D'Orazi, Cecchinelli et al. 2002). This DDR enzyme is localized in the nucleus (Siepi, Gatti et al. 2013) and, under normal conditions (i.e. without genotoxic stress), inactivated by the E3 ubiquitin-protein ligase SIAH1 (Hwang, Lee et al. 2013). Upon DNA damage, SIAH1 becomes phosphorylated by ATM, which causes it to disassociate from HIPK2 and HIPK2 accumulates in the cells (Winter, Sombroek et al. 2008). HIPK2 in turn phosphorylates p53 at ser46, thus stimulating its transactivating activity. This was shown to be the case for cells exposed to ultraviolet light (D'Orazi, Cecchinelli et al. 2002, Hofmann, Moller et al. 2002), ionising radiation (Dauth, Kruger et al. 2007) and doxorubicin (Puca, Nardinocchi et al. 2009). Here, we demonstrate for the first time, that alkylating agents, notably the S_N1 methylating agent TMZ, is able to trigger this pathway. Since MGMT expressing cells, in which the TMZ-induced damage *O*^{6}MeG is quickly repaired, do not show HIPK2 activation and p53ser46 phosphorylation, we conclude that this specific lesion is responsible for eliciting the response. Thus, *O*^{6}MeG is a highly effective inducer of the SIAH1-HIPK2 pathway, which is remarkable as TMZ, like other S_N1 methylating agents, induces 13 different DNA lesions, with the minor lesion *O*^{6}MeG (amounting to maximally 8% of total methylation products) being so effective in killing cells (Kaina, Christmann et al. 2007). It is conceivable that the major *N*-alkylations are also cytotoxic, but this is only the case if *O*^{6}MeG is completely repaired by MGMT and cells were exposed to much higher doses of TMZ or other S_N1 methylating genotoxic drugs.

We also demonstrate that upon TMZ, HIPK2 is the only kinase phosphorylating p53 at serine 46, which is considered to be a pro-apoptotic event. p-p53ser46 was previously demonstrated to transcriptionally activate several pro-apoptotic target genes, including *PTEN* (Mayo, Seo et

al. 2005) and *NOXA* (Ichwan, Yamada et al. 2006). However, we did not find an effect of HIPK2 knockdown on the upregulation of these genes, nor on *BBC3* (PUMA) and *BAX* in TMZ treated p53wt glioblastoma cells. Another transcriptional target of p53 is the death receptor FAS (Muller, Wilder et al. 1998, Pohl, Wagenknecht et al. 1999), which has been shown to be induced by TMZ in a p53-dependent manner (Roos, Batista et al. 2007). The expression of FAS mRNA and protein was enhanced following O^6MeG induction and reduced if HIPK2 was knocked down. At the same time, the TMZ-induced level of apoptosis was significantly reduced, suggesting that the HIPK2/p-p53Ser46/FAS pathway is decisively triggered in TMZ-induced apoptosis. This was further substantiated by blocking the FAS pathway following DN-FADD expression, which abrogated the HIPK2 driven apoptotic response. Under the treatment conditions (50 µM TMZ) necrosis was only marginally induced, which indicates that the O^6MeG response played the major role. Previously, we showed that for p53wt glioblastoma cells, lower doses of TMZ were required to induce a given apoptosis level than in p53mt cells. p53mt cells undergo O^6-MeG triggered apoptosis through utilizing the mitochondrial pathway, which is, however, less responsive to signals elicited by O^6-MeG/MMR. Whether the data can be translated to the therapeutic situation remains to be seen. Downregulation of either SIAH1, SIAH2 or both SIAH1&2 revealed that SIAH1 is the principle regulator of HIPK2 upon exposure of glioblastoma cells to TMZ. It is striking that gliomas frequently overexpress SIAH1 and, therefore, it is conceivable that this fraction of tumors is impaired in activating the FAS driven cell death pathways. It is, therefore, reasonable to estimate that downregulation, or pharmacological inhibition, of SIAH1 has a positive impact on therapy with TMZ.

It is also worth to note that the modulation of the HIPK2 pathway had no significant effect on the killing response of glioma cells to CCNU treatment, which is sometimes used concomitantly with TMZ or as second-line therapeutic. CCNU induces O^6-chloroethylguanine and secondary inter-strand crosslinks (ICL), which are highly cytotoxic lesions through blocking transcription and replication (Nikolova, Roos et al. 2017). It thus appears that ICL do not trigger the HIPK2 pathway as efficiently as O^6-MeG/MMR derived lesions do.

5.5 Concluding remarks

In the first project, the data demonstrated that there is no threshold for TMZ-induced apoptosis, senescence or autophagy, while p53 plays an essential role in the DNA damage response induced by TMZ, p53 deficient cells showed less sensitivity than p53 proficient cells, phosphorylated p53ser15 and p53ser46 accumulated with time, p53ser46 signal went up later than p53ser15, it can be seen as a marker for apoptosis, the results also provide the basis for the study of HIPK2 and p53 in the second project, the mechanism behind needs to be further studied, LN308 and LN229 cells display the same amount of DSBs after TMZ exposure, why do they show such a different response to TMZ-induced cell death and apoptosis?

In the second HIPK2-p53 project, the data revealed a new DDR pathway triggered by the cytotoxic (and mutagenic) DNA lesion O^6MeG. These findings have clear therapeutic implications, paving the way for new strategies in fostering death functions and blocking survival traits in tumor cells. This very likely pertains not only to treatments with TMZ, but also other anticancer drugs such as dacarbazine (DTIC), procarbazine and streptozotozine (Kaina, Christmann et al. 2007, Fu, Calvo et al. 2012), which act on molecular level in the same way as TMZ and are being used in the therapy of other cancers such as malignant melanoma, Hodgkin lymphoma and island cell carcinoma. Although O^6-MeG is an important clinically relevant DNA damage, it is also induced by methylating environmental and food-borne carcinogens (Lijinsky 1999, Fu, Calvo et al. 2012). Therefore, the identification of the SIAH1/HIPK2/p-p53ser46 axis triggered by O^6-MeG is not only important for cancer therapy but has also far-reaching implications for carcinogenesis, as cells harboring mutagenic and carcinogenic O^6-MeG lesions may selectively be removed through this death pathway.

6 References

Agarwal, S., D. K. Jangir, P. Singh and R. Mehrotra (2014). "Spectroscopic analysis of the interaction of lomustine with calf thymus DNA." Journal of Photochemistry and Photobiology B: Biology **130**: 281-286.

Al-Mefty, O., J. E. Kersh, A. Routh and R. R. Smith (1990). "The long-term side effects of radiation therapy for benign brain tumors in adults." Journal of neurosurgery **73**(4): 502-512.

Asthagiri, A. R., N. Pouratian, J. Sherman, G. Ahmed and M. E. Shaffrey (2007). "Advances in brain tumor surgery." Neurologic clinics **25**(4): 975-1003.

Batista, L. F., W. P. Roos, M. Christmann, C. F. Menck and B. Kaina (2007). "Differential sensitivity of malignant glioma cells to methylating and chloroethylating anticancer drugs: p53 determines the switch by regulating xpc, ddb2, and DNA double-strand breaks." Cancer research **67**(24): 11886-11895.

Bayer, N., D. Schober, E. Prchla, R. F. Murphy, D. Blaas and R. Fuchs (1998). "Effect of bafilomycin A1 and nocodazole on endocytic transport in HeLa cells: implications for viral uncoating and infection." Journal of virology **72**(12): 9645-9655.

Beranek, D. T. (1990). "Distribution of methyl and ethyl adducts following alkylation with monofunctional alkylating agents." Mutation Research/Fundamental and Molecular Mechanisms of Mutagenesis **231**(1): 11-30.

Bitomsky, N., E. Conrad, C. Moritz, T. Polonio-Vallon, D. Sombroek, K. Schultheiss, C. Glas, V. Greiner, C. Herbel and F. Mantovani (2013). "Autophosphorylation and Pin1 binding coordinate DNA damage-induced HIPK2 activation and cell death." Proceedings of the National Academy of Sciences: 201310001.

Black, P. M. (1991). "Brain tumors." New England Journal of Medicine **324**(22): 1555-1564.

Bradford, M. M. (1976). "A rapid and sensitive method for the quantitation of microgram quantities of protein utilizing the principle of protein-dye binding." Analytical biochemistry **72**(1-2): 248-254.

Branch, P., G. Aquilina, M. Bignami and P. Karran (1993). "Defective mismatch binding and a mutator phenotype in cells tolerant to DNA damage." Nature **362**(6421): 652-654.

Brierley, J. D., T. Panzarella, R. W. Tsang, M. K. Gospodarowicz and B. O'Sullivan (1997). "A comparison of different staging systems predictability of patient outcome: thyroid carcinoma as an example." Cancer: Interdisciplinary International Journal of the American Cancer Society **79**(12): 2414-2423.

Bulavin, D. V., S. Saito, M. C. Hollander, K. Sakaguchi, C. W. Anderson, E. Appella and A. J. Fornace (1999). "Phosphorylation of human p53 by p38 kinase coordinates N‐terminal phosphorylation and apoptosis in response to UV radiation." The EMBO journal **18**(23):

6845-6854.

Canner, J., M. Sobo, S. Ball, B. Hutzen, S. DeAngelis, W. Willis, A. Studebaker, K. Ding, S. Wang and D. Yang (2009). "MI-63: a novel small-molecule inhibitor targets MDM2 and induces apoptosis in embryonal and alveolar rhabdomyosarcoma cells with wild-type p53." British journal of cancer **101**(5): 774.

Chang, S., X. Shan, X. Li, W. Fan, S. Q. Zhang, J. Zhang, N. Jiang, D. Ma and Z. Mao (2015). "Toxoplasma gondii rhoptry protein ROP16 mediates partially SH-SY5Y cells apoptosis and cell cycle arrest by directing Ser15/37 phosphorylation of p53." International journal of biological sciences **11**(10): 1215.

Choi, C. Y., Y. H. Kim, H. J. Kwon and Y. Kim (1999). "The homeodomain protein NK-3 recruits Groucho and a histone deacetylase complex to repress transcription." Journal of Biological Chemistry **274**(47): 33194-33197.

Choi, D. W., Y.-M. Seo, E.-A. Kim, K. S. Sung, J. W. Ahn, S.-J. Park, S.-R. Lee and C. Y. Choi (2008). "Ubiquitination and degradation of homeodomain-interacting protein kinase 2 by WD40 repeat/SOCS box protein WSB-1." Journal of Biological Chemistry **283**(8): 4682-4689.

Conrad, E., T. Polonio-Vallon, M. Meister, S. Matt, N. Bitomsky, C. Herbel, M. Liebl, V. Greiner, B. Kriznik and S. Schumacher (2016). "HIPK2 restricts SIRT1 activity upon severe DNA damage by a phosphorylation-controlled mechanism." Cell death and differentiation **23**(1): 110.

Crone, J., C. Glas, K. Schultheiss, J. Moehlenbrink, E. Krieghoff-Henning and T. G. Hofmann (2011). "Zyxin is a critical regulator of the apoptotic HIPK2-p53 signaling axis." Cancer research: canres. 3486.2010.

D'Orazi, G., B. Cecchinelli, T. Bruno, I. Manni, Y. Higashimoto, S. Saito, M. Gostissa, S. Coen, A. Marchetti, G. Del Sal, G. Piaggio, M. Fanciulli, E. Appella and S. Soddu (2002). "Homeodomain-interacting protein kinase-2 phosphorylates p53 at Ser 46 and mediates apoptosis." Nat Cell Biol **4**(1): 11-19.

D'Orazi, G., B. Cecchinelli, T. Bruno, I. Manni, Y. Higashimoto, S. i. Saito, M. Gostissa, S. Coen, A. Marchetti and G. Del Sal (2002). "Homeodomain-interacting protein kinase-2 phosphorylates p53 at Ser 46 and mediates apoptosis." Nature cell biology **4**(1): 11.

Dandy, W. E. (1933). Benign tumors in the third ventricle of the brain: diagnosis and treatment, Classics of Surgery Library.

Darzynkiewicz, Z. (2011). "Novel strategies of protecting non-cancer cells during chemotherapy: Are they ready for clinical testing?" Oncotarget **2**(3): 107.

Dauth, I., J. Krüger and T. G. Hofmann (2007). "Homeodomain-interacting protein kinase 2 is the ionizing radiation–activated p53 serine 46 kinase and is regulated by ATM." Cancer research **67**(5): 2274-2279.

Dauth, I., J. Kruger and T. G. Hofmann (2007). "Homeodomain-interacting protein kinase 2 is the ionizing radiation-activated p53 serine 46 kinase and is regulated by ATM." Cancer Res **67**(5): 2274-2279.

Davis, F. G., S. Freels, J. Grutsch, S. Barlas and S. Brem (1998). "Survival rates in patients with primary malignant brain tumors stratified by patient age and tumor histological type: an analysis based on Surveillance, Epidemiology, and End Results (SEER) data, 1973–1991." Journal of neurosurgery **88**(1): 1-10.

de la Vega, L., K. Fröbius, R. Moreno, M. A. Calzado, H. Geng and M. L. Schmitz (2011). "Control of nuclear HIPK2 localization and function by a SUMO interaction motif." Biochimica et Biophysica Acta (BBA)-Molecular Cell Research **1813**(2): 283-297.

de la Vega, L., I. Grishina, R. Moreno, M. Krüger, T. Braun and M. L. Schmitz (2012). "A redox-regulated SUMO/acetylation switch of HIPK2 controls the survival threshold to oxidative stress." Molecular cell **46**(4): 472-483.

DeAngelis, L. M. (2001). "Brain tumors." New England Journal of Medicine **344**(2): 114-123.

Di Stefano, V., G. Blandino, A. Sacchi, S. Soddu and G. D'orazi (2004). "HIPK2 neutralizes MDM2 inhibition rescuing p53 transcriptional activity and apoptotic function." Oncogene **23**(30): 5185.

DiPiro, J. T., R. L. Talbert, G. C. Yee, G. R. Matzke, B. G. Wells and L. M. Posey (2014). Pharmacotherapy: a pathophysiologic approach, McGraw-Hill Education New York.

Drabløs, F., E. Feyzi, P. A. Aas, C. B. Vaagbø, B. Kavli, M. S. Bratlie, J. Peña-Diaz, M. Otterlei, G. Slupphaug and H. E. Krokan (2004). "Alkylation damage in DNA and RNA—repair mechanisms and medical significance." DNA repair **3**(11): 1389-1407.

Drappatz, J., D. Schiff, S. Kesari, A. D. Norden and P. Y. Wen (2007). "Medical management of brain tumor patients." Neurologic clinics **25**(4): 1035-1071.

Eich, M., W. P. Roos, T. Nikolova and B. Kaina (2013). "Contribution of ATM and ATR to the resistance of glioblastoma and malignant melanoma cells to the methylating anticancer drug temozolomide." Molecular cancer therapeutics **12**(11): 2529-2540.

Eich, M., W. P. Roos, T. Nikolova and B. Kaina (2013). "Contribution of ATM and ATR to the resistance of glioblastoma and malignant melanoma cells to the methylating anticancer drug temozolomide." Mol Cancer Ther **12**(11): 2529-2540.

Esteller, M., J. Garcia-Foncillas, E. Andion, S. N. Goodman, O. F. Hidalgo, V. Vanaclocha, S. B. Baylin and J. G. Herman (2000). "Inactivation of the DNA-repair gene MGMT and the clinical response of gliomas to alkylating agents." N Engl J Med **343**(19): 1350-1354.

Esteller, M., S. R. Hamilton, P. C. Burger, S. B. Baylin and J. G. Herman (1999). "Inactivation of the DNA repair gene O6-methylguanine-DNA methyltransferase by promoter hypermethylation

is a common event in primary human neoplasia." Cancer Res **59**(4): 793-797.

Fang, Z., M. Kulldorff and D. I. Gregorio (2004). "Brain cancer mortality in the United States, 1986 to 1995: a geographic analysis." Neuro-oncology **6**(3): 179-187.

Foertsch, F., A. Szambowska, A. Weise, A. Zielinski, B. Schlott, F. Kraft, K. Mrasek, K. Borgmann, H. Pospiech and F. Grosse (2016). "S100A11 plays a role in homologous recombination and genome maintenance by influencing the persistence of RAD51 in DNA repair foci." Cell Cycle **15**(20): 2766-2779.

Franken, N. A., H. M. Rodermond, J. Stap, J. Haveman and C. Van Bree (2006). "Clonogenic assay of cells in vitro." Nature protocols **1**(5): 2315.

Fu, D., J. A. Calvo and L. D. Samson (2012). "Balancing repair and tolerance of DNA damage caused by alkylating agents." Nat Rev Cancer **12**(2): 104-120.

Fukunaga-Takenaka, R., K. Fukunaga, M. Tatemichi and H. Ohshima (2003). "Nitric oxide prevents UV-induced phosphorylation of the p53 tumor-suppressor protein at serine 46: a possible role in inhibition of apoptosis." Biochemical and biophysical research communications **308**(4): 966-974.

Goodenberger, M. L. and R. B. Jenkins (2012). "Genetics of adult glioma." Cancer genetics **205**(12): 613-621.

Guo, A., P. Salomoni, J. Luo, A. Shih, S. Zhong, W. Gu and P. P. Pandolfi (2000). "The function of PML in p53-dependent apoptosis." Nature cell biology **2**(10): 730.

Hammond, E. M., N. C. Denko, M. J. Dorie, R. T. Abraham and A. J. Giaccia (2002). "Hypoxia links ATR and p53 through replication arrest." Mol Cell Biol **22**(6): 1834-1843.

Han, E.-S., F. L. Muller, V. I. Pérez, W. Qi, H. Liang, L. Xi, C. Fu, E. Doyle, M. Hickey and J. Cornell (2008). "The in vivo gene expression signature of oxidative stress." Physiological genomics **34**(1): 112-126.

Happold, C., P. Roth, W. Wick, N. Schmidt, A. M. Florea, M. Silginer, G. Reifenberger and M. Weller (2012). "Distinct molecular mechanisms of acquired resistance to temozolomide in glioblastoma cells." J Neurochem **122**(2): 444-455.

Haupt, S., M. Berger, Z. Goldberg and Y. Haupt (2003). "Apoptosis-the p53 network." Journal of cell science **116**(20): 4077-4085.

Hegi, M. E., A. C. Diserens, T. Gorlia, M. F. Hamou, N. de Tribolet, M. Weller, J. M. Kros, J. A. Hainfellner, W. Mason, L. Mariani, J. E. Bromberg, P. Hau, R. O. Mirimanoff, J. G. Cairncross, R. C. Janzer and R. Stupp (2005). "MGMT gene silencing and benefit from temozolomide in glioblastoma." N Engl J Med **352**(10): 997-1003.

Hirose, Y., M. S. Berger and R. O. Pieper (2001). "p53 effects both the duration of G2/M arrest

and the fate of temozolomide-treated human glioblastoma cells." Cancer Res **61**(5): 1957-1963.

Hochberg, F. H. and A. Pruitt (1980). "Assumptions in the radiotherapy of glioblastoma." Neurology **30**(9): 907-907.

Hock, A. K., A. M. Vigneron, S. Carter, R. L. Ludwig and K. H. Vousden (2011). "Regulation of p53 stability and function by the deubiquitinating enzyme USP42." The EMBO journal **30**(24): 4921-4930.

Hofmann, T. G., A. Möller, H. Sirma, H. Zentgraf, Y. Taya, W. Dröge, H. Will and M. L. Schmitz (2002). "Regulation of p53 activity by its interaction with homeodomain-interacting protein kinase-2." Nature cell biology **4**(1): 1.

Hofmann, T. G., A. Moller, H. Sirma, H. Zentgraf, Y. Taya, W. Droge, H. Will and M. L. Schmitz (2002). "Regulation of p53 activity by its interaction with homeodomain-interacting protein kinase-2." Nat Cell Biol **4**(1): 1-10.

Hofseth, L. J., S. P. Hussain and C. C. Harris (2004). "p53: 25 years after its discovery." Trends in pharmacological sciences **25**(4): 177-181.

Hwang, J., S. Y. Lee, J. R. Choi, K. S. Shin, C. Y. Choi and S. J. Kang (2013). "SIRT1 negatively regulates the protein stability of HIPK2." Biochem Biophys Res Commun **441**(4): 799-804.

Ichwan, S. J., S. Yamada, P. Sumrejkanchanakij, E. Ibrahim-Auerkari, K. Eto and M. A. Ikeda (2006). "Defect in serine 46 phosphorylation of p53 contributes to acquisition of p53 resistance in oral squamous cell carcinoma cells." Oncogene **25**(8): 1216-1224.

Ichwan, S. J. A., S. Yamada, P. Sumrejkanchanakij, E. Ibrahim-Auerkari, K. Eto and M. Ikeda (2006). "Defect in serine 46 phosphorylation of p53 contributes to acquisition of p53 resistance in oral squamous cell carcinoma cells." Oncogene **25**(8): 1216.

Kaina, B., M. Christmann, S. Naumann and W. P. Roos (2007). "MGMT: key node in the battle against genotoxicity, carcinogenicity and apoptosis induced by alkylating agents." DNA Repair (Amst) **6**(8): 1079-1099.

Kaina, B., M. Christmann, S. Naumann and W. P. Roos (2007). "MGMT: key node in the battle against genotoxicity, carcinogenicity and apoptosis induced by alkylating agents." DNA repair **6**(8): 1079-1099.

Kaina, B., A. Ziouta, K. Ochs and T. Coquerelle (1997). "Chromosomal instability, reproductive cell death and apoptosis induced by O 6-methylguanine in Mex−, Mex+ and methylation-tolerant mismatch repair compromised cells: facts and models." Mutation Research/Fundamental and Molecular Mechanisms of Mutagenesis **381**(2): 227-241.

Karran, P. and M. Bignami (1992). "Self-destruction and tolerance in resistance of mammalian

cells to alkylation damage." Nucleic Acids Res **20**(12): 2933-2940.

Keinan-Boker, L., E. Friedman and B. G. Silverman (2018). "Trends in the incidence of primary brain, central nervous system and intracranial tumors in Israel, 1990–2015." Cancer epidemiology **56**: 6-13.

Kim, E.-J., J.-S. Park and S.-J. Um (2002). "Identification and Characterization of HIPK2 Interacting with p73 and Modulating Functions of the p53 Familyin Vivo." Journal of Biological Chemistry **277**(35): 32020-32028.

Kim, Y. H., C. Y. Choi, S.-J. Lee, M. A. Conti and Y. Kim (1998). "Homeodomain-interacting protein kinases, a novel family of co-repressors for homeodomain transcription factors." Journal of Biological Chemistry **273**(40): 25875-25879.

Knizhnik, A. V., W. P. Roos, T. Nikolova, S. Quiros, K.-H. Tomaszowski, M. Christmann and B. Kaina (2013). "Survival and death strategies in glioma cells: autophagy, senescence and apoptosis triggered by a single type of temozolomide-induced DNA damage." PloS one **8**(1): e55665.

Kondziolka, D., A. Patel, L. D. Lunsford, A. Kassam and J. C. Flickinger (1999). "Stereotactic radiosurgery plus whole brain radiotherapy versus radiotherapy alone for patients with multiple brain metastases." International Journal of Radiation Oncology* Biology* Physics **45**(2): 427-434.

Kracikova, M., G. Akiri, A. George, R. Sachidanandam and S. Aaronson (2013). "A threshold mechanism mediates p53 cell fate decision between growth arrest and apoptosis." Cell death and differentiation **20**(4): 576.

Langleben, D. D. and G. M. Segall (2000). "PET in differentiation of recurrent brain tumor from radiation injury." Journal of Nuclear Medicine **41**(11): 1861-1867.

Lee, M.-G., J. Han, S.-I. Jeong, N.-G. Her, J.-H. Lee, T.-K. Ha, M.-J. Kang, B.-K. Ryu and S.-G. Chi (2014). "XAF1 directs apoptotic switch of p53 signaling through activation of HIPK2 and ZNF313." Proceedings of the National Academy of Sciences **111**(43): 15532-15537.

Lijinsky, W. (1999). "N-Nitroso compounds in the diet." Mutat Res **443**(1-2): 129-138.

Lin, Z., H. Kong, M. Nei and H. Ma (2006). "Origins and evolution of the recA/RAD51 gene family: evidence for ancient gene duplication and endosymbiotic gene transfer." Proceedings of the National Academy of Sciences **103**(27): 10328-10333.

Loughery, J., M. Cox, L. M. Smith and D. W. Meek (2014). "Critical role for p53-serine 15 phosphorylation in stimulating transactivation at p53-responsive promoters." Nucleic Acids Res **42**(12): 7666-7680.

Loughery, J., M. Cox, L. M. Smith and D. W. Meek (2014). "Critical role for p53-serine 15 phosphorylation in stimulating transactivation at p53-responsive promoters." Nucleic acids

research **42**(12): 7666-7680.

Martin, V., E. Moyal, M. Delannes, L. Padovani, M. Sunyach, L. Feuvret, F. Dhermain, G. Noël and A. Laprie (2013). "Radiotherapy for brain tumors: which margins should we apply?" Cancer radiotherapie: journal de la Societe francaise de radiotherapie oncologique **17**(5-6): 434-443.

Matsukado, Y., C. S. MacCarty and J. W. Kernohan (1961). "The growth of glioblastoma multiforme (astrocytomas, grades 3 and 4) in neurosurgical practice." Journal of neurosurgery **18**(5): 636-644.

Mayo, L. D., Y. R. Seo, M. W. Jackson, M. L. Smith, J. R. Guzman, C. K. Korgaonkar and D. B. Donner (2005). "Phosphorylation of human p53 at serine 46 determines promoter selection and whether apoptosis is attenuated or amplified." Journal of Biological Chemistry **280**(28): 25953-25959.

Mayo, L. D., Y. R. Seo, M. W. Jackson, M. L. Smith, J. Rivera Guzman, C. K. Korgaonkar and D. B. Donner (2005). "Phosphorylation of human p53 at serine 46 determines promoter selection and whether apoptosis is attenuated or amplified." J Biol Chem **280**(28): 25953-25959.

Meikrantz, W., M. A. Bergom, A. Memisoglu and L. Samson (1998). "O6-alkylguanine DNA lesions trigger apoptosis." Carcinogenesis **19**(2): 369-372.

Minniti, G., R. Muni, G. Lanzetta, P. Marchetti and R. M. Enrici (2009). "Chemotherapy for glioblastoma: current treatment and future perspectives for cytotoxic and targeted agents." Anticancer research **29**(12): 5171-5184.

Mojas, N., M. Lopes and J. Jiricny (2007). "Mismatch repair-dependent processing of methylation damage gives rise to persistent single-stranded gaps in newly replicated DNA." Genes Dev **21**(24): 3342-3355.

Muller, M., S. Wilder, D. Bannasch, D. Israeli, K. Lehlbach, M. Li-Weber, S. L. Friedman, P. R. Galle, W. Stremmel, M. Oren and P. H. Krammer (1998). "p53 activates the CD95 (APO-1/Fas) gene in response to DNA damage by anticancer drugs." J Exp Med **188**(11): 2033-2045.

Nakagawa, K., Y. Taya, K. Tamai and M. Yamaizumi (1999). "Requirement of ATM in phosphorylation of the human p53 protein at serine 15 following DNA double-strand breaks." Mol Cell Biol **19**(4): 2828-2834.

Newlands, E. S., M. F. Stevens, S. R. Wedge, R. T. Wheelhouse and C. Brock (1997). "Temozolomide: a review of its discovery, chemical properties, pre-clinical development and clinical trials." Cancer Treat Rev **23**(1): 35-61.

Nguyen, Q.-B., R. Amato, R. Riascos, L. Ballester, N. Tandon, A. Blanco and Y. Esquenazi (2018). "Fluciclovine, Anti-1-amino-3-[18F]-fluorocyclobutane-1-carboxylic acid: A Novel Radiotracer for Meningioma." World Neurosurgery.

Nicol, S. M., S. E. Bray, H. D. Black, S. A. Lorimore, E. G. Wright, D. P. Lane, D. W. Meek, P. J. Coates and F. V. Fuller-Pace (2013). "The RNA helicase p68 (DDX5) is selectively required for the induction of p53-dependent p21 expression and cell-cycle arrest after DNA damage." Oncogene **32**(29): 3461.

Nikolova, T., W. P. Roos, O. H. Krämer, H. M. Strik and B. Kaina (2017). "Chloroethylating nitrosoureas in cancer therapy: DNA damage, repair and cell death signaling." Biochimica et Biophysica Acta (BBA)-Reviews on Cancer **1868**(1): 29-39.

Nikolova, T., W. P. Roos, O. H. Kramer, H. M. Strik and B. Kaina (2017). "Chloroethylating nitrosoureas in cancer therapy: DNA damage, repair and cell death signaling." Biochim Biophys Acta **1868**(1): 29-39.

Ochs, K. and B. Kaina (2000). "Apoptosis induced by DNA damage O6-methylguanine is Bcl-2 and caspase-9/3 regulated and Fas/caspase-8 independent." Cancer Res **60**(20): 5815-5824.

Oda, K., H. Arakawa, T. Tanaka, K. Matsuda, C. Tanikawa, T. Mori, H. Nishimori, K. Tamai, T. Tokino and Y. Nakamura (2000). "p53AIP1, a potential mediator of p53-dependent apoptosis, and its regulation by Ser-46-phosphorylated p53." Cell **102**(6): 849-862.

Okamura, S., H. Arakawa, T. Tanaka, H. Nakanishi, C. C. Ng, Y. Taya, M. Monden and Y. Nakamura (2001). "p53DINP1, a p53-inducible gene, regulates p53-dependent apoptosis." Molecular cell **8**(1): 85-94.

Park, J. H., G. A. Widi, D. A. Gimbel, N. Y. Harel, D. H. Lee and S. M. Strittmatter (2006). "Subcutaneous Nogo receptor removes brain amyloid-β and improves spatial memory in Alzheimer's transgenic mice." Journal of Neuroscience **26**(51): 13279-13286.

Parkin, D. M. (2001). "Global cancer statistics in the year 2000." The lancet oncology **2**(9): 533-543.

Patchell, R. A., P. A. Tibbs, W. F. Regine, R. J. Dempsey, M. Mohiuddin, R. J. Kryscio, W. R. Markesbery, K. A. Foon and B. Young (1998). "Postoperative radiotherapy in the treatment of single metastases to the brain: a randomized trial." Jama **280**(17): 1485-1489.

Patchell, R. A., P. A. Tibbs, J. W. Walsh, R. J. Dempsey, Y. Maruyama, R. J. Kryscio, W. R. Markesbery, J. S. Macdonald and B. Young (1990). "A randomized trial of surgery in the treatment of single metastases to the brain." New England Journal of Medicine **322**(8): 494-500.

Pegg, A. E. (2000). "Repair of O 6-alkylguanine by alkyltransferases." Mutation Research/Reviews in Mutation Research **462**(2): 83-100.

Peter, I. D., M. S. Linet and E. F. Heineman (1995). "Etiology of brain tumors in adults." Epidemiologic reviews **17**(2): 382-414.

Pierantoni, G. M., A. Bulfone, F. Pentimalli, M. Fedele, R. Iuliano, M. Santoro, L. Chiariotti, A.

Ballabio and A. Fusco (2002). "The homeodomain-interacting protein kinase 2 gene is expressed late in embryogenesis and preferentially in retina, muscle, and neural tissues." Biochemical and biophysical research communications **290**(3): 942-947.

Pietsch, E. C., S. M. Sykes, S. B. McMahon and M. E. Murphy (2008). "The p53 family and programmed cell death." Oncogene **27**(50): 6507.

Pohl, U., B. Wagenknecht, U. Naumann and M. Weller (1999). "p53 enhances BAK and CD95 expression in human malignant glioma cells but does not enhance CD95L-induced apoptosis." Cell Physiol Biochem **9**(1): 29-37.

Pollak, L., N. Walach, R. Gur and J. Schiffer (1998). "Meningiomas after radiotherapy for tinea capitis-still no history." Tumori Journal **84**(1): 65-68.

Pouratian, N., A. Asthagiri, J. Jagannathan, M. E. Shaffrey and D. Schiff (2007). "Surgery Insight: the role of surgery in the management of low-grade gliomas." Nature Reviews Neurology **3**(11): 628.

Preston-Martin, S. (1996). "Epidemiology of primary CNS neoplasms." Neurologic clinics **14**(2): 273-290.

Puca, R., L. Nardinocchi, A. Sacchi, G. Rechavi, D. Givol and G. D'Orazi (2009). "HIPK2 modulates p53 activity towards pro-apoptotic transcription." Mol Cancer **8**: 85.

Puca, R., L. Nardinocchi, A. Sacchi, G. Rechavi, D. Givol and G. D'Orazi (2009). "HIPK2 modulates p53 activity towards pro-apoptotic transcription." Molecular cancer **8**(1): 85.

Quiros, S., W. P. Roos and B. Kaina (2010). "Processing of O6-methylguanine into DNA double-strand breaks requires two rounds of replication whereas apoptosis is also induced in subsequent cell cycles." Cell cycle **9**(1): 168-178.

Quiros, S., W. P. Roos and B. Kaina (2011). "Rad51 and BRCA2--New molecular targets for sensitizing glioma cells to alkylating anticancer drugs." PLoS One **6**(11): e27183.

Quiros, S., W. P. Roos and B. Kaina (2011). "Rad51 and BRCA2-New molecular targets for sensitizing glioma cells to alkylating anticancer drugs." PloS one **6**(11): e27183.

Radner, H., Y. El-Shabrawi, R. H. Eibl, O. Brüstle, L. Kenner, P. Kleihues and O. D. Wiestler (1993). "Tumor induction by ras and myc oncogenes in fetal and neonatal brain: modulating effects of developmental stage and retroviral dose." Acta neuropathologica **86**(5): 456-465.

Reuss, D. and A. von Deimling (2009). Hereditary tumor syndromes and gliomas. Gliomas, Springer**:** 83-102.

Roos, W., L. Batista, S. Naumann, W. Wick, M. Weller, C. Menck and B. Kaina (2007). "Apoptosis in malignant glioma cells triggered by the temozolomide-induced DNA lesion O 6-methylguanine." Oncogene **26**(2): 186.

Roos, W., M. Baumgartner and B. Kaina (2004). "Apoptosis triggered by DNA damage O6-methylguanine in human lymphocytes requires DNA replication and is mediated by p53 and Fas/CD95/Apo-1." Oncogene **23**(2): 359-367.

Roos, W. P., L. F. Batista, S. C. Naumann, W. Wick, M. Weller, C. F. Menck and B. Kaina (2007). "Apoptosis in malignant glioma cells triggered by the temozolomide-induced DNA lesion O6-methylguanine." Oncogene **26**(2): 186-197.

Roos, W. P. and B. Kaina (2006). "DNA damage-induced cell death by apoptosis." Trends in molecular medicine **12**(9): 440-450.

Roos, W. P., T. Nikolova, S. Quiros, S. C. Naumann, O. Kiedron, M. Z. Zdzienicka and B. Kaina (2009). "Brca2/Xrcc2 dependent HR, but not NHEJ, is required for protection against O 6-methylguanine triggered apoptosis, DSBs and chromosomal aberrations by a process leading to SCEs." DNA repair **8**(1): 72-86.

Roos, W. P., A. D. Thomas and B. Kaina (2016). "DNA damage and the balance between survival and death in cancer biology." Nature Reviews Cancer **16**(1): 20.

Sakai, T., R. Kurokawa, S.-i. Hirano and J. Imai (2019). "Hydrogen Indirectly Suppresses Increases in Hydrogen Peroxide in Cytoplasmic Hydroxyl Radical-Induced Cells and Suppresses Cellular Senescence." International journal of molecular sciences **20**(2): 456.

Scheers, I., J. Palermo, S. Freedman, M. Wilschanski, U. Shah, M. Abu-El-Hajia, B. Barth, D. Fishman, C. Gariepy and M. Giefer (2018). "NCBINCBI Logo Skip to main content Skip to navigation Resources How To About NCBI Accesskeys Sign in to NCBI PubMed US National Library of Medicine National Institutes of Health Search database Search term Clear input Advanced Help Result Filters Format: Abstract Send to J Pediatr Gastroenterol Nutr. 2018 May 9." Journal of Pediatric Gastroenterology and Nutrition.

Shah, V. and P. Kochar (2018). "Brain Cancer: Implication to Disease, Therapeutic Strategies and Tumor Targeted Drug Delivery Approaches." Recent patents on anti-cancer drug discovery **13**(1): 70-85.

Siepi, F., V. Gatti, S. Camerini, M. Crescenzi and S. Soddu (2013). "HIPK2 catalytic activity and subcellular localization are regulated by activation-loop Y354 autophosphorylation." Biochim Biophys Acta **1833**(6): 1443-1453.

Siepi, F., V. Gatti, S. Camerini, M. Crescenzi and S. Soddu (2013). "HIPK2 catalytic activity and subcellular localization are regulated by activation-loop Y354 autophosphorylation." Biochimica et Biophysica Acta (BBA)-Molecular Cell Research **1833**(6): 1443-1453.

Sombroek, D. and T. Hofmann (2009). "How cells switch HIPK2 on and off." Cell death and differentiation **16**(2): 187.

Stupp, R. (2005). "European Organisation for Research and Treatment of Cancer brain tumor and radiotherapy groups; National Cancer Institute of Canada clinical trials group.

Radiotherapy plus concomitant and adjuvant temozolomide for glioblastoma." N Engl J Med **352**: 987-996.

Stupp, R., W. Mason, M. Van Den Bent, M. Weller, B. Fisher, M. Taphoorn, A. Brandes, G. Cairncross, D. Lacombe and R. Mirimanoff (2004). "Concomitant and adjuvant temozolomide (TMZ) and radiotherapy (RT) for newly diagnosed glioblastoma multiforme (GBM). Conclusive results of a randomized phase III trial by the EORTC Brain & RT Groups and NCIC Clinical Trials Group." Journal of Clinical Oncology **22**(14_suppl): 2-2.

Sun, L., A. M. Hui, Q. Su, A. Vortmeyer, Y. Kotliarov, S. Pastorino, A. Passaniti, J. Menon, J. Walling, R. Bailey, M. Rosenblum, T. Mikkelsen and H. A. Fine (2006). "Neuronal and glioma-derived stem cell factor induces angiogenesis within the brain." Cancer Cell **9**(4): 287-300.

Sung, K. S., Y.-A. Lee, E. T. Kim, S.-R. Lee, J.-H. Ahn and C. Y. Choi (2011). "Role of the SUMO-interacting motif in HIPK2 targeting to the PML nuclear bodies and regulation of p53." Experimental cell research **317**(7): 1060-1070.

Taira, N., K. Nihira, T. Yamaguchi, Y. Miki and K. Yoshida (2007). "DYRK2 is targeted to the nucleus and controls p53 via Ser46 phosphorylation in the apoptotic response to DNA damage." Molecular cell **25**(5): 725-738.

Tan, B., C. Tong, Y. Yuan, P. Xu, L. Wen, C. Zhang, Y. Zheng, L. Lin, F. Zhu and S. Gui (2019). "The Regulation of Trophoblastic p53 Homeostasis by the p38-Wip1 Feedback Loop is Disturbed in Placentas from Pregnancies Complicated by Preeclampsia." Cellular physiology and biochemistry: international journal of experimental cellular physiology, biochemistry, and pharmacology **52**(2): 315-335.

Tanaka, T., S. Ohkubo, I. Tatsuno and C. Prives (2007). "hCAS/CSE1L associates with chromatin and regulates expression of select p53 target genes." Cell **130**(4): 638-650.

Tewari, M. and V. M. Dixit (1995). "Fas- and tumor necrosis factor-induced apoptosis is inhibited by the poxvirus crmA gene product." J Biol Chem **270**(7): 3255-3260.

Vakhrusheva, O., C. Smolka, P. Gajawada, S. Kostin, T. Boettger, T. Kubin, T. Braun and E. Bober (2008). "Sirt7 increases stress resistance of cardiomyocytes and prevents apoptosis and inflammatory cardiomyopathy in mice." Circulation research **102**(6): 703-710.

Walter, A. W., M. L. Hancock, C.-H. Pui, M. M. Hudson, J. S. Ochs, G. K. Rivera, C. B. Pratt, J. M. Boyett and L. E. Kun (1998). "Secondary brain tumors in children treated for acute lymphoblastic leukemia at St Jude Children's Research Hospital." Journal of Clinical Oncology **16**(12): 3761-3767.

Wang, B., D. Li and O. Kovalchuk (2013). "p53 Ser15 phosphorylation and histone modifications contribute to IR-induced miR-34a transcription in mammary epithelial cells." Cell Cycle **12**(13): 2073-2083.

Wang, Y., K.-M. Debatin and H. Hug (2001). "HIPK2 overexpression leads to stabilization of p53 protein and increased p53 transcriptional activity by decreasing Mdm2 protein levels." BMC molecular biology **2**(1): 8.

Watson, G. A., R. P. Kadota and J. H. Wisoff (2001). Multidisciplinary management of pediatric low-grade gliomas. Seminars in radiation oncology, Elsevier.

Wei, G., S. Ku, G. K. Ma, S. i. Saito, A. A. Tang, J. Zhang, J.-H. Mao, E. Appella, A. Balmain and E. J. Huang (2007). "HIPK2 represses β-catenin-mediated transcription, epidermal stem cell expansion, and skin tumorigenesis." Proceedings of the National Academy of Sciences **104**(32): 13040-13045.

Winter, M., D. Sombroek, I. Dauth, J. Moehlenbrink, K. Scheuermann, J. Crone and T. G. Hofmann (2008). "Control of HIPK2 stability by ubiquitin ligase Siah-1 and checkpoint kinases ATM and ATR." Nature cell biology **10**(7): 812.

Winter, M., D. Sombroek, I. Dauth, J. Moehlenbrink, K. Scheuermann, J. Crone and T. G. Hofmann (2008). "Control of HIPK2 stability by ubiquitin ligase Siah-1 and checkpoint kinases ATM and ATR." Nat Cell Biol **10**(7): 812-824.

Wu, H.-l., X.-y. Fu, W.-q. Cao, W.-z. Xiang, Y.-j. Hou, J.-k. Ma, Y. Wang and C. Fan (2019). "Fucoxanthin induces apoptosis in human glioma cells by triggering ROS-mediated oxidative damage and regulating MAPKs and PI3K/AKT pathways." Journal of agricultural and food chemistry.

Yeh, H.-S., S. Kashiwagi, J. M. Tew Jr and T. S. Berger (1990). "Surgical management of epilepsy associated with cerebral arteriovenous malformations." Journal of neurosurgery **72**(2): 216-223.

Yoshida, K., H. Liu and Y. Miki (2006). "Protein kinase C δ regulates Ser46 phosphorylation of p53 tumor suppressor in the apoptotic response to DNA damage." Journal of Biological Chemistry **281**(9): 5734-5740.

Young, R. J. and E. A. Knopp (2006). "Brain MRI: tumor evaluation." Journal of Magnetic Resonance Imaging: An Official Journal of the International Society for Magnetic Resonance in Medicine **24**(4): 709-724.

Zhang, Q., Y. Yoshimatsu, J. Hildebrand, S. M. Frisch and R. H. Goodman (2003). "Homeodomain interacting protein kinase 2 promotes apoptosis by downregulating the transcriptional corepressor CtBP." Cell **115**(2): 177-186.

Zhang, X.-P., F. Liu, Z. Cheng and W. Wang (2009). "Cell fate decision mediated by p53 pulses." Proceedings of the National Academy of Sciences **106**(30): 12245-12250.

7 Supplementary information

7.1 Abbreviations

APO-1	Apoptosis antigen 1
ATM	Ataxia Telangiectasia Mutated
ATR	Ataxia telangiectasia and Rad3-related protein
BAX	Bcl-2-associated X protein
BER	Base excision repair
BSA	Bovine serum albumin
Caspase	Cysteinyl-aspartate specific protease
CCNU	N-(2-chloroethyl)-N'-cyclohexyl-N-nitrosourea (Lomustine)
CDKN1A	Cyclin Dependent Kinase Inhibitor 1A
cDNA	Complementary DNA
CD95	Cluster of differentiation 95
CHK1	Checkpoint kinase 1
CHK2	Checkpoint kinase 2
DDB2	DNA damage-binding protein 2
DMEM	Dulbecco's modified Eagle medium
DMSO	Dimethylsulfoxide
DNA	Deoxyribonucleic acid
DN-FADD	Dominant-negative Fas-associated death domain protein
DSB	DNA double-strand break
DTIC	5-(3,3-Dimethyl-1-triazenyl)imidazole-4

	-carboxamide (Dacarbazine)
DTT	Dithiothreitol
EDTA	Ethylenediaminetetraacetic acid
FADD	Fas-associated death domain protein
FAS-L	FAS ligand
FBS	Fetal Bovine Serum
FITC	Fluorescein-isothiocyanate
GBM	Glioblastoma
Gy	Gray
HDAC	Histone deacetylase
HR	Homologous recombination
MGMT	O_6-methylguanine-DNA methyltransferase
MMR	Mismatch repair
MTIC	3-methyl-(triazen-1-yl)imidazole-4-carb oximide
N3MeA	N3-methyladenine
N7MeG	N7-methylguanine
NER	Nucleotide excision repair
O^6BG	*O^6-benzylguanine*
O^6MeG	*O^6-methylguanine*
PBS	Phosphate buffered saline
PI	Propidium iodide
PTEN	Phosphatase and Tensin homolog
PUMA	p53 upregulated modulator of apoptosis
qRT-PCR	Quantitative reverse

	transcription polymerase chain reaction
RNA	Ribonucleic acid
RT	Room temperature
SD	Standard deviation
SDS	Sodium dodecyl sulfate
SDS-PAGE	SDS polyacrylamide gel electrophoresis
SEM	Standard error of the mean
TBS-T	TRIS-buffered saline with Tween
TEMED	Tetramethylethylenediamine
TMZ	Temozolomide
TRIS	Tris(hydroxymethyl)aminomethane
UV	Ultraviolet
wt	wild-type

7.2 Supplementary figures

Does Rad51 play a role in homologous recombination in LN229 cells following TMZ treatment?

LN308 and LN229 cells display the same amount of DSBs after TMZ exposure, but why do they show such a different response to TMZ-induced cell death and apoptosis? A possible hypothesis is that cells are sensitive to DNA damage response because of p53 they express. If the damage is repairable, p-p53ser15 is activated and cells go into the survival pathway; if the damage is severe, p53 is phosphorylated at ser46, then the pro-death pathways start to work. When p53 is absent, and cells may go to an error-free pathway and show more resistance. Based on this hypothesis, in p53 deficient LN308 cells, probably the homologous recombination (HR) is employed. Rad51 is a key factor in HR, the repression of Rad51 was generally associated with decreased *HR* and increased the sensitivity of the cells to DNA damaging agents (Lin, Kong et al. 2006, Foertsch, Szambowska et al. 2016). Whether there is a difference in LN229 and LN308 in Rad51 function is not known. LN229, LN229MGMT and LN308 cells were exposed to TMZ, 2 h after TMZ treatment the Rad51 inhibitor RI-1 was added to the cells to a final concentration of 5 µM. The results showed that there was no difference in the survival fraction in LN229MGMT cells before and after RI-1 treatment (Figure S1 A). In LN308 cells, there was also no significant difference observed before and after RI-1 treatment (Figure S1 A), while in LN229 cells, when treated with RI-1, the survival fraction decreased sharply (Figure S1 B). This shows that HR is essential for cell survival after TMZ exposure in the p53 proficient cells LN229. While it is not as important for LN308 as for LN229, it denied the hypothesis that LN308 cells have more survival because of HR.

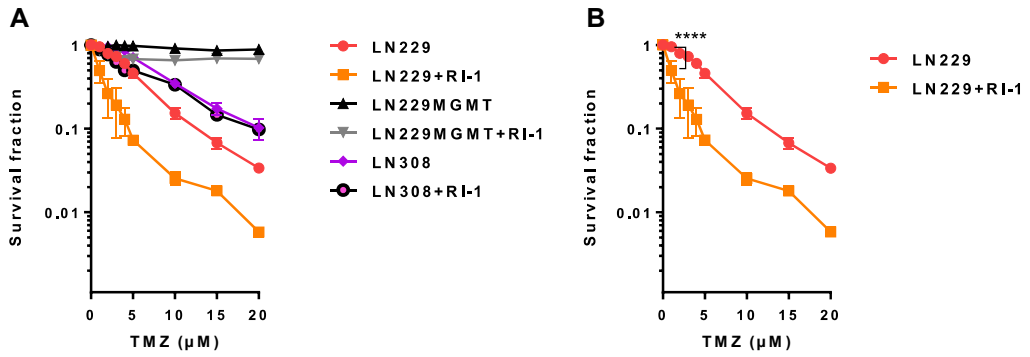

Figure S1 TMZ-induced cell death upon Rad51 inhibition with RI-1 in LN229, LN229MGMT and LN308 cells. (**A**) LN229, LN229MGMT and LN308 cells were exposed to 0-20 μM TMZ with and without RI-1. Survival fractions in each cell line were quantified and plotted on a logarithmic scale. (**B**) Survival fractions in LN229 with and without RI-1. For (**A**) and (**B**), the data were analyzed using the Prism software. p-values of < 0.05 are marked as *, p < 0.01 as *, p-values of < 0.001 as *** and < 0.0001 as ****.

Study on roles of SIAH1 and SIAH2 with Mouse Embryonic Fibroblasts

According to our hypothesis, SIAH1 and/or SIAH2 is the upstream factor that may cause the degradation of HIPK2. Therefore, the Siah1 and Siah2 double knockout mouse cell line MEF SIAH1&2 KO and wild type MEF were employed to test whether SIAH1 and SIAH2 play roles in TMZ-induced apoptosis by regulating the stability of HIPK2. The results didn't show a significant difference between MEF SIAH1&2 KO and wild type MEF cells (Figure S2 A and B), which may due to the p53 status difference between MEF and LN229 (Figure S2 C), TMZ also didn't induce as much apoptosis in MEF cells (~13%) as in LN229 (~33%), the results can be seen as a proof for the importance of p53 in this pathway from the side.

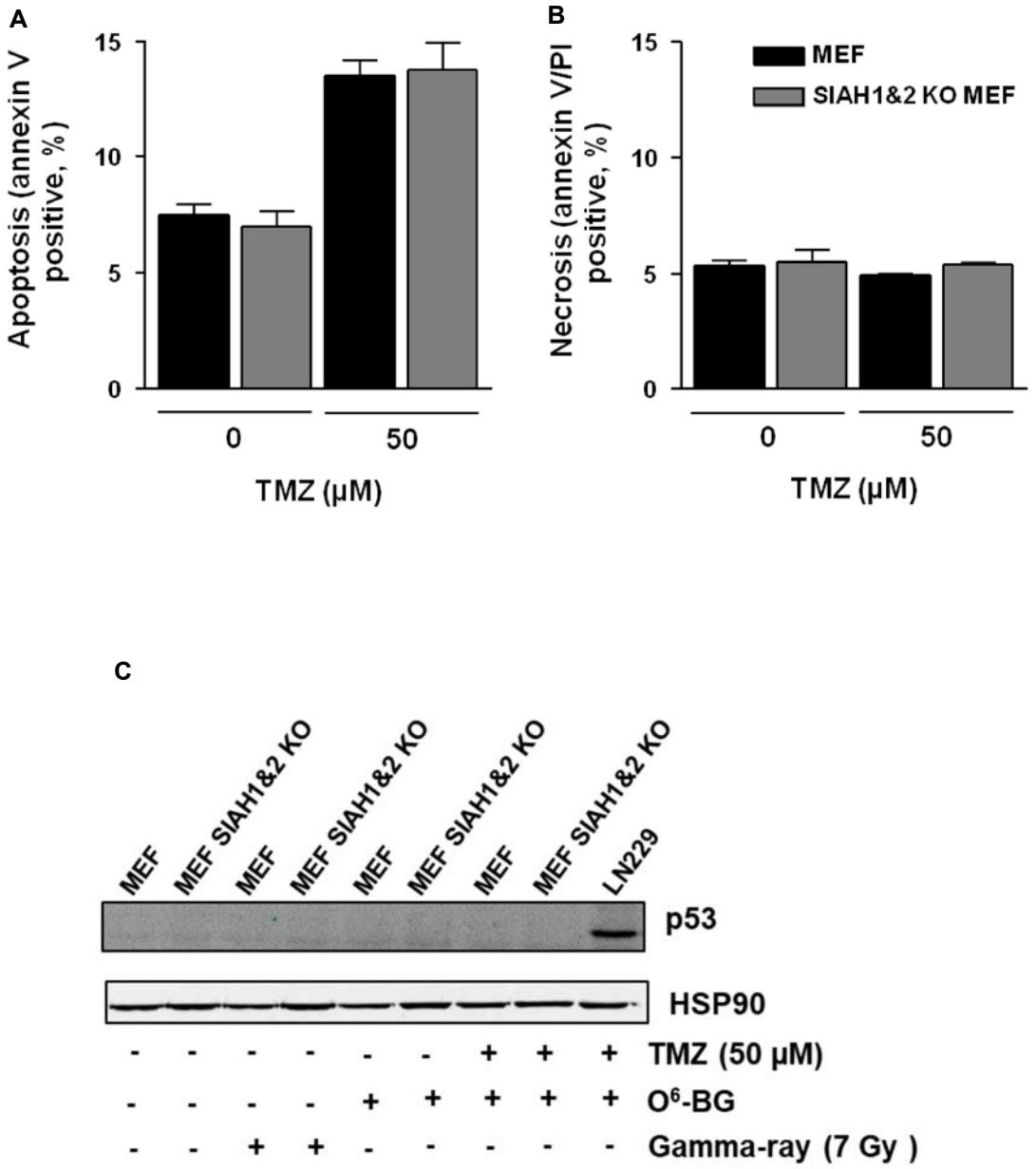

Figure S2 Roles of SIAH1 and SIAH2 in TMZ-induced apoptosis in mouse embryonic fibroblasts. Apoptosis (**A**) and necrosis (**B**) induced by 50 μM TMZ in MEFs knockout for SIAH1 and SIAH2 were measured 144 h after treatment by Annexin V/PI double staining and flow cytometry. (**C**) Western blot analysis p53, protein level in MEF, MEF SIAH1&2 KO and LN229 cells 96 h after TMZ or Gamma-ray exposure, O^6-BG was used 1 h before exposure to clear any possible MGMT. HSP90 was used as the loading control.

7.3 Curriculum vitae

Yang He

Gender: Female **Date of Birth:** June 1989 **Nationality:** Chinese

Affiliation: Institute of Molecular Biology (IMB)/ Institute of Toxicology,

University Medical Center Mainz

Address: Am Rodelberg 55, 55131 Mainz, Germany

Tel: (+49)15902623996

Email: yanghe01@uni-mainz.de

Education

02/2015-01/2019: Ph.D. Candidate, Institute of Molecular Biology (IMB)/ Institute of Toxicology, University Medical Center Mainz, Germany.

Title of the thesis: Regulation of temozolomide-induced death of glioblastoma cells: dose responses and role of HIPK2

09/2011-07/2014: Master of Radiation Medicine/Biophysics, Institute of Modern Physics, University of Chinese Academy of Sciences, Lanzhou, China.

Title of the thesis: Study on Mitochondrial DNA Damage Caused by Carbon-ion Irradiation and the Related Methodology Development

09/2007-07/2011: Dual bachelor's degrees in Biological Technology and Business English Translation, Northwest University, School of Life Science, Xi'an, China

Titles of the theses: 1. Research on Wnt Pathway for Breast Cancer Treatment in Mice 2. Analysis of Esther's Spiritual Crisis in *The Bell Jar* using Freud's theory of Personality Structure

Internships and Employment

05/2018-08/2018 Research Assistant, Institute of Toxicology, University Medical Center Mainz, Germany

2013.10-2014.06 Biology teacher (part-time) in Lanzhou Andeqiyi School, China

06/2010 Internship in Lijun Pharmacy Company, China

07/2010-09/2010 Internship in Microbiology department of the Quality and Technology Supervision Bureau, Shaanxi Province, China

04/2009 Voluntary teacher in Xi'an Bo'aiyuan (for helping children with intellectual disabilities to do recovery training), China

06/2008 Internship in Qinling Pingheliang Nature Reserve, China

Awards

2015-2018 A 3-year fellowship provided by Institute of Molecular Biology (IMB), Mainz, Germany

2011-2014 A 3-year fellowship for excellent master student, provided by Institute of Modern Physics, University of Chinese Academy of Sciences, Lanzhou, China

2013 Excellence Award in Network Information Knowledge Contest, held by the National Science Library, Lanzhou, China

2009-2010 National Scholarship for Encouragement, and second prize scholarship of Northwest University, Xi'an,China

2008-2009 Third prize scholarship of Northwest University, Xi'an,China

2007-2008 National Aspiration Scholarship, and second prize scholarship of Northwest University, Xi'an,China

Publications

1. **He Y.**, Roos W., Wu Q, Hofmann T. G., Kaina B.. The HIPK2-SIAH1-p53 axis regulates temozolomide-induced glioblastoma cell death. Molecular Cancer Research (On review)

2. **He Y.**, Zhou X, Zhang H. Hypoxia Mitochondria and Tumor Radiation Resistance. Nuclear Physics Review, 2013, 30(4): 488-493.

3. **He Y.**, Zhou X., Zhang H.. Mitochondrial DNA Mutations Induced by Carbon Ions Radiation. Cancer Research on Prevention and Treatment, 2014, 41(07): 698-701.

4. Zhou X., Liu X., Zhang X., Zhou R., **He Y.**, Li Q., Wang Z., Zhang H.. Non-randomized mtDNA damage after ionizing radiation via charge transport. Scientific Report, 2012; 2:780.

5. Li H., Zhang H., Xie Y., He Y., Miao G., Yang L., Di C., **He Y.**. Proteomic analysis for testis of mice exposed to carbon ion radiation. Mutation Research, 2013 Aug 15;755(2):148-55.

Language Skills and Qualifications

Chinese: native speaker English: fluent, TOEFL iBT 90 German: B1

7.4 Conferences

2018 IPP Ph.D. Symposium, Mainz. HIPK2 regulates temozolomide-induced glioblastoma cell death in a p53 and FAS-R dependent manner. **Poster presentation**

2018 Symposium of international young scholars at Wenzhou Medical University, Wenzhou. The HIPK2-SIAH1-p53 signaling axis regulates temozolomide-induced glioblastoma cell death. **Oral presentation**

2017 Symposium “DNA damage response, genetic instability and Cancer”, Mainz. HIPK2 is involved in p53-regulated cell death pathways induced by O^6-methylguanine. **Poster presentation**

2017 IPP Ph.D. Symposium, Mainz. HIPK2 is involved in O^6-methylguanine-induced p53 dependent apoptosis by regulating the expression of FAS-R/CD95/Apo-1. **Oral presentation**

2017 4th German-French DNA Repair Meeting, Cologne. HIPK2 is involved in p53-regulated cell death pathways induced by the anticancer drug temozolomide. **Poster presentation**

2016 14th Biennial Conference of the German Society for research on DNA Repair (DGDR), Essen. Identifying factors that switches p53 from a protector to a killer during O^6-mathylguanine triggered signaling. **Poster presentation**

2016 IPP Ph.D. Symposium, Mainz. Identification of factors in the threshold of DNA damage response triggered by O^6-methylguanine. **Poster presentation**